HAL
open science

Développement d'un réfrigérateur à dilution en boucle fermée pour expériences d'astrophysique dans l'espace

Angela Volpe

To cite this version:

Angela Volpe. Développement d'un réfrigérateur à dilution en boucle fermée pour expériences d'astrophysique dans l'espace. Physique [physics]. Université de Grenoble, 2014. Français. NNT : 2014GRENY009 . tel-00993970v2

HAL Id: tel-00993970

https://theses.hal.science/tel-00993970v2

Submitted on 3 Sep 2014

HAL is a multi-disciplinary open access archive for the deposit and dissemination of scientific research documents, whether they are published or not. The documents may come from teaching and research institutions in France or abroad, or from public or private research centers.

L'archive ouverte pluridisciplinaire **HAL**, est destinée au dépôt et à la diffusion de documents scientifiques de niveau recherche, publiés ou non, émanant des établissements d'enseignement et de recherche français ou étrangers, des laboratoires publics ou privés.

UNIVERSITÉ DE GRENOBLE

THÈSE

Pour obtenir le grade de

DOCTEUR DE L'UNIVERSITÉ DE GRENOBLE

Spécialité : **Physique appliquée**

Arrêté ministériel : 7 août 2006

Présentée par

Angela Volpe

Thèse dirigée par **Alain Benoit**

et codirigée par **Gerard Vermeulen**

préparée au sein **l'Institut Néel**

et de **l'École doctorale de Physique**

Development of a closed cycle dilution refrigerator for astrophysical experiments in space

Thèse soutenue publiquement le **31/01/2014**,

devant le jury composé de :

M. Alain Girard

Ingénieur au Service des Basses Températures-CEA, Grenoble, Président

M. Pierre-Jean Nacher

Directeur de recherche au Laboratoire Kastler Brossel, Paris, Rapporteur

M. A.T.A.M. de Waele

Professeur émérite à Technische Universiteit Eindhoven, Rapporteur

M. Paolo De Bernardis

Professeur à l'Université La Sapienza, Rome, Examinateur

M. Alain Benoit

Directeur de recherche à l'Institut Néel, Grenoble, Directeur de thèse

M. Gerard Vermeulen

Chargé de Recherche à l'Institut Néel, Grenoble, Co-Directeur de thèse

Acknowledgements

Firstly I would like to thank the MCBT (Matière Condensée - Basses Températures) department of the Neel Institute to allowed me to work in this renowned institution along with preeminent members of the low temperature physics community.

I acknowledge my supervisor Alain Benoit to have givin me the opportunity to participate in this prestigious project that could represent a breakthrough in the field of the astrophysical detection on satellite.

I thank my co-supervisor Gerard Vermeulen for his assistance, support and availability in any moment throughout these years and generally being a nice guy. I truly appreciated all he has done for me and, in particular, the opportunity to present my results in several international conferences. He has been an example of devotion to work.

I acknowledge Dominique Grand of SERAS (Service Etude et Realisation d'Appareillages Scientifiques-CNRS) for the accurate drawings of the NG-CCDR and Gilles Pont and Pierre Chantib of pôle Cryogénie of the MCBT department for the help in manufacturing and assembling it.

Thanks also to the guys of the liquefacteur for their technical assistance. The assistance of Patrick Belmain of the Service Informatique is also appreciated.

I would like to thank the members of the équipe HELFA to have accepted me in their team and provide a stimulating environment of study and work.

In my acknowledgements I cannot forget Gunaranjian Chaudhry, a former Post-Doc I worked with during my first year of PhD. He first introduced me to the ^{3}He-^{4}He mixture physics and I thank him for the time he spent answering

my questions. I truly appreciated his method "you do, I sit here and watch", forcing me to learn how to handle the experiment.

I also acknowledge the CNES (Centre national d'études spatiales), the industry Air Liquid and ESA (European Space Agency) to found this project and my grant. In particular from these organisation I thank Stéphane d'Escrivan, Sébastien Triquenaux, James Butterworth and Thierry Tirolien for their help and support throughout my PhD and for the nice time spent together during the conferences. A special thank goes to Sébastien Triquenaux who helped me to prepare the presentation for my PhD defense.

I would also like to thank Pierre-Étienne Wolf, the Head of the MCBT departement, for the time he spent to discuss physics with us despite his busy schedule. In particular he deserves my thanks for his precious advice for my final presentation.

I acknowledge the members of my jury, for having read accurately my thesis and for coming the day of my defense. In particular, I thank my two referees, A.T.A.M de Waele and Pierre-Jean Nacher, for having given me precious advice to improve the quality of my manuscript.

And of course I cannot forget my friends in Grenoble: I don't know where to start...maybe I can start listing them: Claudio Attaccalite, Geoffroy Aubry, Andrea Barolini, Nicolas Boudou, Irene Calvo, Martino Calvo, Elena Cannuccia, Lucia Capogna, Ioan Chioar, Valentina Cogoni, Barbara Comis, Francesca Coscia, Antonio D'Addabbo, Liza Herrera Diez, Angelo Di Marco, Carina Faber, Ovidiu Florea, Simone Fratini, Camille Gandioli, Marc Ganzhorn, Martin Jackson, Marco Maccarini, Sophie Saia, Christoph Schenke, Laura Simonelli, Cornelia Schwarz, Robert Schneider, Stefan Thiele,

Tommaso Tosi, Peter Van Zwol, Isabel Zamanillo and all the members of the spaghetti-climbers group. I sincerely thank them for their help in the difficult moments, such as my various accidents. But this is nothing compared to what they have given me every single day I spent in Grenoble: despite I was in a foreign country, far from my family and my boyfriend, they made me feel at home. They have enriched my everyday life in a way I cannot describe: after three years spent with them I feel a better and more complete person. Thanks guys for making this time in Grenoble a wonderful experience, one I will never forget.

Grazie mille a Stefan Thiele for the "writing Sundays": he made the work during the weekend nice and pleasant. Thanks also to Simone Fratini, Elena Cannuccia, Martino Calvo and Johannes Goupy for having read part of my thesis.

Infine ringrazio i miei genitori e il mio ragazzo Pietro. Nonostante la lontananza mi sono stati vicini e pronti ad accorrere nel momento del bisogno.

I hope not having overlooked anybody. I apologise if I have and thanks anyway.

Contents

Introduction **ix**

Introduction **xiv**

1 Cryogenics for astrophysics **1**

1.1 Detecting the Universe 2

1.2 Methods to reach the detectors operating temperature 6

1.3 Planck and future missions 8

2 ^{3}He-^{4}He mixture and dilution refrigerators **13**

2.1 ^{3}He-^{4}He liquid mixture 14

2.1.1 Phase diagram 14

2.1.2 Some thermodynamic properties 16

2.1.3 ^{4}He chemical potential in a ^{3}He-^{4}He mixture 16

2.1.4 The dilution process 19

2.2 Conventional dilution refrigerator 24

2.2.1 Cooling power 29

2.3 OCDR: Open-Cycle Dilution Refrigerator 33

2.4 Conclusions 37

3 Closed-cycle dilution refrigerator **41**

3.1 From the OCDR to the CCDR 42

3.2 CCDR low temperature part 43

3.2.1 Heat exchanger and cold end configuration 45

3.2.2 CCDR cooling power 54

3.2.3 The Kapitza resistance in the cold end 55

3.2.4 Constant x or constant μ_4? 60

3.2.5 Effect of still pressure on the refrigerator performance and on the pre-cooling stage 63

3.3 High temperature part 65

3.3.1 The pre-cooling stage 65

3.3.2 Fountain pump 73

3.4 CCDR operational conditions 82

4 Negative Gravity Vapor Liquid Phase Separation **85**

4.1 Method 86

4.1.1 Materials 87

4.2 Test setup 90

4.2.1 Setup description 90

4.2.2 Test equipment 96

4.2.3 Test procedure 99

4.2.4 Results 101

4.3 Test output for NG-still design 106

5 Negative Gravity CCDR **109**

5.1 Negative-gravity still design 110

5.2 Negative Gravity CCDR test setup 114
5.2.1 Ng-CCDR setup cooling performance 117
5.3 Negative Gravity CCDR test equipment 118
5.4 Negative Gravity CCDR procedure 119
5.4.1 Optimization of the NG-CCDR and its performance . . 119
5.4.2 Verification of the negative gravity operation 121
5.5 NG-CCDR test preliminary results 122
5.6 Conclusions 128

6 Perspectives 131
6.1 The fountain pump in the NG-still design 132
6.2 ^{3}He compressor 132
6.3 Further improvements and open questions 136

A Recalculation of the ^{4}He flow rate 139

B History of the variations of the NG-VLPS setup 143

Conclusions 155

Conclusions 159

References 163

Introduction

To comprehend the physical processes occurring across the universe it is essential to observe over the whole range of electromagnetic radiation. Experiments on satellite are needed because certain wavelengths never reach the Earth surface, due to the atmospheric absorption. Certain kind of detectors need to be cooled at very low temperatures (< 0.3 K) to operate correctly. Such temperatures can be achieved with two systems: the adiabatic demagnetisation refrigerator and the ^{3}He-^{4}He dilution refrigerator. The adiabatic demagnetisation refrigerator absorbs heat by augmenting the entropy of the magnetic moments of the molecules in a paramagnetic salt.The entropy is reduced by applying a magnetic field to align the magnetic moment along its direction. During the reduction of the magnetic field the entropy is conserved, while the temperature is reduced. In a dilution refrigerator, instead, the cooling is obtained by the transfer of ^{3}He atoms from pure liquid ^{3}He into a solution of ^{3}He diluted in ^{4}He. Due to the large enthalpy of the dilute phase, high cooling power is available for the dilution process. The use of both methods poses some issues, due to the constrains of a satellite: limited available space, weight and electrical power, electromagnetic noise and/or stray magnetic field, duty-cycle duration, micro-gravity environment, resistance to

shocks and vibrations, reliability in terms of lifetime and performance. One of the main issues concerning the use of a dilution refrigerator in space is that it is hard to adapt to zero-gravity. Nevertheless, an open-cycle dilution refrigerator, successfully adapted to the micro-gravity environment, has been used on Planck satellite. This system successfully delivered a cooling power of a 0.2 μW at 100 mK for a lifetime of 2.5 years. In this refrigerator the two isotopes, mixed from different reservoirs, are ejected into space. The lifetime and the cooling power of the mission are therefore limited by the amount of gas embarked at launch. Future space missions demand a higher cooling power (1 μW) at a lower temperature (50 mK) for a lifetime of five-ten years. Such requirements cannot be fulfilled by an open-cycle.

This has driven to the need of developing a new gravity-insensitive dilution refrigerator in which the mixture is not ejected into space but separated out into its components which are then re-injected into the system. Even if closing the cycle is a solution to overcome the limitations of the open-cycle, it introduces problems caused by the zero-g environment.

In this context I present my thesis work. I will illustrate the progress made in the last three years on the development and the comprehension of this system, that builds on previous work carried out in collaboration with a former PhD student and a post-doc. The work is divided in two parts: the first part focused on the improvements of the cooling performance under required conditions and on the better comprehension of the system; the second part where the main focus is to solve the problems connected to the micro-gravity environment.

In the first chapter I will remind the general context and the motivation

of the project. I will describe the scientific interest of placing an experiment above the atmosphere and why it is necessary to cool the detectors to very low temperatures. I will explain very shortly the functioning of the two methods for cooling at very low temperature, dwelling on the Plank mission as an example of dilution refrigeration used in space. After specifying more ambitious cryogenic requirements of future missions, it will be clear that the open-cycle dilution refrigerator cannot be employed for these projects.

The second chapter is devoted to explain the principle of the dilution refrigeration. I will begin discussing some important thermodynamic properties of the ^{3}He-^{4}He mixture. These properties are then used to explain the functioning of the conventional dilution refrigerator, which exploits gravity to localize the phase separation interfaces in the still and in the mixing chamber. Then I will describe more in details the open-cycle dilution refrigerator, where the gravity problems are eliminated suppressing the still and using a mixing chamber where surface tension replaces gravity.

In the third chapter I will discuss the CCDR (Closed-Cycle Dilution Refrigerator) design, which is based on the open-cycle refrigerator. The major difference between the two systems is the addition of a separation-circulation system. After a description of this system I will present the different parts of the refrigerator: the low temperature part (the counter-flow heat exchanger, the cooling power at the mixing chamber exit, and the Kapitza resistance relevant for thermal contact to a detector assembly); and the high temperature part (the fountain pump and the heat load on the pre-cooling stage). The different parts have been characterized with respect to the cooling performance required by future space missions and in order to specify the interface

of the CCDR with the rest of a satellite.

The fourth chapter is devoted to a crucial issue: the confinement of the liquid mixture in the still in zero-gravity conditions. In conventional dilution refrigerators the liquid-vapor phase interface is localized by gravity in the still. In a zero-gravity environment another method has to be found to achieve the phase separation. The method we used is based on the liquid confinement by capillary forces in a porous material. I will describe the setup we have built and characterized to test the confinement in negative-gravity and under required conditions (to reach the optimum cooling performance). The output of these experiments has been very important for the design of a negative-gravity still, presented at the end of this chapter.

In the fifth chapter I will present the negative-gravity still design. The new still has been integrated in an "upside-down" version of the CCDR prototype described in chapter 3. In this new design the the mixing chamber and the heat exchanger are placed above the still. This choice to simulate negative gravity and so to verify if a dilution refrigerator can work in such extreme condition. The main focus of this setup is to test the new still design. After presenting the new CCDR design, I will illustrate the procedure, developed in the context of the ESA-ITI contract, to apply during the measurements. I will conclude the chapter presenting the experimental results and the problems met during the measurements.

In the last chapter I will describe the outstanding issues to be solved in order to finalise the project. I will start explaining how we thought to verify and solve the problems met during the tests performed on the prototype described in chapter 5. Then I will address an important topic: the choice

of a space qualified compressor to circulate the ^{3}He in the system. I will conclude the chapter with some suggestions to improve the system further and discussing some open questions.

This project has been carried out at the Institut Neel, CNRS (Centre national de la recherche scientifique) and it is co-founded by the CNES (Centre national d'études spatiales) and the industry Air Liquid. The project receives funding also from ESA (European Space Agency) by means of an ITI contract.

Introduction

Pour comprendre les processus physiques qui se produisent à travers l'univers, il est essentiel de l'observer sur toute la plage du rayonnement électromagnétique. En raison de l'absorption atmosphèrique à longueurs d'onde, il est nécessaire de réaliserdes observations avec des détecteurs embarqués sur satellite. Certain types de détecteurs doivent être refroidis à des températures très basses (< 0.3 K) pour fonctionner correctement. Ces températures sont obtenues avec deux types des systèmes : le réfrigérateur à démagnétisation adiabatique et le réfrigérateur à dilution ^{3}He-^{4}He. Le réfrigérateur à demagnetisation adiabatique absorbe la chaleur en augmentant l'entropie des moments magnétiques des molécules dans un sel paramagnétique. Les moments sont alignés par un champ magnétique le long de sa direction. Au cours de la réduction du champ magnétique de l'entropie est conservée, tandis que la température est réduite. Dans un réfrigérateur à dilution le refroidissement est obtenu par transfert d'atomes d'^{3}He à partir d'^{3}He pur liquide dans une solution d'^{3}He dilué dans l'^{4}He. En raison de la grande enthalpie de la phase diluée , une puissance frigorifique élevée est rendue disponible par le processus de dilution. L'utilisation des deux méthodes implique quelques complications. Sur un satellite plusieurs contraintes sont

à prendre en compte : l'encombrement , le poids et la puissance électrique disponibles limités, le bruit électromagnétique et/ou champ magnétique parasite, le duty-cycle, la microgravité, la tenue aux chocs et aux vibrations , la fiabilité en termes de durée de vie et des performances. Le principal problème avec un réfrigérateur à dilution est son utilisation en apesanteur. Néanmoins, un réfrigérateur à dilution en boucle ouverte, adapté avec succès à la microgravité, a été utilisé sur le satellite Planck. Ce système a livré une puissance frigorifique de 0.2 μW à 100 mK avec une durée de vie de 2,5 ans. Dans ce réfrigérateur les deux isotopes, mélangés à partir de deux différents réservoirs, sont éjectées dans l'espace. La durée de vie et la puissance frigorifique de la mission sont donc limitées par la quantité de gaz embarqué au lancement. Les futures missions spatiales exigent une puissance frigorifique plus élevée (1 μW) à une température inférieure (50 mK) pour une durée de vie de cinq à dix ans. Ces exigences ne peuvent pas être satisfaites avec un système à cycle ouvert.

Ceci a conduit à la nécessité de développer un nouveau réfrigérateur à dilution non sensible à la gravité , où le mélange n'est pas éjecté dans l'espace , mais séparé en ses composants qui sont ensuite réinjecté dans le système. Même si la fermeture du cycle est une solution pour surmonter les limites du réfrigérateur en boucle ouverte , il introduit des problèmes causés par la microgravité.

C'est dans ce contexte qui s'inscrit mon travail de thèse. Je vais illustrer les progrès réalisés au cours des trois dernières années sur le développement et la compréhension de ce système, qui s'appuie sur des travaux antérieurs réalisés en collaboration avec un ancien doctorant et un post-doc. Le travail

est divisé en deux parties: la première partie est dedié à l'amélioration des performance de refroidissement dans les conditions requises et à une meilleure compréhension du système; la deuxième partie a pour objectif principal de résoudre les problèmes liés à la microgravité.

Dans le premier chapitre, je vais rappeler le contexte général et la motivation du projet. Je vais décrire l'intérêt scientifique de placer une expérience endehors de l'atmosphère et pourquoi il est nécessaire de refroidir les détecteurs à très basse température. Je vais expliquer brièvement le fonctionnement des deux méthodes pour refroidir à très basse température, en prenant le systèm utilisé sur la mission Planck comme exemple de réfrigération à dilution utilisés dans l'espace. Après avoir spécifié les exigences cryogéniques des missions futures, nous verrons clairement que le réfrigérateur à dilution en cycle ouvert ne peut pas être utilisé pour ces projets.

Le deuxième chapitre est consacré à l'explication du principe de la réfrigération à dilution. Je commencerai par evoquer les propriétés thermodynamiques du mélange ^{3}He-^{4}He. Ces propriétés seront ensuite utilisées pour expliquer le fonctionnement du réfrigérateur à dilution classique , qui exploite la gravité pour localiser les interfaces de séparation de phases dans le bouilleur et dans la chambre à mélange. Ensuite , je vais décrire plus en détails le le fonctionnement du réfrigérateur à dilution en boucle ouverte , où les problèmes de gravité sont éliminés en supprimant le bouilleur et en utilisant une chambre à mélange où la tension de surface remplace la gravité.

Dans le troisième chapitre , je vais discuter le design du réfrigérateur à dilution en cycle fermé , le CCDR (Closed Cycle Dilution Refrigerator) , qui est basé sur le réfrigérateur en cycle ouvert. La différence majeure en-

tre les deux systèmes est l'ajout d'un système de séparation et de circulation. Après une description de ce système, je vais présenter les différentes parties du réfrigérateur : la partie à basses températures (l'échangeur de chaleur à contre-courant , la puissance frigorifique à la sortie de la chambre de mélange, et la résistance de Kapitza pour le contact thermique avec ensemble des détecteur) , et la partie à hautes températures (la pompe à pression fountaine et la charge thermique sur l'étage de pré-refroidissement). Les différentes parties ont été caractérisées par rapport aux performances de refroidissement requis par les futures missions spatiales et afin de préciser l'interface du CCDR avec le reste du satellite.

Le quatrième chapitre est consacré à la question cruciale du confinement du mélange liquide dans le bouilleur dans en l'absence de gravité. Dans les réfrigérateurs à dilution classiques l'interface de phase liquide-vapeur est localisée par gravité dans le bouilleur. En l'absence de gravité une autre méthode doit être trouvé pour obtenir la séparation de phase. Le procédé que nous avons utilisé est basé sur le confinement du liquide par la force capillaire dans un matériau poreux. Je vais décrire la configuration que nous avons construite et caractérisé pour tester le confinement en gravité négative et dans les conditions requises (pour atteindre les performances de refroidissement optimale). Les résultats de ces expériences ont été très important pour la conception d'un bouilleur qui marche en gravité négative.

Dans le cinquième chapitre, je vais présenter le design du bouilleur qui fonctionne en gravité négative. Le nouveau bouilleur a été intégré dans version à l'envers du prototype de CCDR décrit dans le chapitre 3. Avec cette nouvelle conception la chambre de mélange et l'échangeur de chaleur sont placés

au-dessus du bouilleur. Ce choix a été fait pour simuler la gravité négative et ainsi pour vérifier si un réfrigérateur à dilution peut travailler dans telles conditions extrêmes. L'objectif principal de cette configuration est de tester le nouveau design du bouilleur. Après avoir présenté le nouveau design du réfrigerateur , je vais illustrer la procédure développée dans le cadre du contrat ESA -ITI , à appliquer pendant les mesures . Je vais conclure le chapitre en présentant les résultats expérimentaux et les problèmes rencontrés lors des mesures.

Dans le dernier chapitre , je vais décrire les questions en suspen à résoudre afin de finaliser le projet. Je commencerai par à expliquer comment nous allons vérifier et résoudre les problèmes rencontrés lors des tests effectués sur le prototype décrit dans le chapitre 5. Ensuite, je vais aborder un sujet important : le choix d'un compresseur qualifié pour l'espace pour la circulation de l'^{3}He dans le système. Je vais conclure le chapitre avec des suggestions pour améliorer le système et en discutant quelques questions ouvertes.

Ce projet a été réalisée à l'Institut Néel , CNRS (Centre national de la recherche scientifique) et il est co-fondée par le CNES (Centre national d'Etudes Spatiales) et l'industrie Air Liquide. Le projet reçoit également un financement de l'ESA (Agence spatiale européenne) avec un contrat ITI .

Chapter 1

Cryogenics for astrophysics

An observation over the whole range of electromagnetic radiation is necessary to study the universe. The atmospheric absorption prevents certain wavelengths to reach the Earth surface. It is, therefore, indispensable to put experiments on satellite. Certain kind of detectors, such as the bolometers, need to be cooled down at very low temperatures to operate properly. This can be done with different methods: one of these is by using a ^{3}He-^{4}He dilution refrigerator adapted to zero-gravity. The first, and for the moment the only, dilution refrigerator ever used in space is the open-cycle dilution refrigerator of the Planck satellite. In this system, successfully adapted to the micro-gravity environment, the two helium isotopes are mixed from different reservoirs and then the mixture is ejected into space. As a consequence the lifetime and the cooling power are limited by the amount of gas embarked at launch. More demanding cooling requirements of future missions render this system impractical. For this reason an evolution of this refrigerator, able to meet future mission specifications, has been conceived.

1.1 Detecting the Universe

For centuries humanity has looked up in the sky wondering about the universe. The tool used by astronomers, astrophysicists and cosmologists to get information about the universe is the electromagnetic radiation[1] coming form astronomical objects (among the others planets, stars, galaxies, black holes, cosmic microwave background). The observation of the universe started from the visible part of the electromagnetic spectrum, where our eyes can see. For a complete understanding of the physical processes occurring across the universe an exploration of the whole range of electromagnetic radiation is essential. The problem is that most of electromagnetic radiation from space never reaches the surface of the Earth. Figure 1.1 shows the depth of penetration of different wavelengths into the Earth's atmosphere. It is evident that only the visible and radio wavelengths achieve the surface without being absorbed. A limited amount of infra-red light also reaches the ground and it can be observed from mountain tops or by flying instruments in an aircraft. Experiments can also be taken up to altitudes of about 40 km by stratospheric balloons (avoiding most of the atmosphere) or by rockets at about 200 Km (completely above the atmosphere). The problem with this two methods is the short observation time: few months for balloons, few minutes for rockets. In most case, to obtain accurate scientific results and to obtain a valid statistics, it is necessary to map the sky for years. In order to avoid the atmosphere and obtain longer observation times, the best solution is to place experiments on a satellite.

[1] Of course there also are scientists who study directly the dark matter or the gravitational waves.

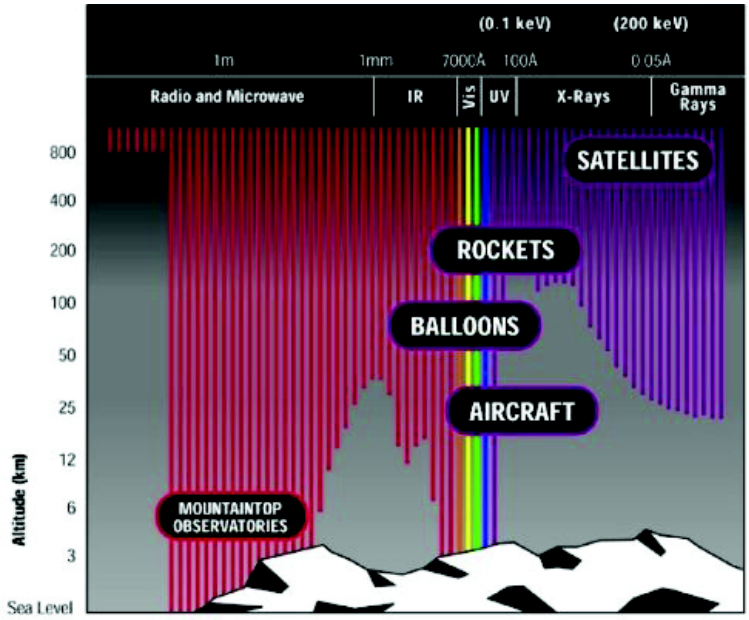

Figure 1.1: Depth of penetration of different wavelengths of electromagnetic radiation into the Earth's atmosphere.

To detect the radiation different kinds of sensors are used, depending on the energy of the photons. Traditionally for short wavelengths (< 200 μm), the energy of a single photon hitting the detector is high enough to produce an observable physical quantity due to some quantum effect (i.e. an electric current due to the photoelectric effect). For long wavelengths (>200 μm) the photons energy is too low to produce quantum effects effectively exploitable. Therefore, the use of thermal detectors becomes indispensable. In this kind of sensors a parameter, for example the detector resistance, changes due to the heating produced by the cumulative effect of many low energy photons. The detector becomes actually sensitive to this low energy radiation when its noise, which depends on the sensor temperature, is lower than the astrophysical signal one wants to detect. To reduce the noise it is necessary to cool sensor at low temperatures (typically < 1 K). Fig. 1.2 shows the

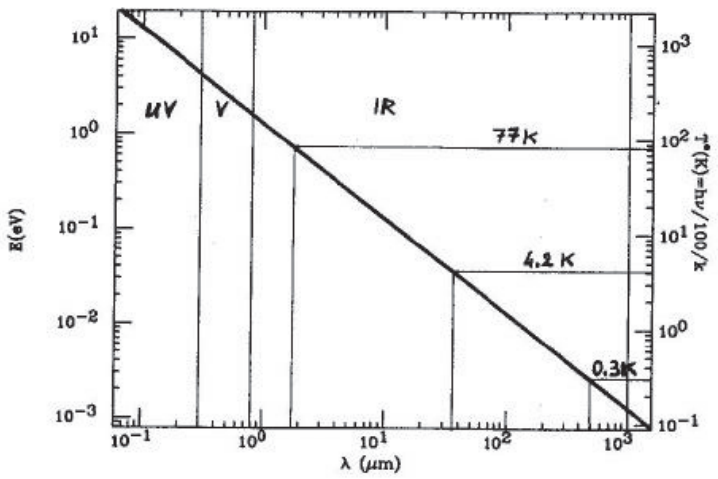

Figure 1.2: Comparison between the photons energy (left y-axis) and the the detector noise temperature (right y-axis) as a function of the wavelength (UV = Ultraviolet, V = visible, IR = infrared). The detector temperature is obtained imposing that the sensor thermal energy is one hundred times smaller than that of the photons($kT = h\nu/100$). This plot gives an idea of the temperature at which the detectors have to be cooled so that their noise is not higher than the astrophysical signal one wants to detect.

photons energy (left side y-axis) as a function of the wavelength. At the right y-axis there is the detector temperature obtained imposing that the sensor thermal energy is one hundred times smaller than that of the photons ($kT = h\nu/100$). This plot is not to be taken literally, but it gives a general idea of the temperature at which detectors have to be cooled so that their noise is lower than the astrophysical signal.

The most common thermal detectors are the bolometers. A bolometer consists of an absorbing element whose resistance depends strongly on its temperature. It is connected through a thermal link to a heat sink, a body of constant temperature. The result is that any radiation impinging on the absorbing element raises its temperature above that of the heat sink. As a

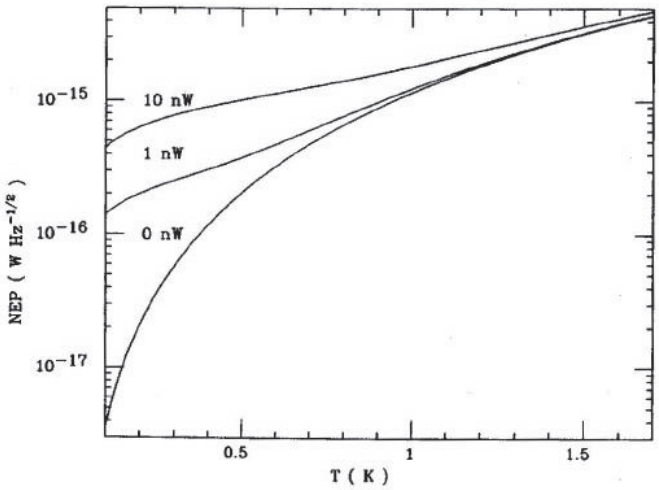

Figure 1.3: Total fundamental noise (Noise Equivalent Power) of a bolometer for different values of radiative background. For low radiative backgrounds, which are necessary in many kinds of astrophysical experiments, it is worthy to decrease the temperature because of significant detector noise reduction.

consequence of the temperature raise, the bolometer resistance changes. For sub-millimeter and millimeter wavelengths, bolometers are among the most sensitive available detectors. To achieve the best sensitivity, they have be cooled down to temperatures below 0.3 K (the typical temperature range is 300-50 mK). Fig. 1.3 shows the total fundamental noise (Noise Equivalent Power) of a bolometer. The different curves represent different values (nW) of the radiative background (for example due to the IR thermal emission of the mirrors). It is evident that for low radiative backgrounds, which are often required in astrophysical experiments, it is worth to decrease the detector temperature because of the significant noise reduction.

Similar cooling requirements are shared by technologies exploiting superconducting materials, such as transition edge sensors or kinetic inductance detectors, to cool down the sensors well below the critical temperature.

1.2 Methods to reach the detectors operating temperature

To cool down the detectors below 0.3 K, there are two main methods: the Adiabatic Demagnetisation Refrigerator (ADR) (suggested by Debije [1] and Giauque [2] in the late 1920s) and the ^{3}He-^{4}He dilution refrigerator (suggested by London in 1951 [4], then realised by Das, Ouboter and Taconis in 1965 [5]).

The ADR is a cyclic cooling system. It alternates between two states: the first step is to use a magnetic field to align along its direction the magnetic moments of molecules composing a paramagnetic salt, while the paramagnetic salt is connected to an heat sink (usually an ^{4}He bath at 2 K) to keep its temperature stable. During this process the entropy is reduced. Then the heat switch to the sink is opened, and the magnetic field is decreased. The process occurs in adiabatic conditions, since the heat switch is open. During the reduction of the magnetic field, the entropy is conserved while the temperature is reduced. To cycle it again it is necessary to reconnect the salt to the heat sink to realign the magnetic moments that moved out of alignment due to the absorption of heat (for more details refer to [7]). This technique is appealing for space applications, since it does not require gravity for its operation. However, this system is not able to operate at constant temperature for a long time and needs a periodic recycling. To achieve continuous

cooling more ADRs can be used at the same time. This solution render the all system massive and heavy, introducing problems regarding the massive supports that have to be used to sustain such a device.

The functioning of the dilution refrigerator will be expounded in details in the next chapter. The general idea is to exploit the properties of the liquid mixture of ^{3}He and ^{4}He: the cooling is obtained by the transfer of ^{3}He atoms from pure liquid ^{3}He into a solution of ^{3}He diluted in ^{4}He. Due to the large enthalpy of the dilute phase, high cooling power is available by the dilution process. Compared to ADR, this refrigerator has the advantage of being a continuously working device and it does not require the use of magnetic fields, which can negatively affect other components of the experiment (for instance the detectors). Moreover, its mass is very low on the coldest stages and the cooling power can be distributed on large focal planes avoiding thermal links and heavy supports required by an ADR. It also allows to cool the mechanical supports and the electrical wires (by intercepting the heat transported from higher temperatures along its counterflow heat exchanger) without affecting the minimum temperature (see ref. [8]).

It could be argued that dilution refrigerators require gravity for their operation, so they cannot be used for space applications. This is in fact true in standard terrestrial dilution refrigerators, which exploit gravity to localize the phase separation interfaces in the still and in the mixing chamber. In the next chapter we will see that it is possible to suppress gravity problems and that a dilution refrigerator can be successfully used on a satellite. For the first time, in fact, an open-cycle dilution refrigerator [9, 10, 12, 13] has been used aboard Planck satellite to cool down its High-Frequency Instrument.

The dilution refrigerator is the coldest stage of Planck's cooling chain. An example of cooling chain in space is describe by DiPirro, Johnson and Shirron [6] (here the last stage is an ADR).

1.3 Planck and future missions

The ESA's Planck mission [14, 15] was designed to image the anisotropies in temperature of the Cosmic Microwave Background radiation (CMB) over the whole sky. The CMB is a snapshot of the oldest light in our Universe, imprinted on the sky when its age was just 380 000 years. This radiation, filling the observable universe almost uniformly, has a black body spectrum with a temperature of 2.725 K and its spectral density peaks at microwave frequencies. The CMB is the main tool to study the evolution of our Universe in terms of its general characteristics, elements composition and formation of structures.

Planck, with its unprecedented sensitivity and angular resolution, will provide a major source of information relevant to several cosmological and astrophysical issues, such as testing theories of the early universe and the origin of cosmic structures. Figure 1.4 shows the map of the anisotropies of the CMB as observed by Planck. It shows tiny temperature fluctuations (from -500 μK to 500 μK) that correspond to regions of slightly different densities, representing the seeds of all future structures: the stars and galaxies of today.

The High Frequency Instrument (HFI), one of the two instruments on the satellite, has completed its survey of the remnant light from the Big Bang.

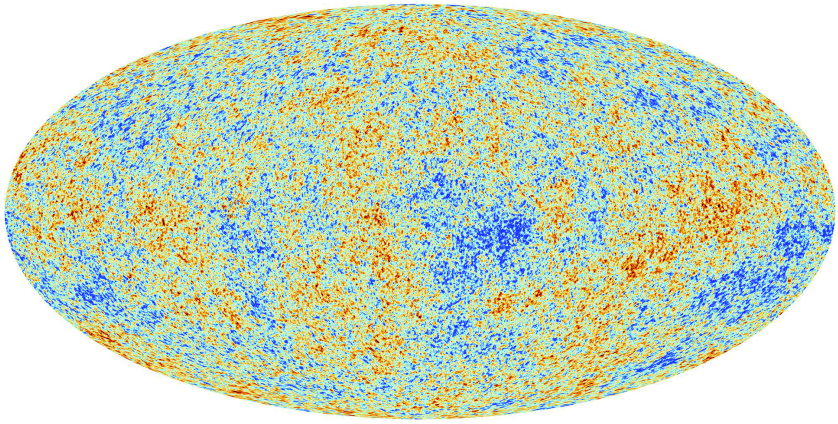

Figure 1.4: Map of the anisotropies of the CMB as observed by Planck.

The sensors ran out of coolant on January 2012 as expected, ending its ability to detect this faint energy. Planck was launched in May 2009, and the minimum requirement for success was to complete two whole surveys of the sky. In the end, Planck worked perfectly for 30 months, about twice the span originally required, and completed five full-sky surveys with both instruments. Being able to work at slightly higher temperatures than HFI, the Low Frequency Instrument will continue its survey of the sky for a large part of 2013, providing even more data to improve Planck final results.

For the HFI, the required sensitivity ($\Delta T/T \sim 10^{-6}$) is achieved by using an array of bolometers cooled down to 100 mK by an Open-Cycle Dilution Refrigerator (OCDR) [9, 10, 12, 13]. The OCDR operates by flowing both ^{3}He and ^{4}He from separate reservoirs, mixing them to provide cooling and ejecting the mixture into space without recycling it (unlike it happens in con-

ventional dilution refrigerators). This design works in zero-gravity since (a) the still, which requires gravity to separate the liquid and vapour phases, is completely eliminated, and (b) in its mixing chamber design surface tension replaces gravity to separate the concentrated and dilute phases.

The disadvantage is that the lifetime of the mission is limited by the quantity of ^{3}He and ^{4}He embarked at launch. So, to obtain continuous operation for 2 or 3 years it is indispensable to work with small flow rates. As a consequence the cooling power, proportional to the flow rates, is limited too.

In the case of Planck a cooling power of 0.2 μW at a temperature of 100 mK for a lifetime of at least 15 months were required. The flow rates necessary to reach these specifications are: 6 $\mu mol/s$ for the ^{3}He and 18 $\mu mol/s$ for the ^{4}He. Therefore, it was necessary to store aboard the satellite, at high pressure (300 bar), 12 m^3 of ^{3}He and 36 m^3 of ^{4}He (values at STP). In the end, the OCDR successfully cooled the HFI instrument for twice the lifetime required.

Instruments aboard future space missions such as SPICA or ATHENA, respectively for astrophysics in far-IR and X-Ray bands, require a higher cooling power (1 μW) at a lower temperature (50 mK). Therefore higher flow rates are needed: about 18 $\mu mol/s$ for the ^{3}He and 360 $\mu mol/s$ for the ^{4}He. These missions are also projected to have longer operating times (5-10 years). This would mean a larger amount of gas to be embarked on the satellite: 90 m^3 of ^{3}He and 1800 m^3 of ^{4}He (values at STP). It is evident that such an amount of gas is not adapted to the space and weight constrains of a satellite. The OCDR is therefore unable to satisfy the needs of future missions. Table 3.4 recapitulates Planck and future missions specifications.

In this thesis I will discuss the development of a close-cycle dilution refrigerator, adapted from the open-cycle refrigerator, able to fulfill future missions cooling requirements remaining within the constrains of a space mission.

Mission	Planck	Spica/Athena
Temperature (K)	0.100	0.050
Cooling power (μW)	0.2	1
Lifetime (years)	2.5	5
^{3}He flow rate (μmol/s)	6	18
^{4}He flow rate (μmol/s)	18	360
^{3}He storage aboard the satellite (m^3)	12	90
^{4}He storage aboard the satellite (m^3)	36	1800

Table 1.1: Comparison between Planck and future missions specifications.

Chapter 2

^{3}He-^{4}He mixture and dilution refrigerators

In this chapter I will discuss the functioning of a dilution refrigerator. First I will describe some important properties of the ^{3}He-^{4}He mixture, beginning from its phase diagram. Then I will explain a peculiar characteristic of superfluid ^{4}He: its tendency to flow to equalize its chemical potential. This feature has to be considered when devising a dilution refrigerator. I will continue illustrating the difference between the irreversible and the reversible mixing: the last process, used in the mixing chamber of a dilution refrigerator, allows cooling below 180 mK. Then I will present the design of a conventional dilution refrigerator, which depends on gravity for its operation. After comparison with the open-cycle dilution refrigerator of the Planck satellite, it will appear clear that the solutions adopted for the latter design render this device usable in a micro-gravity environment (but at the cost of having less cooling power).

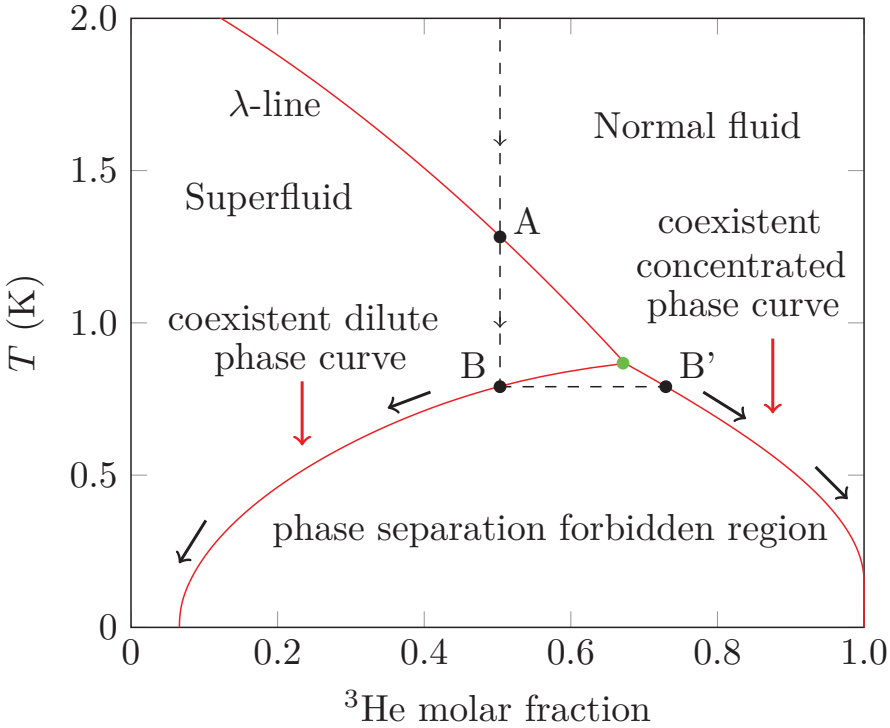

Figure 2.1: Phase diagram of ^{3}He-^{4}He mixtures at saturated vapour pressure. The tricritical point (in green) occurs at 0.87 K and 67% ^{3}He molar fraction [16].

2.1 ^{3}He-^{4}He liquid mixture

2.1.1 Phase diagram

For a deep understanding of the dilution refrigerator it is necessary to know the properties of ^{3}He-^{4}He mixture. In fig. 2.1 the mixture phase diagram is shown. Consider a 50/50 solution cooled from high temperatures along the vertical line. Above 1.3 K the solution is a normal fluid. Then, after going through the λ-line, point A in figure 2.1, it becomes a ^{4}He-like superfluid (the λ-transition for pure ^{4}He occurs at 2.17 K. The addition of ^{3}He to the liquid ^{4}He lowers the λ-temperature, as it is shown in figure 2.1).

Then at about 0.8 K at point B in figure 2.1, the single phase solution becomes unstable (it saturates). Therefore, it separates in two components: a ^{3}He-rich phase, starting to form at point B', referred to as the concentrated phase, and a ^{4}He-rich phase, referred to as the dilute phase. In a gravitational field the lighter concentrated phase floats on top of the heavier dilute phase. As the temperature is reduced further, the concentration difference between the two phases widens, following the coexistence curves, until at 0 K the concentrated phase becomes virtually pure ^{3}He, while the diluted phase still contains 6.6% ^{3}He. Since the dilution process is endothermic under certain conditions, cooling is produced by inducing dissolution of ^{3}He atoms from the concentrated phase into the dilute phase. We can compare this process to the vapour-liquid cooling where atoms leave the liquid phase to go into the gas phase, absorbing the latent heat from the surroundings. However, the dilution process is more advantageous than the vapour-liquid cooling. This advantage is given by finite solubility of the ^{3}He in the dilute mixture at low temperatures. The Clausius-Clapeyron equation relates the vapour pressure to the latent heat for a vapour-liquid system, while it relates the osmotic pressure (depending on the percentage of ^{3}He dissolved in ^{4}He) to the latent heat for a ^{3}He-^{4}He mixture. The vapour pressure goes exponentially to zero as the temperature is reduced. The osmotic pressure, instead, decreases quadratically to a finite value because of the Fermi statistics since the solubility of the ^{3}He in the dilute mixture approaches a finite value. This means that the technical difficulties to go to zero temperature increase less rapidly for dilution cooling than for evaporational cooling (although the latent heat remains finite for a ^{3}He liquid-vapour system, but goes to zero for

a ^{3}He-^{4}He mixture).

2.1.2 Some thermodynamic properties

2.1.3 ^{4}He chemical potential in a ^{3}He-^{4}He mixture

The properties of the liquid ^{3}He-^{4}He mixture are treated in many text books (for example refer to [7]). Here I report some of them, necessary to entirely understand the operations and the design of a dilution refrigerator. According to one of the basic equations of the two-fluid model of superfluid ^{4}He in the linear approximation (the term $\vec{v}_s \cdot \vec{\nabla}\vec{v}_s$ is neglected) [17]:

$$M_4 \frac{\partial v_s}{\partial t} = -\nabla \mu_4 \tag{2.1}$$

the ^{4}He superfluid component flows to equalize the ^{4}He chemical potential. In the above equation v_s is the velocity of the ^{4}He superfluid component, μ_4 is the partial chemical potential of ^{4}He in a ^{3}He-^{4}He mixture. Since μ_4 is per mole of ^{4}He the left hand of the equation has to multiplied by the ^{4}He molar mass, M_4. Therefore, in a steady state:

$$\nabla \mu_4 = 0 \tag{2.2}$$

from which follows that μ_4 is constant everywhere in a such a state[1].

$\mu_4(P, T, x)$ is a quantity that indicates where the ^{4}He prefers to go: it decreases with decreasing pressure, increasing temperature and increasing ^{3}He concentration. This means the ^{4}He goes from high to low pressures, from low to high temperature and from low to high ^{3}He concentrations.

Now consider the three chambers, A, B and C, in fig. 2.2 connected by a superleak[2]. Chamber A is filled with pure ^{4}He (green) at zero pressure and temperature. In chamber B the temperature is raised to the value T. Chamber C contains a ^{3}He-^{4}He mixture (yellow) of concentration x and at the same temperature T. According to eq. 2.2, μ_4 is the same in all three chambers at equilibrium:

$$\mu_4(0, 0, 0) = \mu_4(P_f(T), T, 0) = \mu_4(P_f(T) + \Pi(x, T), T, x) \tag{2.3}$$

As a consequence of eq. 2.3 a pressure difference $\Delta P = P_C - P_A = P_C$ ($P_A = 0$) develops between the two containers A and C:

$$\Delta P = P_C = P_f(T) + \Pi(x, T) \tag{2.4}$$

[1]This relation is valid only for low superfluid velocities (lower than the critical velocity). In this case there is no dissipation due to mutual friction between the normal and superfluid components. In certain parts of a dilution refrigerators this is true. But we will see later that in our system and that of Planck certain elements, such as the one-phase heat exchanger, are conceived exploiting the fact that there the velocity difference between the superfluid and the normal components exceeds the critical velocity beyond which mutual friction occurs. In other parts, such as the fountain pump, the velocity exceeds a certain value (related to the Reynolds number), above which the flow becomes turbulent and the superfluid and normal components are locked together

[2]A superleak is a porous plug with nanometer-scale pores, that effectively acts as a semi-permeable membrane. It offers no resistance to the flow of superfluid ^{4}He, but does not allow ^{3}He , or the normal component of the ^{4}He, to pass.

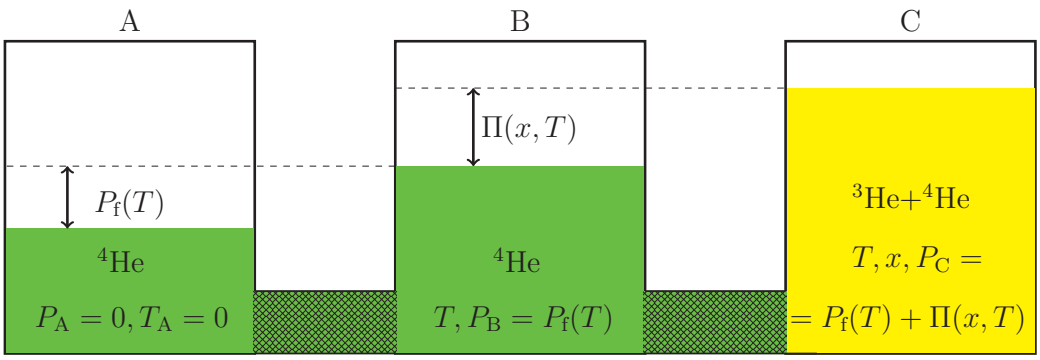

Figure 2.2: The pressure difference developed between chambers containing pure ^{4}He and ^{3}He-^{4}He mixture and connected by superleaks. The pressures indicated in figure are at the level of the superleaks; at the top of the liquid columns the pressures are equal to the vapour pressure. For simplicity the vapour pressure and the hydrostatic pressure have not been taken into account.

where P_f(T) denotes the pressure, referred to as fountain pressure, that develops when a temperature difference establish in superfluid ^{4}He; $\Pi(x,T)$ represents the pressure, referred to as osmotic pressure, associated with the solute ^{3}He. To compensate the raise in temperature between chamber A and B the pressure in chamber B has to increase (by an amount of P_f(T)); if ^{3}He is added in chamber C at the same temperature, again the pressure has to increase (by an amount of $\Pi(x,T)$ more).

It is possible to define these two pressures (P_f(T) and $\Pi(x,T)$) from eq. 2.3. The general thermodynamic relation:

$$d\mu_4 = \left(\frac{\partial \mu_4}{\partial P}\right)_{T,x} dP + \left(\frac{\partial \mu_4}{\partial T}\right)_{P,x} dT + \left(\frac{\partial \mu_4}{\partial x}\right)_{T,P} dx \tag{2.5}$$

can be integrated obtaining:

$$\mu_4(P_C,T,x)-\mu_4(0,0,0)=\int_0^{P_C}\underbrace{\left(\frac{\partial\mu_4}{\partial P}\right)_{T=0,x=0}}_{v_4}dP+$$
$$+\int_0^{T}\underbrace{\left(\frac{\partial\mu_4}{\partial T}\right)_{P=P_C,x=0}}_{-s_4}dT'+\int_0^{x}\left(\frac{\partial\mu_4}{\partial x}\right)_{T,P=P_C}dx' \tag{2.6}$$

where v_4 is the ^{4}He molar volume, assumed independent of P, and s_4 is the ^{4}He molar entropy. Considering that $\mu_4(P_C,T,x)-\mu_4(0,0,0)=0$ we obtain:

$$P_C=\underbrace{\frac{1}{v_4}\int_0^T s_4dT}_{P_f(T)}\underbrace{-\frac{1}{v_4}\int_0^x\left(\frac{\partial\mu_4}{\partial x}\right)_{T,P}dx}_{\Pi(x,T)} \tag{2.7}$$

Concluding I can say that the property of μ_4 to be constant in a steady state leads to the relation between the pressures[3]:

$$P-P_f-\Pi=constant \tag{2.8}$$

2.1.4 The dilution process

Irreversible mixing

Consider the two containers in fig. 2.3, one filled with pure ^{3}He, the other with pure ^{4}He and separated by a partition. The two fluids are at the same temperature. The partition is taken off and the two isotopes mix. The mixing is realised at constant pressure. Suppose that the quantity of

[3]In the case I show in fig. 2.2 $P_A=0$, so we have: $P_C-P_f-\Pi$=0. This relation can be generalized in eq. 2.8.

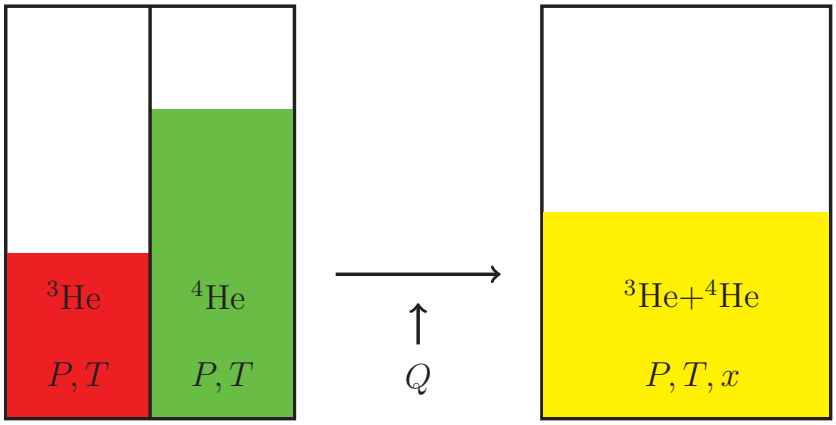

Figure 2.3: ^{3}He-^{4}He irreversible mixing. The two fluids are separated by a partition and they are at same temperature and pressure. When the partition is taken off the two fluids mix, exchanging a certain amount of heat with the surroundings, so that the temperature is maintained constant.

^{3}He is low enough to dilute completely in ^{4}He and so forming a single-phase mixture. In order to keep the temperature constant, a certain amount of heat Q must be exchanged with the surroundings. The exchanged heat per mole of mixture, $q = \frac{Q}{n_3+n_4}$, will be:

$$q = h_m(x, T) - (xh_3(T) + (1-x)h_4(T)) \tag{2.9}$$

where $h = \frac{H}{n_3+n_4}$ is the enthalpy of the mixture per mole of mixture, $h_3 = \frac{H_3}{n_3}$ the enthalpy of pure ^{3}He per mole of ^{3}He and $h_4 = \frac{H_4}{n_4}$ the enthalpy of pure ^{4}He per mole of ^{4}He, $x = \frac{n_3}{n_3+n_4}$ is the ^{3}He concentration, n_3 and n_4 are the ^{3}He and ^{4}He numbers of moles. The heat exchanged is the difference between the molar enthalpy of the mixture and the sum, weighted by the concentrations, of the molar enthalpies of pure components. This is exactly the definition of the excess molar enthalpy, h_E. In fact for a generic mixture it is possible to define the excess molar value, Y_E, of a certain quantity Y

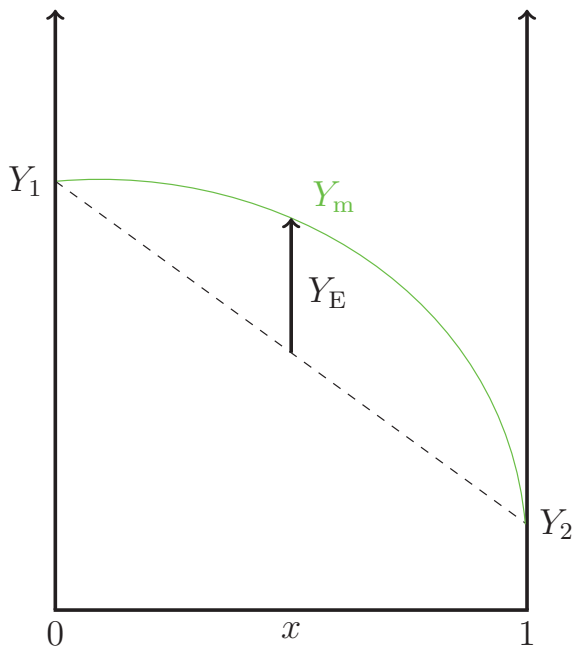

Figure 2.4: A generic excess quantity, Y_E, defined as the difference between the molar value of this quantity for the mixture, Y_m, and the sum, weighted by the concentrations, of molar values of the same quantity for the pure components, Y_1 and Y_2, as a function of the solute concentration.

as the difference between the molar value of this quantity for the mixture, (Y_m, green curve in fig. 2.4) and the sum, weighted by the concentrations, of molar values of the same quantity for the pure components, Y_1 and Y_2. For an ideal mixture this difference is zero. This means that Y_m, as a function of the solute concentration, can be approximated to a straight line (dashed straight line in the figure 2.4).

The excess enthalpy has been calculated by Kuerten et al. [18] for temperatures below 250 mK and concentrations below 7 % and by Chaudhry et al. [19] for temperatures between 200 mK and 1.8 K and high concentrations. Figure 2.5 shows the excess enthalpy having a positive deviation from an ideal mixture, at least above a temperature of 180 mK and a concentration

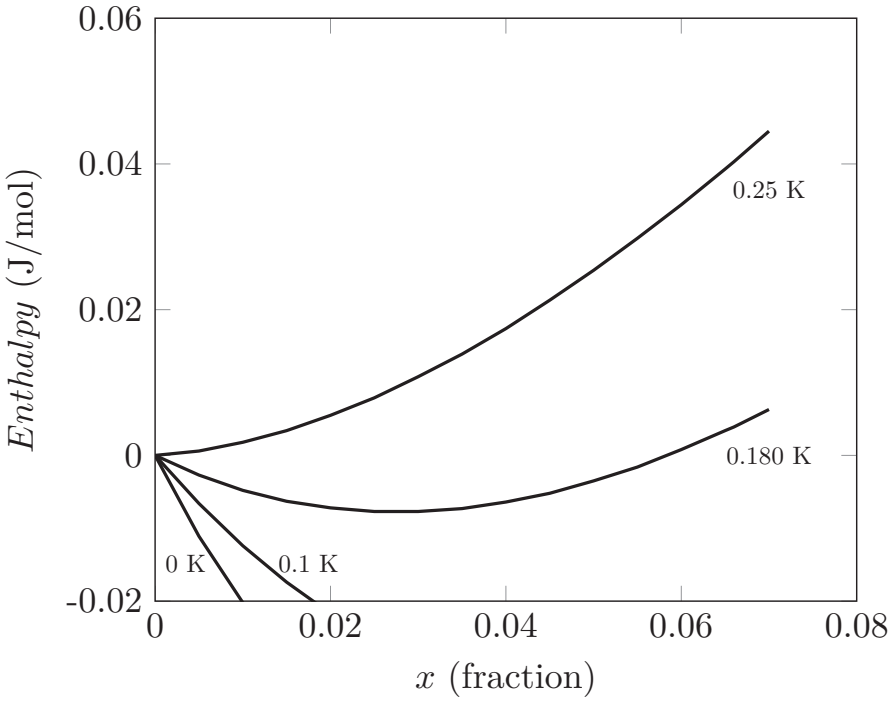

Figure 2.5: Excess enthalpy of the ^{3}He-^{4}He mixture as a function of the ^{3}He concentration for different temperatures.9 This plot is taken from [18].

of 6 %. This means that the mixture produced during the mixing process absorbs a certain amount of heat from the surroundings to keep the temperature constant. This property of the mixture can be exploited to provide cooling. As shown in figure 2.5, the excess enthalpy becomes negative below 180 mK. Therefore, in the configuration considered in figure 2.3, the mixture cannot cool down below this temperature. The explanation is that this configuration leads to irreversible mixing where the dilution process is not realised in a state of quasi-equilibrium and the chemical potentials of pure ^{4}He and pure ^{3}He before and after the mixing are not the same.

Reversible mixing

Consider the container in figure 2.6 (a), filled with concentrated mixture (red) floating on top of dilute mixture (yellow). The fluids are separated by the phase separation surface: nothing happens because they are in equilibrium. The dilute phase is connected by a superleak to infinite reservoir containing pure ^{4}He (green) at zero temperature and pressure, having the same chemical potential as the ^{4}He in the dilute phase. Now imagine to reduce the ^{3}He concentration in the dilute phase by a factor ϵ. This can be done adding some ^{4}He from the reservoir, acting with the piston on the saturated mixture (red arrows in figure 2.6). The reduction of ^{3}He concentration decreases the chemical potential in the dilute phase, creating a non-equilibrium situation. The system will tend to correct it by diluting a certain amount of ^{3}He from the concentrated phase, producing a cooling power proportional to the quantity of ^{3}He dissolved. In every moment during the process the

system is in equilibrium. We can reverse the process by acting on the piston, removing the ^{4}He from the dilute phase (black arrows in figure 2.6)[4].

The cooling power produced in a reversible mixing process does not depend on the excess enthalpy, but on the osmotic enthalpy, which is always positive (for concentration higher than 6.6%). With reversible mixing it is possible to cool below 180 mK. This topic is addressed more in detail in section 2.2.1.

2.2 Conventional dilution refrigerator

A diagram of the basic components and layout of a conventional dilution refrigerator is shown in figure 2.7. The volumes of ^{3}He and ^{4}He are adjusted so that the concentrated-dilute phase interface is situated in the mixing chamber, where cooling occurs, and the liquid-gas interface in the still. In principle the two phases in the mixing chamber are in equilibrium, so there is no heat exchange between them and no cooling is produced. Now the basic task is to devise a practical way of removing ^{3}He atoms from lower dilute phase to create a non-equilibrium situation (as I explained in section 2.1.4). In this way the system will tend to correct it by allowing a net transfer of ^{3}He atoms that, from the upper phase, dilute into the lower phase, providing cooling. This is achieved by connecting the dilute phase through a capillary to a still, as shown in figure 2.7, and applying heat to the still. The ^{3}He has a higher vapour pressure and is more volatile than ^{4}He: it evaporates from the dilute mixture in the still. Therefore, the ^{3}He removed in the still is

[4] In this representation I neglected the hydrostatic pressure: a 1 cm column of dilute phase corresponds to 0.1 mbar, negligible compared the other pressures involved. Therefore the only role played by the gravity here is to separate the concentrated and the dilute phases.

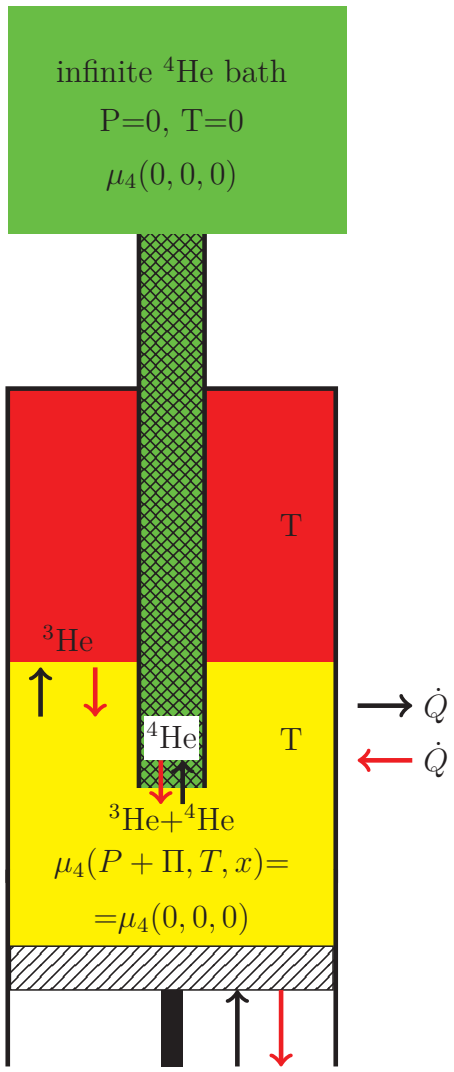

Figure 2.6: ^{3}He-^{4}He reversible mixing process. The two fluids, a saturated dilute mixture (yellow) and pure ^{3}He (red), are separated by the phase separation surface. The dilute phase is connected by a superleak to a infinite reservoir containing pure ^{4}He (green) at zero temperature and pressure, having the same chemical potential as the ^{4}He in the dilute phase. Acting with the piston on the dilute mixture, some ^{4}He can be added from the reservoir to the dilute phase or removed from it. The first case, indicated with red arrows, produces dilution and therefore cooling. The second case (black arrows) produces de-mixing and therefore heating.

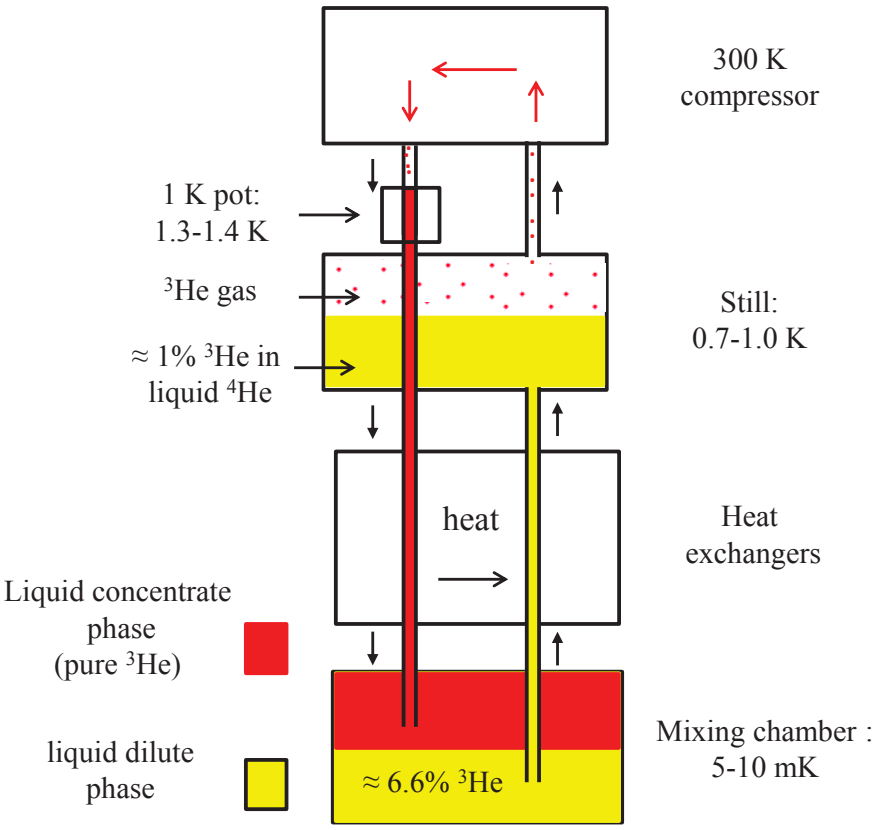

Figure 2.7: Highly stylised diagram of the basic components and layout of a conventional dilution refrigerator.

replaced by dilution in the mixing chamber. Note that, in this design there is no net ^{4}He flow. Continuous cooling is achieved by pumping out the ^{3}He evaporated by means of a high temperature compressor, that circulates it back in the system. The gas is condensed at the 1 K ^{4}He pot and, before being injected again in the mixing chamber, it is first pre-cooled in the still and then by counterflow heat exchangers. The performance of a particular dilution refrigerator depends on the efficiency of these heat exchangers. Typical temperatures in different parts of the refrigerator are indicated in figure 2.7. In this design gravity is exploited in the mixing chamber, to separate the concentrated and dilute phases, and in the still to separate the liquid and vapour phases.

Since ^{4}He is stationary, $\nabla\mu_4 = 0$ and so μ_4 is equal in the mixing chamber and in the still: $\mu_4(P_{MC}, T_{MC}, x_{MC}) = \mu_4(P_{still}, T_{still}, x_{still})$. From the mixing chamber to the still the temperature increases, while the pressure is approximately constant. As a consequence, to keep μ_4 constant, the ^{3}He concentration decreases: typically in the mixing chamber it is about 6.6%, in the still about 1%. Figure 2.8 shows some lines at constant μ_4 plotted in the ^{3}He-^{4}He phase diagram. It is evident that along these lines as the temperature increases, the concentration decreases.

Due to this low concentration in the still, the ^{3}He vapour pressure is also low. Therefore, to re-cycle it back in the system, a suitable pumping installation is necessary. This is not a concern on Earth, but it could be in space, because a complex pumping system would be too massive and would require too much power to operate on a satellite. We will see later how this problem can be solved.

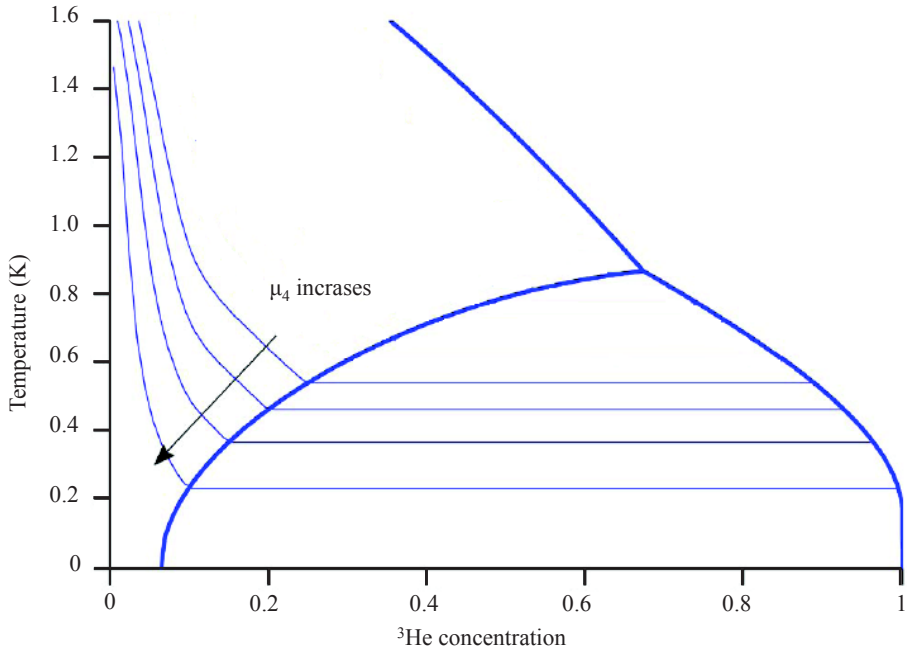

Figure 2.8: Lines at constant μ_4 in the ^{3}He-^{4}He phase diagram [20]. Along these lines, as the temperature increases, the concentration decreases.

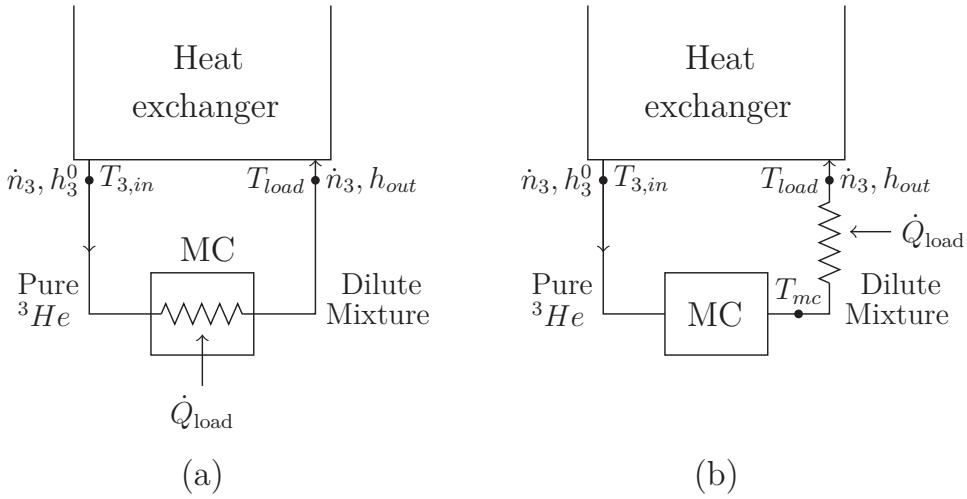

Figure 2.9: Mixing chambers of conventional dilution refrigerator with (a) heat load directly applied to it and (b)heat load applied to stream exiting it.

2.2.1 Cooling power

Consider the mixing chamber in figure 2.9 (a). It has a heat input $\dot{Q}_{load}$, which is what we want to know. It is possible to write it in terms of the inlet and outlet properties of the respective streams. The First Law of Thermodynamics in a control volume is:

$$\frac{dE}{dt} = \dot{Q} - \dot{W} + \sum_{ports} \dot{n}h \tag{2.10}$$

where E is the total internal energy in the control volume, $\dot{Q}$ is the rate of heat transfer into the control volume, $\dot{W}$ is the rate of work transfer from the control volume, $\dot{n}$ is the molar flow rate of the components that flow in and out the control volume, and h is their molar enthalpy. Application of the First Law in steady state to the mixing chamber (figure 2.9), without

performing work on the environment, gives:

$$\dot{Q}_{load} = \dot{n}_3 h_{out}(T_{load}) - \dot{n}_3 h_3^0(T_{3,in}) \tag{2.11}$$

where $\dot{n}_3$ is the ^{3}He flow rate, h_{out} the molar enthalpy of the dilute phase leaving the mixing chamber, h_3^0 the molar enthalpy of the concentrated phase entering the mixing chamber, T_{load} the mixture temperature after absorbing the heat load and $T_{3,in}$ the temperature at which the ^{3}He leaves the heat exchanger to enter the mixing chamber. Note, that $\dot{n}_4 = 0$ in an ideal classical dilution refrigerator.

The difficulty is to calculate h_{out}, because it involves moving ^{3}He inside stationary superfluid ^{4}He. Ebner and Edwards [21] derived h_{out} for a system where the average velocities of the ^{3}He and ^{4}He atoms are not the same. In their derivation they used the osmotic enthalpy defined as:

$$H_{os} = H_m - N_4\mu_4 = U + PV - N_4\mu_4 \tag{2.12}$$

where $H_m = U + PV$ is the mixture enthalpy and N_4 the ^{4}He number of moles. The term $N_4\mu_4$ is of the same order of magnitude as H_m.

A similar osmotic enthalpy (subtracting $V_4\Pi$ instead of $N_4\mu_4$) has already been introduced by London, Clarke, and Mendoza [22] to ignore the ^{4}He contribution to the thermodynamic analysis and so simplifying it to that of a one-component system: the concentrated phase then plays the part of a 'liquid' which, in the mixing chamber of the refrigerator, 'evaporates' into the dilute phase which plays the part of the 'vapour'. The differential of H_{os}

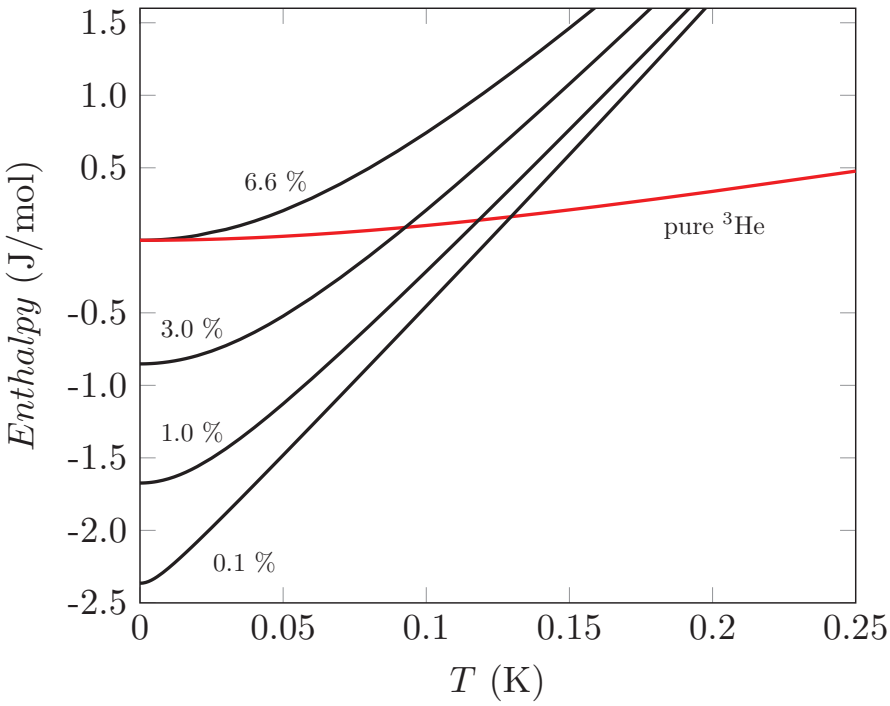

Figure 2.10: Osmotic enthalpy per mole of ^{3}He as a function of temperature for various ^{3}He concentrations [18].

is:

$$dH_{os} = \underbrace{TdS - PdV + \mu_3 dN_3 + \mu_4 dN_4}_{dU} + \underbrace{PdV + VdP}_{d(PV)} - \underbrace{\mu_4 dN_4 - N_4 d\mu_4}_{d(\mu_4 N_4)} =$$
$$= TdS + VdP + \mu_3 dN_3 - N_4 d\mu_4 \tag{2.13}$$

The one-component analogy is based on the idea that if $d\mu_4 = 0$ the number of the independent variables is reduced to three and the thermodynamic equations are formally similar to a one-component system.

Using the definition of osmotic enthalpy and the condition $d\mu_4 = 0$ it can be demonstrated that the enthalpy associated with a dilute phase mixture

leaving the mixing chamber is the osmotic enthalpy of the dilute phase on the phase separation line, h_d^{os}. Therefore eq. 2.11 can be rewritten as:

$$\frac{\dot{Q}_{load}}{\dot{n}_3} = h_d^{os}(T_{load}) - h_3^0(T_{3,in}) \tag{2.14}$$

For concentrations higher than 6.6%, the region where a dilution refrigerator operates, the osmotic enthalpy is always higher than that of pure ^{3}He at the same temperature (figure 2.10), thus making the cooling below 180 mK possible. If we consider an ideal counterflow heat exchanger, so that the inlet temperature $T_{3,in}$ is identical to T_{load}, and that the enthalpies at low temperature are fairly linear with T^2, then eq. 2.14 becomes (for temperatures below 50 mK):

$$\frac{\dot{Q}_{mc}}{\dot{n}_3} = 82T_{load}^2 \tag{2.15}$$

This result is due to the fact that the dilution process is realised in a state of equilibrium and so we could use the condition $\mathrm{d}\mu_4 = 0$, thus obtaining a cooling power depending on the osmotic enthalpy instead of on the excess enthalpy. The cooling power depends also on where the heat load is applied. Typically it is applied either directly to the mixing chamber (the case I described above) or to the stream exiting the mixing chamber (figure 2.9 (b)). Chaudhry and Vermeulen [23] demonstrated that in the latter case the specific cooling power is (assuming an ideal counterflow heat exchanger and for temperatures below 150 mK):

$$\frac{\dot{Q}_{load}}{\dot{n}_3} = (h^{os}(T_{load}) - h_3^0(T_{load})) = 48T_{load}^2 \tag{2.16}$$

where $h^{os}(T_{load})$ is the osmotic enthalpy of a single-phase mixture along the constant μ_4 line. h_d^{os} is not the same as h^{os}: in the former case we refer to the mixture in the mixing chamber during the dilution process (on the phase separation line); in the latter we refer to the mixture on its way to return to the still after the dilution process (along the constant μ_4 line). Note that applying the heat load to the stream exiting the mixing chamber results in a lower cooling power.

2.3 OCDR: Open-Cycle Dilution Refrigerator

As I said in the previous chapter, the OCDR has successfully delivered a cooling power of 0.2 μW at a temperature of 100 mK on the Planck satellite for a lifetime of 2.5 years.

In figure 2.11 a schematic diagram of this refrigerator is shown. This design is completely different from that of a conventional dilution refrigerator: here both ^{3}He and ^{4}He circulate from different reservoirs, through capillaries (D<0.5 mm), they mix in the mixing chamber providing cooling and then the mixture is not recycled but ejected into space. The mixture produced is used to pre-cool the pure streams by means of a counterflow heat exchanger (HX in figure in figure 2.11), before being ejected into space. The heat exchanger consists of three capillaries soldered together in parallel and joined at one end by an junction forming the mixing chamber.

This design works in zero-gravity since (a) the still, which requires gravity to

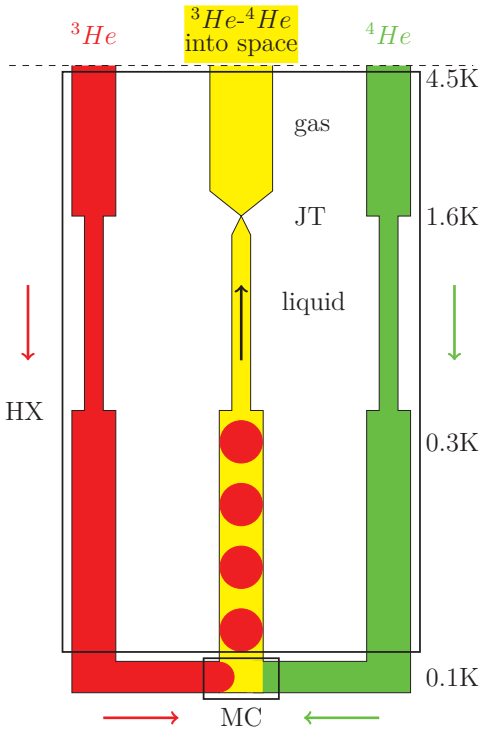

Figure 2.11: OCDR schematic sketch. HX: heat exchanger. MC: mixing chamber.

separate the liquid and vapour phases, is suppressed, and (b) in this mixing chamber design (MC in figure in figure 2.11) surface tension replaces gravity to separate the concentrated and the dilute phases. Moreover, suppressing the still and using the space vacuum as a pump, complex pumping installations have been avoided.

The isotopes are pre-cooled with external cooling power down to 4.5 K. Further cooling to less than 1.6 K is achieved through an internal Joule Thomson (JT) expansion process on the mixture return line. This is another difference compared to the refrigerator described in section 2.2: a conventional dilution refrigerator needs an external cooling source to pre-cool and condense the ^{3}He down to 1.3-1.4 K. On the contrary the OCDR provides his own 1.6 K stage.

In this condition, along the return capillary, μ_4 cannot be constant, as in a conventional dilution refrigerator. Imagine that the ^{3}He and ^{4}He are injected in the mixing chamber to obtain a certain ^{3}He concentration (about 6.6%). Since the ^{4}He superfluid component is free to flow equalizing μ_4, at higher temperatures, about 1.6 K the concentration in the return capillary would be practically 0%. Therefore, it is not possible to extract the same ^{3}He quantity that has been injected. It is therefore necessary to break the continuity of μ_4, which means to try to extract at constant ^{3}He concentration. This is achieved by injecting more than 6.6% ^{3}He, so that a part of it goes into the dilute phase providing cooling; some of it stays in the concentrated phase forming ^{3}He droplets, as shown in figure 2.11. The droplets lock together the superfluid and the normal components of ^{4}He in the dilute slugs, preventing the superfluid to equalize μ_4. At higher temperatures, about 0.3 K, when the

^{3}He droplets dissolve, the capillary size is reduced to drive the flow velocity above the critical velocity beyond which mutual friction between ^{3}He and ^{4}He establishes. Mutual friction cannot really lock together the superfluid and the normal components, because to have mutual friction there must be a velocity difference between the two components. Nevertheless it breaks the continuity of μ_4 and consequently it keeps a high concentration along the return capillary (even if not exactly constant). Actually in our refrigerator the mechanism that keeps the two components locked together is the turbulence of the ^{3}He normal component (see section 3.3.2.)

Another difference compared to a conventional dilution refrigerator is the cooling power. In the case of Plank the heat load is applied to the stream exiting the mixing chamber due to the small dimension of the mixing chamber. Here the mixture is not single-phase, as in a conventional dilution refrigerator, but two-phase. In this case the specific cooling power is [23]

$$\frac{\dot{Q}_{load}}{\dot{n}_4} = \underbrace{\frac{x_d(T_{load})}{1 - x_d(T_{load})} \left[h_d^{os}(T_{load}) - h_3^0(T_{load})\right]}_{dissolved \qquad {}^3He} - \underbrace{\left[\mu_4(T_{mc}) - \mu_4(T_{load})\right]}_{d\mu_4 \neq 0} \quad (2.17)$$

where x_d is the ^{3}He fraction going into the dilute phase. Cooling is produced by the injected ^{3}He going into the dilute phase[5]. However, in this case, not all the injected ^{3}He goes into the dilute phase; some of it stays in the concentrated phase. This is a disadvantage for the cooling process because the ^{3}He that does not dilute does not contribute to the cooling process, but it has

[5]The specific cooling power in eq. 2.17 has been defined as $\frac{\dot{Q}_{load}}{\dot{n}_4}$ rather than $\frac{\dot{Q}_{load}}{\dot{n}_3}$, because all the injected ^{4}He ends up in the dilute phase and contributes to the cooling process.

to be pre-cooled in anyway, charging the the heat exchanger with an extra heat load. Moreover, also the heat exchange in the heat exchanger is less effective: along the return capillary the enthalpy (at constant x) associated to a two-phase mixture is lower than the enthalpy (at μ_4 constant) associated to a single dilute phase mixture. The result is that the cooling power of a gravity-insensitive dilution refrigerator is almost half the amount of a conventional dilution refrigerator.

This model, developed in [23], is valid under the assumption that the average ^{3}He concentration inside the mixture return capillary is constant and equal to $x_{app} = \frac{\dot{n}_3}{\dot{n}_3+\dot{n}_4}$ (x_{app} is the ^{3}He concentration calculated using the flow rates. The subscript 'app' means applied by the flow rate.). We will see in the next chapter that this is not exactly the case.

The specific cooling power can be written in the form $\frac{\dot{Q}_{load}}{\dot{n}_4} = cT_{load}^2$, where the parameter c depends on the ^{3}He concentration. For a concentration of 0.1 $c \sim 3$, while for a concentration of 0.2 $c \sim 3.3$ [23].

2.4 Conclusions

The most important points discussed in this chapter are:

- The fact that the ^{3}He-^{4}He mixture separates in two components at low temperatures can be exploited to provide cooling. Since the dilution process is endothermic, cooling is produced by inducing dissolution of ^{3}He atoms from the concentrated phase into the dilute phase. In comparison with a liquid-vapour system we have argued that the finite solubility of the ^{3}He in the dilute mixture is an advantage since the

osmotic pressure remains finite, even at zero temperature.

- An important property of superfluid ^{4}He is that it flows to equalize the chemical potential. This means that in a steady state the chemical potential is constant. This condition has to be considered when devising a dilution refrigerator.

- To cool below 180 mK it is necessary to realise a reversible dilution process: in this case the enthalpy involved is the osmotic enthalpy, which is always positive and higher than that of pure ^{3}He (for concentration larger than 6.6%). In an irreversible process the enthalpy involved is the excess enthalpy, which is negative below 180 mK, not allowing to cool below this temperature.

- We compare two dilution refrigerator design: the conventional one and the OCDR. In the first design, where only ^{3}He is circulated, gravity is exploited in in the mixing chamber, to separate the concentrated and dilute phases, and in the still to separate the liquid and vapour phases. In the OCDR, where both isotopes circulates, gravity problems are eliminated suppressing the still and using a mixing chamber where surface tension replaces gravity. In this design μ_4 cannot be constant along the return capillary. This leads to a different relation for the cooling power.

- The zero-gravity operation comes at a cost: the OCDR has intrinsically less cooling power than a conventional dilution refrigerator. In fact, in the OCDR we are forced to cool an astrophysical detector system at

the mixing chamber exit instead of directly in the mixing chamber, due to the small dimension of the mixing chamber. Moreover, also the fact that not all the mixture is not single-phase but two-phase reduces the performance for two reasons: firstly the ^{3}He that does not goes into the dilute phase does not contribute to the cooling process, but it has to be pre-cooled anyway, charging the the heat exchanger with an extra heat load. Secondly, the heat exchange in the heat exchanger is less effective because along the return capillary the enthalpy (at constant x) associated to a two-phase mixture is lower than the enthalpy (at μ_4 constant) associated to a single dilute phase mixture. The result is that the cooling power of a gravity-insensitive dilution refrigerator is almost half the amount of a conventional dilution refrigerator.

Chapter 3

Closed-cycle dilution refrigerator

Here, I will discuss the CCDR (Closed-Cycle Dilution Refrigerator) design considerations and describe the apparatus. After a short description of the isotopes separation-circulation system, I will present first the low temperature part of the refrigerator (heat exchanger, mixing chamber and thermal contact), which has been characterized with respect to the cooling performance required by future space missions. Then I will focus on the high temperature part (fountain pump for the circulation the ^{4}He and still for the separation of the ^{3}He and the ^{4}He). The effects of the operating conditions of this part on the performance of the low temperature part has been characterized in order to specify the interface of the CCDR with the rest of a satellite.

3.1 From the OCDR to the CCDR

As I already pointed out in the first chapter, more ambitious requirements of future missions render the open cycle dilution refrigerator impractical, because the amount of gas required is too large to be stored on the satellite at launch. This has driven the development of a new gravity-independent dilution refrigerator in which the mixture is not ejected into space but separated out into its components which are then re-injected into the system (see figure 3.1).

The low temperature part of the CCDR is very similar to Planck's OCDR, other than that it has been optimized for greater cooling powers at lower temperatures. The major difference between this new refrigerator and the OCDR is the addition of a separation-circulation system. The returning mixture enters the still, where the two components are separated. The ^{3}He is recovered by pumping the gas phase, much richer in ^{3}He ($> 90\%$) than the liquid phase ($\sim 10\%$), as we do in a conventional dilution refrigerator. This requires the use of a ^{3}He compressor, which has been avoided in Planck's refrigerator. But we saw in the previous chapter that keeping deliberately the returning mixture two-phase allows to ensure a high ^{3}He concentration in the still. Therefore, the still pressure is significantly higher than in a conventional dilution refrigerator, relaxing the constraints on the ^{3}He circulator and allowing it to be within the range of a reasonably-sized compressor. The ^{4}He liquid in the still flows through a superleak and is circulated by a fountain effect pump operating at about 2 K.

After the separation, the two streams are first pre-cooled (the ^{3}He is also

re-condensed) by a thermal reservoir at 1.7 K (a 1K pot), then in the still at about 1.1-1.2 K, and finally by a counterflow heat exchanger (HX in figure 3.1). The ^{3}He and ^{4}He are then mixed in a mixing chamber (MC in figure 3.1), providing cooling. The mixture then enters the counterflow heat exchanger and pre-cools the pure streams on its way to the still. Figure 3.1 shows a schematic diagram of the CCDR.

The functionality of this separation-circulation system has been demonstrated by F. Martin in his thesis [24] (where the methods and the thermometry are described in detail), while the counterflow heat exchanger has been optimized by G. Chaudhry [25, 26].

Closing the cycle requires a vapour-liquid interface similar to the interface in the still of a classical dilution refrigerator but adapted to zero-gravity. We planned to achieve the phase separation in a porous material confining the liquid into the still. Next chapters of this thesis are devoted to this issue.

3.2 CCDR low temperature part

The low temperature part consists in the counterflow heat exchanger and the cold end (mixing chamber the load heater). In our experiments we verified the performance of our refrigerator by varying the applied heat load and measuring the temperatures in its various parts and the ^{3}He flow rate. The ^{4}He flow rate is controlled by the fountain pump as it is explained in section 3.3.2. We also tested the refrigerator performance at different still pressures, that we regulate by means of a valve with a feedback loop where the still pressure is the set point. The purpose of varying the still pressure is to find

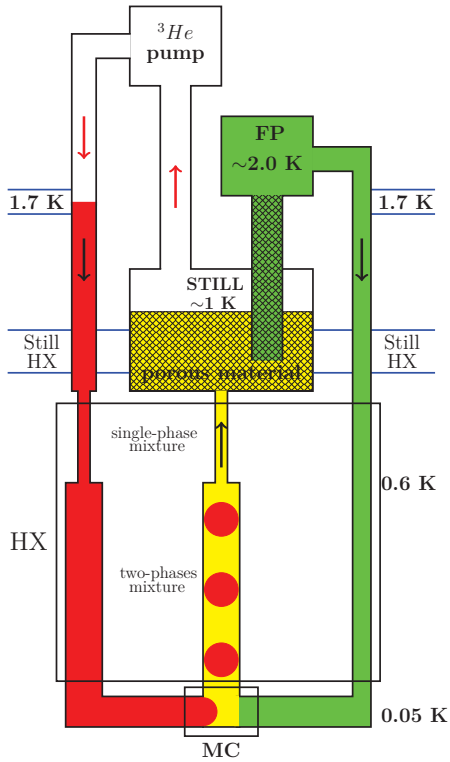

Figure 3.1: A schematic of the closed-cycle gravity-insensitive dilution refrigerator diagram. HX: heat exchanger. MC: mixing chamber.

the highest values of pressure at which the refrigerator is still able to produce 1 μW at temperatures below 50 mK. I remind that high still pressures are favorable to relax the requirements on the ^{3}He compressor. In the following sections I will describe in detail the different parts of the refrigerator and show their performance.

3.2.1 Heat exchanger and cold end configuration

The counterflow heat exchanger design is substantially identical to the configuration of the Planck's refrigerator ([27]): three Cu-Ni capillaries soldered together in parallel and joined at one end by an Y-shaped junction forming the mixing chamber. Two capillaries are for pure ^{3}He and ^{4}He entering the heat exchanger at the still temperature. They are pre-cooled by the returning mixture flowing in the third capillary. The difference compared to Planck design are the larger diameters and length in order to provide a larger heat exchange surface and and so increase the effectiveness of the heat exchange.

The optimization of the heat exchanger and of the cold end has been made with the help of a numerical model, developed to predict the temperatures profiles along the heat exchanger and in the cold end. In this model the ^{4}He contribution was ignored for two reasons: (a) the analysis of three streams is considerably more involved than the analysis of a two streams, and (b) since pure ^{4}He at temperatures below 1 K has a specific heat that is much lower than the specific heats of pure ^{3}He and ^{3}He-^{4}He mixtures, we can ignore the

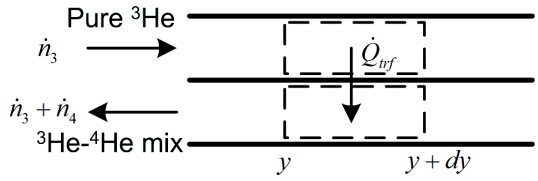

Figure 3.2: Control volumes used to derive the governing equations of the heat exchanger.

effect of the ^{4}He stream altogether, because the amount of heat that needs to be removed from it to cool it down from 1 K to about 0.1 K is much smaller than the corresponding number for the ^{3}He stream.

The energy balances for pure ^{3}He and mixture flows (figure 3.2) are:

$$\begin{aligned} \dot{n}_3 c_3 \frac{dT_3}{dy} &= -\dot{Q}_{trf} + \dot{Q}_{visc,3} \\ -(\dot{n}_3 + \dot{n}_4) c_m \frac{dT_m}{dy} &= \dot{Q}_{trf} - \dot{Q}_{visc,m} \end{aligned} \tag{3.1}$$

where $\dot{n}_3$ and $\dot{n}_4$ represent the molar flow rates of the ^{3}He and ^{4}He components respectively, c_3 the specific heat of pure ^{3}He at constant pressure, c_m is the specific heat of a mixture at constant pressure and constant x, $\dot{Q}_{trf}$ the heat transferred per unit length y from the hot stream to the cold stream, $\dot{Q}_{visc,3}$ and $\dot{Q}_{visc,m}$ the heat loads per unit length due to viscous dissipation in the pure ^{3}He and the mixture stream respectively. The heat transfer between the two streams is governed by many factors, but the dominant is the Kapitza resistances of the two wall-fluid interfaces. Therefore, in the model only this factor has been considered. Regarding the viscous dissipation, being the two flows laminar, a relation of the following form:

$$\dot{Q}_{visc} = \frac{128 \eta \dot{n}^2 v^2}{\pi D^4} \tag{3.2}$$

has been considered for both streams. Here v is the molar specific volume of the fluid, η its viscosity (scaling with T^{-2}), D the capillary diameter.

The axial conduction through the heat exchanger walls as well as through the flowing liquids have been neglected. For more detail on the model see the CNES report [26] and ref. [28, 23].

The heat exchanger consists of two sections (figure 3.4). The one-phase section is 1 metre in length and consists of capillaries with an inner diameter of 0.2 mm. The two-phase section is 6 metres in total length and consists of larger-diameter capillaries. The difference in capillary sizes between the one-phase and two-phase sections is ultimately driven by the need to keep the ^{3}He concentration of the flowing mixture constant. In fact, as I already mentioned, in the one-phase section this is obtained by keeping the flow velocity above the critical velocity to ensure that the ^{3}He and ^{4}He components are locked together. For this reason the diameter in this section is lower than that in the two-phase section, but at the cost of greater viscous dissipation (eq. 3.2). However, viscous dissipation is generally not a critical issue at high temperatures (due to the inverse relationship between η and T^2). Since at lower temperatures it becomes more significant, in the two-phase section the diameter is kept relatively high. However, choosing too large a capillary may make it hard for the flow to return at constant concentration, since the ^{3}He droplets may deform and so they may not be able to fill completely the capillary. In fact we have to consider the capillary length $l_c = \sqrt{\sigma/\Delta\rho g}$, where σ denotes the surface tension of the fluid-fluid interface, $\Delta\rho$ the difference between the dilute mixture density and the concentrated phase density and g is the gravitational acceleration. Using $\sigma = 0.023\,\mathrm{erg/cm^2}$ [29] we find 0.2 mm:

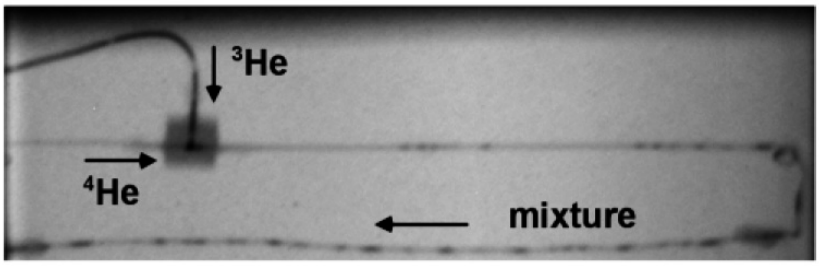

Figure 3.3: Formation of ^{3}He droplets into ^{4}He inside the return capillary (neutron radiograph measurement at the ILL in 2005).

droplets with a radius larger than this value are not spherical anymore. The model has been used as a guide to optimize the diameters (larger is better), but with the capillary length in mind. Actually saying that the only forces that act on a droplets are the surface tension and gravity is a naive simplification. There are other effects that can act on a droplets (for example effects due to the fact that the droplets are moving or due to viscosity). Moreover the fact that if a droplets is not spherical anymore it cannot fill the capillary is too simplistic: even if deformed it could still fill it (our system still works with capillaries five times larger than the capillary length).

For the same reasons, the diameter of the return capillary from the mixing chamber back to the two-phase section of the heat exchanger is most important because of the increasing dissipation as the temperatures decrease.

Figure 3.3 shows a neutron radiograph measurement carried out at the ILL in 2005, showing the formation of ^{3}He droplets into ^{4}He inside the return capillary, as described previously. This observation is possible only using a neutron flux, because ^{3}He droplets absorbs neutrons and appear dark, while ^{4}He is transparent to these particles. The video of this experiment can be found in following web link: http://www.ill.eu/index.php?id=131#.

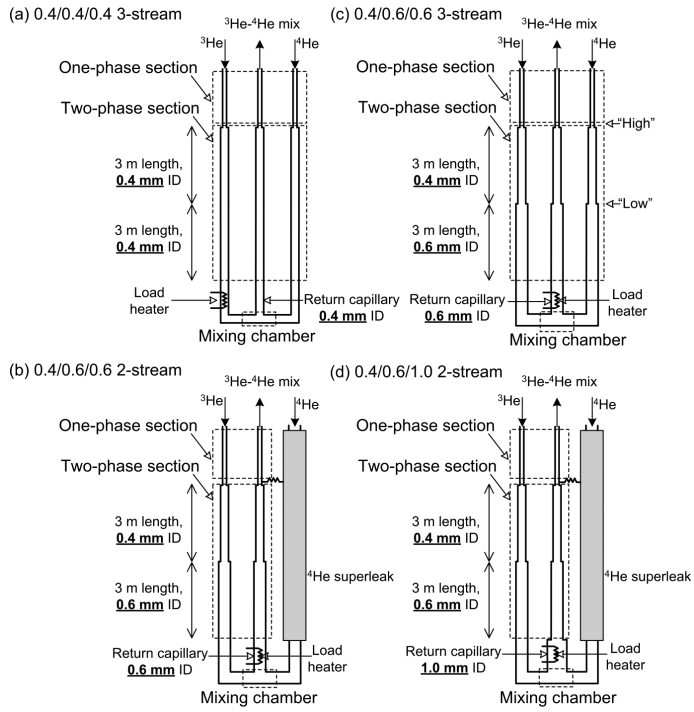

Figure 3.4: The different heat-exchanger/cold-end configurations tested over the years. ID: inner diameter.

Different sizes for the two-phase heat-exchanger/cold-end configurations have been tested before my arrival and in the beginning of my PhD. It is worth defining a nomenclature system to keep track of them. Different sizes of capillaries for the top (hot) half of the two-phase heat exchanger, for the bottom (cold) half of the two-phase heat exchanger, and for the cold end containing the mixing chamber and the load heater have been used. We designate a heat exchanger as a/b/c where a is the inner diameter in mm of the capillaries in the top half of the heat exchanger, b the inner diameter in mm of the capillaries in the bottom half, and c the inner diameter in mm of the return capillary leading from the mixing chamber back to the heat exchanger (see figure 3.4). Moreover we refer to the heat exchanger config-

uration in figure 3.4 (a) as 3-capillary heat exchanger, while we refer to the configuration in figure 3.4 (b) as 2-capillary heat exchanger. In this second configuration the ^{4}He capillaries was replaced by a superleak. I will explain why shortly. The heat exchangers tested are (a) 3-stream 0.4/0.4/0.4, (b) 2-stream 0.4/0.6/0.6, (c) 3-stream 0.4/0.6/0.6, and (d) 2-stream 0.4/0.6/1.0 respectively (figure 3.4).

I only participate in the test of the last two configurations. In configuration (b), (c) and (d) the (3-m long) top half part has an inner diameter is of 0.4 mm, while the (3-m long) bottom half part has an inner diameter is of 0.6 mm. The superleak in configuration (b) and (d) was built because it was suspected that the ^{3}He could diffuse up the ^{4}He capillary, causing heating due to mutual friction, and so putting an extra heat load on the heat exchanger. The superleak precludes this. It is thermally isolated from the heat exchanger except for a single thermal short to prevent a conduction heat leak from the still to the mixing chamber. The ^{4}He superleak is a 9 cm long SS316L tube with an inner diameter of 2.6 mm. The material inside the superleak is aluminium oxide with pores size smaller than 75 nm.

Comparing configuration (b) and (c) we observed that the performance of the 2-capillary design was very similar to that of the 3-capillary. The 2-capillary heat exchanger performed slightly better: T_{load} was typically about 1-2 mK lower than that for the 3-capillary design. However, the tests performed with the 2-capillary configuration helped us to understand that there actually was a mutual-friction-induced-heating in the ^{4}He capillary, due to the ^{3}He diffusing up the ^{4}He capillary. There are two indications (see figure 3.5 [25, 28]): (a) the temperature profiles of the ^{3}He and mixture in the

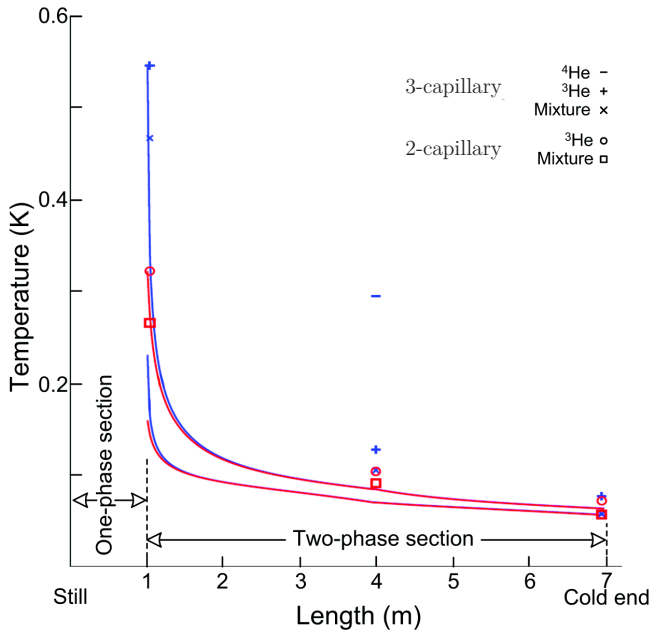

Figure 3.5: Temperature profiles for the two designs (markers) at $\dot{n}_3 = 25$ μmol/s, $\dot{n}_4 = 325$ μmol/s, $T_{still} = 1.05$ K and a heat load of 1 μW. Also shown are the modelled profiles (blue lines - 3-capillary, red lines - 2-capillary) for the two cases. For each design the highest calculated profile is for the ^{3}He stream.

3-capillary design were significantly higher than those in the 2-capillary configuration; (b) the temperatures of the ^{4}He stream in the 3-capillary design were much higher than the corresponding temperatures of the ^{3}He stream. However, since the ultimate T_{load}'s for the two configurations are very close, it appears that there was enough exchange area in the 3-capillary design to compensate for the heating .

In figure 3.5 also are shown the calculated temperature profiles for the two configurations. It appears clear that the results of the 2-capillary heat exchanger are in better agreement with the model than those of the 3-capillary design. The high temperatures of the ^{4}He stream in the 3-capillary heat exchanger suggests that its role cannot be neglected, although it was ignored in all our analysis. As mentioned in the beginning of this section, there was not expected to be a significant load on the mixture stream associated with cooling the ^{4}He down, and the temperature of the ^{4}He stream was expected to mirror the temperature of the mixture stream. It is obvious from the data that the temperature of the ^{4}He stream is much higher than either of the other streams. However, it is hard to get a theoretical estimate of this heating and so considering it in the model. On the other hand, in the 2-capillary heat exchanger the superleak prevents this problem, avoiding the ^{3}He to diffuse up the ^{4}He capillary and so it offers a cleaner comparison with the model.

A schematic of the cold end, consisting of a mixing chamber and a load heater, is shown in (figure 3.6). The return capillary is wound around and soldered to three cylindrical copper mounts. Each spiral is about 50 cm in length; therefore the total length of the return capillary is around 1.5 me-

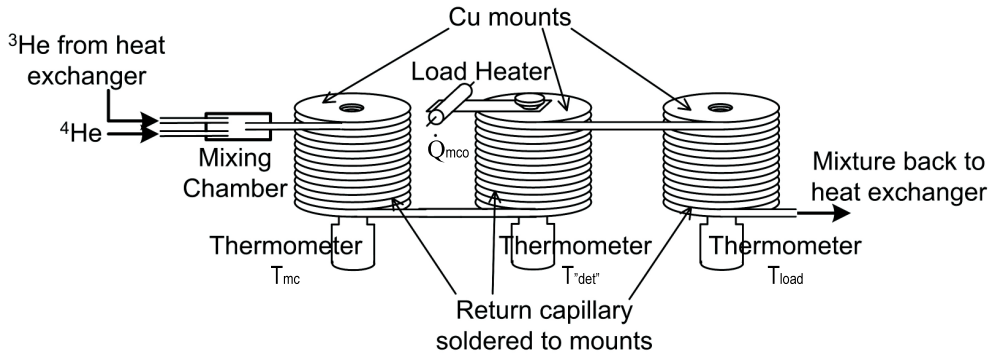

Figure 3.6: The cold-end configuration. See explanation in the tex.t

tres. The thermometer on the first mount measures the temperature of the mixture exiting the mixing chamber, T_{mc}. The second mount supporting a load heater $\dot{Q}_{mco}$ and a thermometer $T_{"det"}$ acts as a detector simulator. The thermometer on the third mount measures the temperature of the mixture after it has absorbed the load, T_{load}. Heater $\dot{Q}_{mco}$ and thermometers $T_{"det"}$ and T_{load} allow to measure the Kapitza resistance between the detector simulator and the liquid (see section 3.2.3). After the third mount, the mixture returns to the heat exchanger. With 1-mm return capillary (configuration (d)) we obtained a T_{load} of about 45 mK at 1μW and at a still pressure of 5 mbar [25, 28]. This solution significantly improved the performance with respect to previous configurations: with a 0.6 mm return capillary in the cold end T_{load} was, in the best case, 55 mK (at 5 mbar).

As a conclusion of this section, I can say that the configuration that performed better is the 0.4/.6/1.0 (configuration (d)). In this case our dilution refrigerator can provide a cooling power of 1 μW to temperatures as low as 45 mK at a still pressure of 5 mabr (see table 3.4 for the other values of pressure).

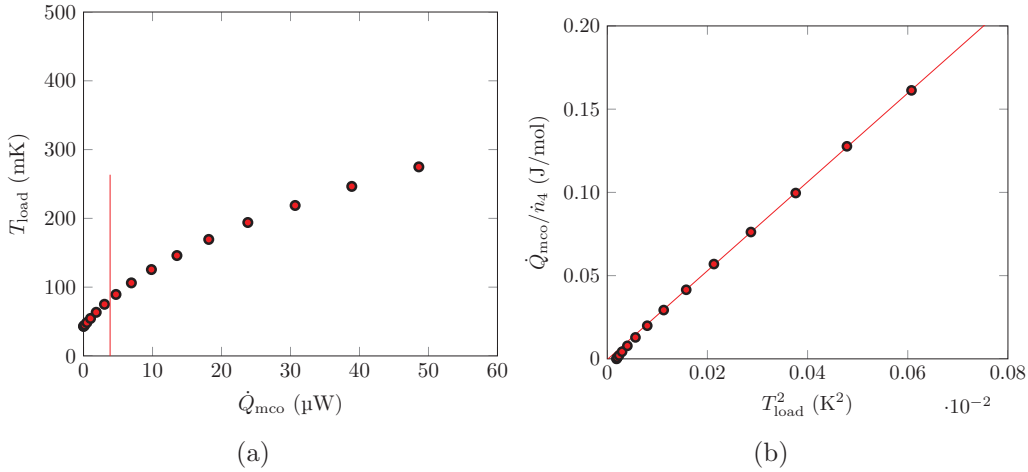

Figure 3.7: (a) T_{load} as a function of cooling power $\dot{Q}_{mco}$ at a still pressure of 0.4 mbar. (b) The specific cooling power $\dot{Q}_{mco}$ as a function of T^2_{load} for the same data. The data have been taken with the 04/06/06 heat exchanger configuration.

3.2.2 CCDR cooling power

In previous sections I showed T_{load} at a cooling power of 1 μW. The refrigerator was also tested at different heat loads to verify the model developed in [23] for the cooling power: $\dot{Q}_{mco}/\dot{n}_4 = 2.9T^2_{load}$. In figure 3.7(a) T_{load} is shown as a function of the cooling power $\dot{Q}_{mco}$ for a series of data taken with the 04/06/06 heat exchanger configuration. We can identify two features: for $\dot{Q}_{mco}$ less than about 5 μW data show a linear trend; then they follow the typical quadratic behaviour for the cooling power. The linear behaviour could be caused by the finite dimension of the heat exchanger, and so of the heat exchange surface. This is a concern because, at the low temperatures reached in the cold end, the Kapitza resistance significantly increases. When the $\dot{Q}_{mco}$ increases, and so the temperatures, the Kapitza resistance decreases enough so that data in figure 3.7(a) bend starting to follow the typ-

ical quadratic behaviour. Therefore the theoretical relation can be applied for $\dot{Q}_{mco}$ higher than 5 μW. Figure 3.7(b) shows the specific cooling $\dot{Q}_{mco}/\dot{n}_4$ as a function of T^2_{load} and the linear fit performed for $\dot{Q}_{mco}$ higher than 5 μW. The slope found is 2.67. For this series of data we obtained the best fit (for other experiments the slope we find is typically between 2 and 2.5).

The explanation we offer for the discrepancy between theory and experiment is the following: the model builds on the assumption that the average ^{3}He concentration inside the mixture return capillary is constant and equal to the applied concentration $x_{app} = \dot{n}_3/(\dot{n}_3 + \dot{n}_4)$. This may not necessarily be so. In section 3.2.4 an indication of this hypothesis is given.

3.2.3 The Kapitza resistance in the cold end

With the 04/06/1.0 configuration the refrigerator is capable of removing 1 μW of heat at about 45 mK. This is the temperature of the mixture stream, T_{load}, after it has absorbed 1 μW of heat. If there is perfect thermal contact between the load heater and the flowing stream, the load heater is at the same temperature as the mixture ($T_{"det"} = T_{load}$=45mK). In practice, however, there is always a thermal resistance between the load heater and the mixture stream because of which a temperature difference establishes between them. In general, the heat transfer $\dot{Q}$ between a solid at T_{solid} and a fluid at T_{fluid} below 1K can be written as:

$$\dot{Q} = \frac{A}{4\rho_K}(T^4_{solid} - T^4_{fluid}) = \alpha(T^4_{solid} - T^4_{fluid}) \tag{3.3}$$

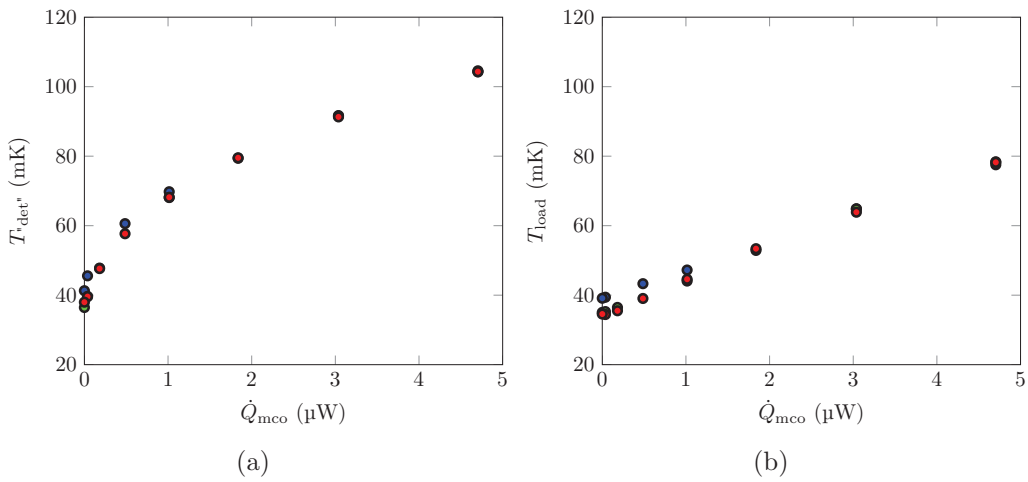

Figure 3.8: $T_{"det"}$ (a) and T_{load} (b) as a function of the applied load $\dot{Q}_{mco}$ for one of the four configurations we tried (1-mm Cu-Ni return capillary). The different colors represent different still pressure (red points - 0.3 mbar, green points - 5.0 mbar, blue points - 10 mbar). Because of the thermal resistance between the load heater and the mixture stream $T_{"det"}$ is higher than T_{load}.

where A is the contact area between the fluid and the solid, and ρ_K is a coefficient, called Kapitza resistance, depending on the fluid, the solid material and the temperature. I define $\alpha \equiv A/4\rho_K$.

We used the setup shown in figure 3.6 to obtain an estimate for the Kapitza resistance (in this setup T_{load} would be T_{fluid}, while $T_{"det"}$ would be T_{solid}). Thermometer $T_{"det"}$ and load heater $\dot{Q}_{mco}$ are mounted downstream of the mixing chamber on the mixture return capillary and thermometer T_{load} is mounted even further downstream, such that the heat transported from $\dot{Q}_{mco}$ to T_{load} by the flowing mixture is much larger than the heat conducted through the walls of the capillary. In the idealised limiting case where $\rho_K \to 0$, $T_{"det"} \to T_{load}$. In a real system, $T_{"det"} > T_{load}$ (figure 3.8). It is, therefore, desirable to maximize the value of the factor α in eq. 3.3. We

measured it for four different configurations:

a) a 0.4/0.6/0.6 configuration with Cu-Ni return capillary.

b) a 0.4/0.6/1.0 configuration with Cu-Ni return capillary.

c) a 0.4/0.6/1.0 configuration with a return capillary made of Cu-Ni etched with acid.

d) a 0.4/0.6/1.0 configuration with a sintered Ag return capillary: the section of the capillary in contact with the load heater is made of a 1.0 Ag capillary with a 50 μg deposit of a Ag sinter.

For each configuration we measured $T_{"det"}$ and T_{load} at different values of $\dot{Q}_{mco}$ and at different pressures. Figure 3.9 shows the experimental data in the form of eq. 3.3 for the the four configurations listed above. ρ_K is obtained by using the definition $\alpha \equiv A/4\rho_K$ and its experimental value, obtained from a linear fit. The contact area is obtained considering that the capillary is wound a certain number n of turns round the load heater mount. Knowing the inner (d_i) and the outer (d_o) diameter of the capillary and that of the mount (D) we can calculate the length useful for heat exchange ($L = n\pi(D + d_o)$) and thus the area ($A = \pi d_i L$). Table 3.1 shows the values of these geometrical parameters for each configurations. For configuration (d) it is not possible to calculate the contact area: it is bigger than the inner surface of the capillary because of the silver sinter, but we cannot evaluate it. For this configuration I give the value of the slope, but not the calculated Kapitza resistance. The results are summarized for each configuration in table 3.2. Among the three configurations where we could calculate ρ_K, we

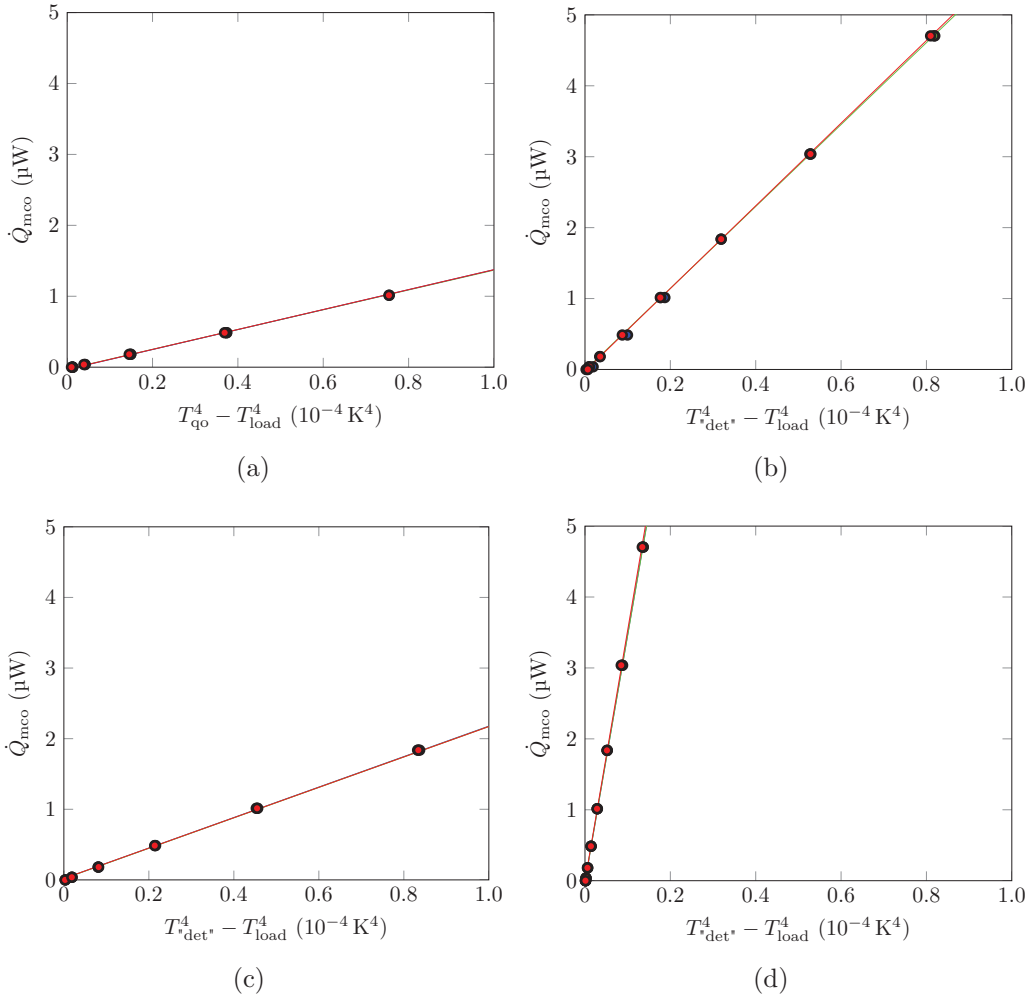

Figure 3.9: The applied load $\dot{Q}_{mco}$ as a function of $T^4_{\text{"}det\text{"}} - T^4_{load}$ or the four different configurations described in the text. The different colors (they are not so distinguishable because the data are overlapped) represent different still pressure (red points - 0.3 mbar, green points - 5.0 mbar, blue points - 10 mbar).

d_ixd_o(mm)	material	n	D (mm)	L (m)	A (m^2)
0.6x0.8	Cu-Ni	12	8	0.33	$6.3{\cdot}10^{-4}$
1.0x1.5	Cu-Ni	-	-	0.42	$1.3{\cdot}10^{-2}$
1.0x1.5	Acid treated Cu-Ni	13.5	10.53	0.51	$1.6{\cdot}10^{-2}$
1.0x1.5	Ag with Ag sinter	12.5	10.95	0.49	-

Table 3.1: Geometrical parameters for each configurations. For the second configuration, which has been disassembled, we calculated and noted down only the information about the length, but we lost the information about n and D.

Configuration	slope(W/K^4)	$\rho_K(K^4m^2/W)$	$T_{"det"}$(mK)	T_{load} (mK)
0.6x0.8 Cu-Ni	$1.4{\cdot}10^{-2}$	0.011	95.4	52.2
1.0x1.5 Cu-Ni	$5.9{\cdot}10^{-2}$	0.0056	68.2	44.6
Acid	$2.1{\cdot}10^{-2}$	0.019	84.7	49.1
Ag sinter	$3.5{\cdot}10^{-1}$	-	51.7	45.0

Table 3.2: Kapitza resistances for different configurations at a cooling power of 1 μW and a still pressure of 5 mbar.

obtained the lowest value (0.0056 K^4m^2/W) for configuration (b). In fact among these three configurations it is the one that performed better.

Figure 3.9 and table 3.2 show that the configuration with the sintered Ag capillary performed better than the others: at 1 μW and a still pressure of 5 mbar $T_{"det"}$ fell to 51.7 mK for a T_{load} of about 45 mK. Moreover, it shows a value of α a factor 10 higher than the other configurations.

In our calculations we consider T_{fluid} constant. Actually it is not constant because it changes from T_{mc} to T_{load}. To check the consequences of this simplification I performed the same analysis described above for $T_{"det"}$ and T_{mc}. For configuration (b) and (c) α is respectively 14% and 28% lower than that calculated in previous analysis, while for the sintered Ag capillary I obtained a very similar value (less than 1% different). For configuration (a)

I could not perform the comparison, because T_{mc} has been not measured. I can conclude that for the configuration (d), that we are interested in, the assumption that T_{fluid} is constant is correct.

The main result described in this section is that in its present state, the closed-cycle dilution refrigerator can deliver a cooling power of 1 μW to temperatures as low as 45 mK, which means a temperature for the load very near to 50 mK, at a still pressure of 5 mbar. This is obtained thank to a sintered Ag return capillary, which increases the contact surface between the fluid and load heater.

3.2.4 Constant x or constant μ_4?

Figure 3.10 shows T_{load} as a function of the cooling power $\dot{Q}_{mco}$ for experiments performed with the 04/0.6/1.0 heat exchanger configuration. The three different plots indicate different P_{still} (0.3, 5.0, 10.0 mbar) and different colors indicate different ^{3}He flow rate, $\dot{n}_3$ (the values are shown in 3.10: magenta is the lowest value, cyan the highest). In figure 3.10 we can identify three features: for $\dot{Q}_{mco}$ less than 5 μW data show a linear trend; then they follow the typical quadratic behaviour for the cooling power until a sudden jump. The first two have been already described in 3.2.2. Here for P_{still} above 0.3 mbar a jump in temperature appears and, in our opinion, it is an indication of the fact that the ^{3}He droplets dissolve. For the same P_{still} they dissolve at lower temperatures when $\dot{n}_3$ is lower, because lower $\dot{n}_3$ implies lower x_{app}.

The temperature at the jump gives us an indication of the local concentra-

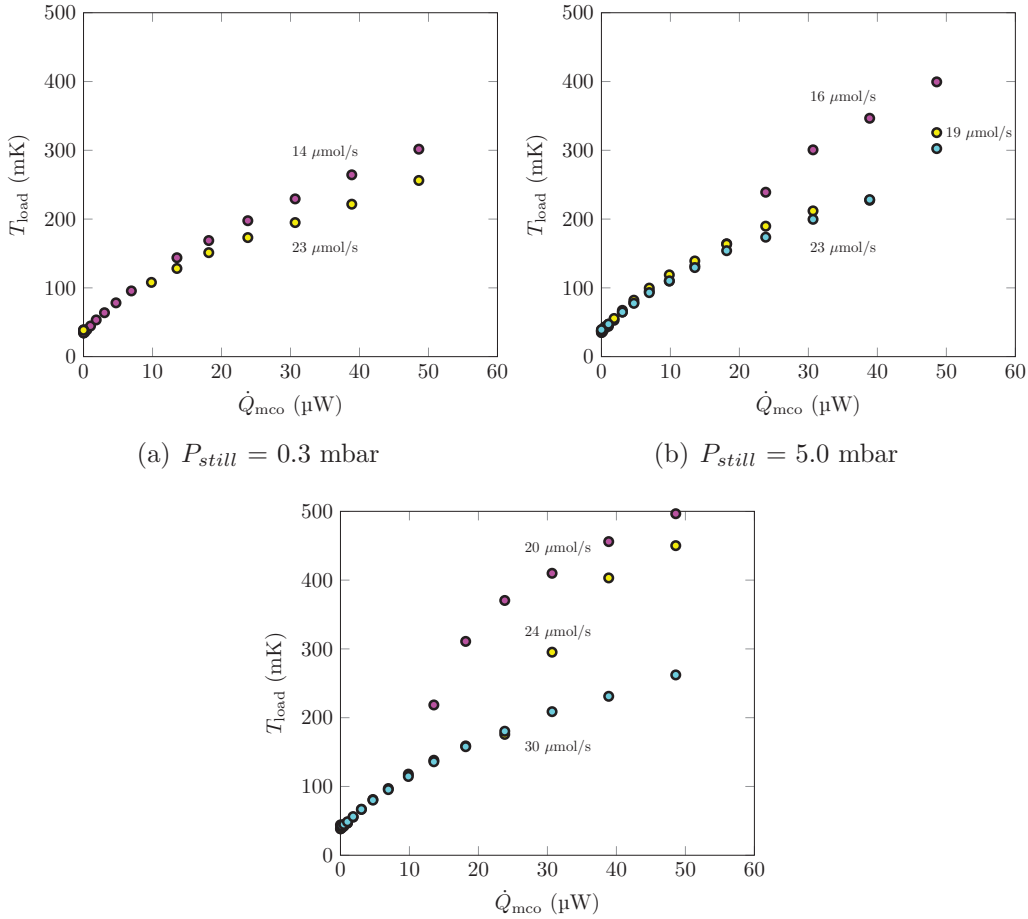

(a) $P_{still} = 0.3$ mbar

(b) $P_{still} = 5.0$ mbar

(c) $P_{still} = 10$ mbar

Figure 3.10: T_{load} as a function of the cooling power $\dot{Q}_{mco}$. The three different plots indicate different P_{still} (0.3, 5.0, 10.0 mbar) and different colors indicate different $\dot{n}_3$ (magenta is the lowest value, cyan the highest).

$P_{still\ (mbar)}$	$\dot{n}_3\ (\mu mol/s)$	$\dot{n}_4\ (\mu mol/s)$	$x_{app\ fraction}$	$x_{loc\ fraction}$
0.3	14.1	383.8	0.035	-
0.3	23.4	358.2	0.061	-
5.0	16.0	341.3	0.045	0.10
5.0	19.2	301.0	0.060	-
5.0	23.6	345.7	0.064	0.12
10.0	20.5	308.6	0.062	-
10.0	23.9	312.2	0.071	0.12
10.0	30.0	307.2	0.089	-

Table 3.3: The local concentration, x_{loc}, calculated by measurements of temperature at the jump in fig 3.10, assuming that at the jump the ^{3}He droplets dissolve. For comparison I report the concentration x_{app} calculated from measurements of $\dot{n}_3$ and $\dot{n}_4$ flow rates at the jump.
For the lowest pressure curves I did not calculate x_{loc}, because they show no jump. For some of the high pressure curves I could not calculate x_{loc} because we did not take enough points to be sure where the jump is located. For the curves where I could not calculate x_{loc} I show the the main value of x_{app} over the $\dot{Q}_{mco}$ sweep. In general x_{app} varies slightly during the $\dot{Q}_{mco}$ sweep (10% in the worst experimental runs).

tion, x_{loc}, that we can compare with x_{app} (results in table 3.3). In this way we can verify whether the assumption that along the return capillary the average ^{3}He concentration inside the mixture return capillary is constant and equal to x_{app}. Table 3.3 shows that the local concentration is actually higher than the applied concentration.

Another indication that x_{loc} is higher than x_{app} is given by observing T_{load} and x_{app} for the data at 0.3 mbar. For example for the magenta curve we have a load temperature of 45 mK for a x_{app} of 3.5%. If the local concentration was equal to 3.5%, cooling would be possible only above 70 mK (see for example [42]). However we observe it at lower temperatures, meaning that the local concentration has to be higher enough to allow it. Therefore the assumption, on which the model for calculating the cooling power is based, is

not true. More probably along the return capillary the situation is between the two ideal ones: constant concentration and constant ^{4}He chemical potential. This could explain the discrepancy between theory and experiments I described in section 3.2.2. However, it is still unclear how to modify the model.

3.2.5 Effect of still pressure on the refrigerator performance and on the pre-cooling stage

As mentioned earlier, it is desirable that the still pressure P_{still} be as high as possible so as to relax the requirements on the ^{3}He compressor. However, the performance of the refrigerator deteriorates as the still pressure increases. In fact higher P_{still} corresponds to a higher T_{still} which raises the temperature of ^{3}He stream entering the counterflow heat exchanger, posing a higher load on it. Experimentally, higher P_{still} implies also need of higher x_{app} (or higher $\dot{n}_3$ for the same $\dot{n}_4$) or the dilution refrigerator will not work. This affects negatively the minimum temperature because, as I said in previous chapter, the extra ^{3}He that does not goes into the dilute phase does not contribute to the cooling process, but it has to be pre-cooled in the heat exchanger anyway. Moreover, the specific heat of the dilute mixture per mole of ^{3}He decreases with increasing ^{3}He concentration. Therefore, it is more difficult to pre-cool the incoming ^{3}He stream when the concentration of the mixture is higher. An incoming ^{3}He stream not well pre-cooled results in a higher T_{load} (see table 3.4).

Another negative effect to have a high P_{still} is that the percentage of ^{3}He

in the vapour boiling off from the still reduces as the pressure (and thus the temperature) increases. With a ^{3}He concentration in the liquid of about 10%, the ^{3}He concentration in the vapour changes from above 95% at 1.1 K (P_{still} = 5 mbar) to about 85% at 1.3 K (P_{still} = 10 mbar) to about 70% at 1.5 K (P_{still} = 15 mbar). As a result, the room temperature pump, which circulates only ^{3}He at low still temperatures, ends up circulating some ^{4}He at high still temperatures. This effects negatively the effectiveness of the heat exchanger: the ^{4}He in the ^{3}He stream increases the enthalpy of the incoming flow. Therefore it is more difficult for the exiting mixture to pre-cool the incoming stream, resulting again in a higher T_{load} (see table 3.4).

Results of testing the system at still pressures up to 15 mbar are tabulated in Table 3.4[1]: it shows that, when the still pressure is raised from the lowest value (about 0.3 mbar) to 10 mbar, T_{load} increases by 5% (from 44.0 mK to 46.7 mK). For a pressure of 15 mbar the deterioration of the performance is more significant (about 15%), due to the degradation of the heat exchange I explained above.

The still pressure affects negatively also the pre-cooling stage: the heat load on the 1.7 K stage increases significantly with the still pressure (because higher quantity of ^{3}He needs to be liquefied). The heat load on the pre-cooling stage is an important parameter: it has to be as low as possible to relax the requirements on the external 1.7 K cooling source, that provides the interface between the refrigerator and the rest of the cooling chain (see

[1]The ^{4}He flow rates in table 3.4 are lower than those published in [25] and in [28], because we found an error in the measurement of the heating power, $\dot{Q}_{fp}$, applied to the fountain pump (see appendix A). Actually, $\dot{Q}_{fp}$ is 3 % to 4 % higher than we thought meaning that $\dot{n}_4$ is 3 % to 4 % lower than we have published until now.

P_{still} (mbar)	T_{still} (K)	x_v (%)	$\dot{n}_3$ (μmol/s)	$\dot{n}_4$ (μmol/s)	T_{load} (mK)	$T_{"det"}$ (mK)
0.3	0.7	100	16.5	382.6	44.0	50.7
5.0	1.1	95	18.1	332.8	45.0	51.4
10.0	1.3	85	28.4	327.8	46.7	52.6
15.0	1.5	70	56.3	278.3	51.8	56.5

Table 3.4: The minimum T_{load} and $T_{"det"}$ temperatures achieved with a 1 μW heat load at various still pressures (and corresponding still temperature). The table also shows the values of the flow rates at which these temperatures are reached.

section 3.3.1).

Summarising, a high still pressure, necessary to relax the requirements on the ^{3}He compressor, deteriorates the refrigerator performance and increase the heat load on the 1.7 K stage. Therefore an optimum for the operational conditions must to be found. Before drawing conclusions about the operational parameters, I will treat the heat load on the pre-cooling stage and the operation of the fountain pump.

3.3 High temperature part

3.3.1 The pre-cooling stage

Our refrigerator requires a pre-cooling stage at a temperature of about 1.7 K to cool the ^{3}He gas from 4.2 K (and condense it) and to cool the ^{4}He exiting the fountain pump. The function of the pre-cooling stage is to reduce the heat load on the still due to the circulation of the helium isotopes to an acceptable value. The specifications of the ^{3}He Joule Thompson expansion cooler planned for the SPICA mission are our principal benchmark for the 1.7

K cooling source, which is the high temperature interface of our refrigerator with the rest of the cooling chain in a space mission. This cooler has a nominal cooling power of 10 mW at 1.7 K [30] to be shared between two scientific instruments. Therefore, it would provide our refrigerator with a pre-cooling power of 5 mW at 1.7 K. Our goal is to keep the heat load on this stage below this value.

Our system is immersed in a liquid helium bath at 4.2 K and the pre-cooling stage consists in a pot continuously filled with helium from the main bath through a capillary and pumped to reach the temperature of about 1.7 K. The impedance between the bath and the pre-cooling stage can be varied by means of a needle valve operated at room temperature. The needle valve is controlled by a feedback system to maintain the pressure in the pre-cooling stage at the set point value that we choose. Figure 3.11 shows the 1.7 K pot with the still and the fountain pump of our refrigerator. ^{3}He gas (red dashed arrow) is pumped from the still by a ^{3}He compressor (not shown), it passes through the 4.2 K bath, the ^{3}He heat exchanger in the 1.7 K pot and then it is injected in the ^{3}He still heat exchanger. The superfluid ^{4}He is pumped from the still by the fountain pump through the superleak, it passes through the ^{4}He heat exchanger in the 1.7 K pot and then it is injected in the ^{4}He still heat exchanger.

The presence of the needle makes our 1 K pot work differently with respect to the most common devices (see for example [31]).

We have tried to calculate and measure the heat load on the pre-cooling stage due to the circulation of the two helium isotopes.

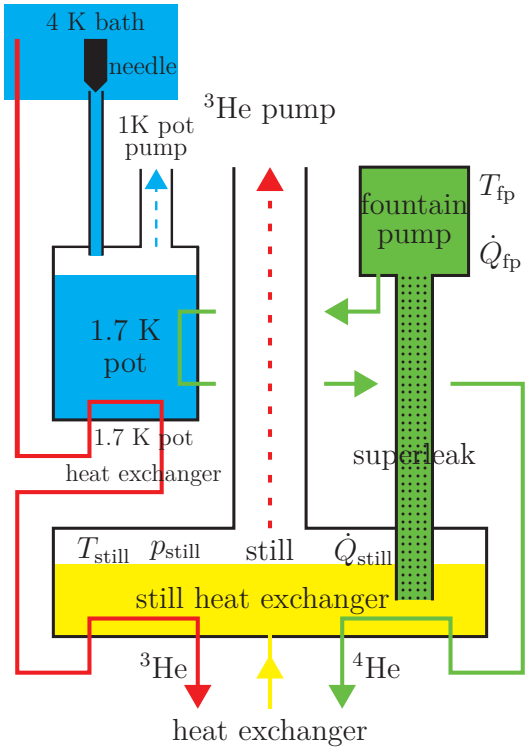

Figure 3.11: The 1.7 K pot with the still and the fountain pump of our closed-cycle dilution refrigerator.

The heat load on the pre-cooling stage due to the ^{3}He flow

The heat load on the pre-cooling stage $\dot{Q}_{pot,\dot{n}_3}$ due to the ^{3}He flow depends on the latent heat of condensation and on the specific heat at constant pressure of the liquid and vapour phases. We can write $\dot{Q}_{pot,\dot{n}_3}$ as follow:

$$\dot{Q}_{pot,\dot{n}_3} = \dot{n}_3(C_{p,vapour}(T_{bath} - T_{sat}) + L(T_{sat}) + C_{p,liquid}(T_{sat} - T_{pot})) \quad (3.4)$$

where $\dot{n}_3$ is the ^{3}He flow rate, L is the molar latent heat, $C_{p,vapour}$ and $C_{p,liquid}$ are the molar specific at constant pressure of the vapour and liquid respectively, T_{bath} is the temperature of the ^{4}He bath at which the mixture flow is cooled before entering the pot, T_{pot} is the temperature of the pre-cooling stage, and T_{sat} is the saturated vapour temperature. T_{sat} depends through the saturated vapour pressure on the pressure distribution in the condensing line. Currently, we cannot measure the saturated vapour pressure because of the pressure drop in the ^{3}He injection capillaries between the ^{3}He injection pressure gauge at room temperature and the pre-cooling stage heat exchanger. Therefore, T_{sat} is unknown and so we make the simplifying assumption that $T_{sat} = T_{pot}$. Therefore, we assume that vapour enters the 1.7 K pot and just completely liquefies in it. We approximate the specific heat of the vapour as that of an ideal gas and, considering that the circulating ^{3}He can be contaminated by up 5-30% ^{4}He (depending on the ^{3}He concentration in the liquid in the still and on the still temperature) the latent heat as $x_v L_3^0(T_{pot}) + (1 - x_v)L_4^0(T_{pot})$. x_v is the ^{3}He concentration in the vapour[2]

[2]Estimation of x_v: given the ^{3}He concentration of the liquid in the still, x_{still}, and the still temperature (> 1 K), we inferred x_v by interpolating the data from [32]. We estimated x_{still} from measurements of pressures and temperatures in the still and by interpolating

and L_3^0 and L_4^0 are the latent heats[3] of pure ^{3}He and pure ^{4}He. In the end we obtain:

$$\dot{Q}_{pot,\dot{n}_3} = \dot{n}(\frac{5}{2}R(T_{bath} - T_{pot}) + x_v L_3^0(T_{pot}) + (1 - x_v)L_4^0(T_{pot})) \tag{3.5}$$

The heat load on the pre-cooling stage due to the ^{4}He flow

The heat load on the pre-cooling stage due to the ^{4}He circulated by the fountain pump, $\dot{Q}_{pot,\dot{n}_4}$, is simply:

$$\dot{Q}_{pot,\dot{n}_4} = \dot{n}_4(h_4^0(T_{fp}) - h_4^0(T_{pot})) \tag{3.6}$$

where $\dot{n}_4$ is the ^{4}He flow rate, h_4^0 the molar enthalpy of pure liquid ^{4}He, T_{fp} the temperature of the fountain pump.

The heat load on the pre-cooling stage inferred from its ^{4}He consumption

We assume that the total heat load on the pre-cooling stage can be inferred from its ^{4}He consumption. So we added a flow meter at the exit of the pump to measure the gas flow rate, $\dot{n}_{4,pot}$, and an additional heater, $\dot{Q}_{heater}$, on the pre-cooling stage so that we can write the heat load, $\dot{Q}_{fm}$ (the subscript 'fm' means flow meter), as:

$$\dot{Q}_{fm} = \dot{n}_{4,pot}L_4^0 = \dot{Q}_{leak} + \dot{Q}_{pot,\dot{n}_3} + \dot{Q}_{pot,\dot{n}_4} + \dot{Q}_{heater} \tag{3.7}$$

data from [33]. For still temperature < 1 K we assume x_v=1.

[3]We estimated the latent heats from measurements of the pot temperature and by fitting data from [35] (for L_3^0) and by interpolating data from [34] (for L_4^0)

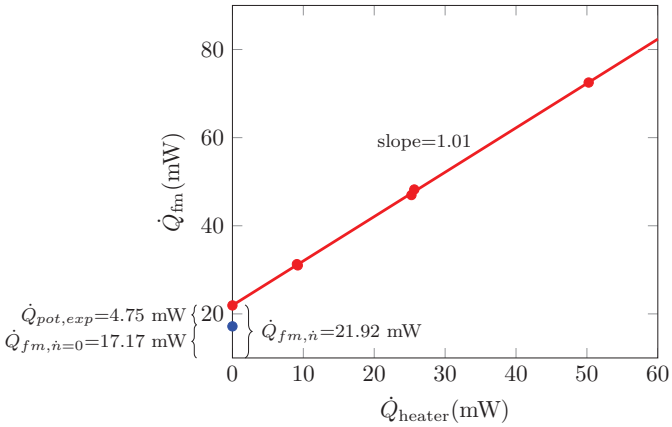

Figure 3.12: The heat load inferred by measurements of ^{4}He gas flow rate, $\dot{Q}_{fm}$, as a function of $\dot{Q}_{heater}$. See explanation in the text.

where L_4^0 is the ^{4}He evaporation latent heat, $\dot{Q}_{pot,\dot{n}_3}$ and $\dot{Q}_{pot,\dot{n}_4}$ are the heat loads due to the circulation of the ^{3}He and ^{4}He and $\dot{Q}_{leak}$ is the heat load due to other heat leaks in the experiment setup. We assume that, for constant $\dot{n}_3$ and $\dot{n}_4$ and at fixed T_{pot}[4] those quantities are practically constant. Therefore the only variable is $\dot{Q}_{heater}$ and eq. 3.7 can be described by a straight line of slope 1. If our experimental data can be described by eq. 3.7, the heat load due to the helium isotopes flows is equal to the decrease of $\dot{Q}_{fm}$ when we set the flow rates to zero ($\dot{Q}_{pot,\dot{n}_3} + \dot{Q}_{pot,\dot{n}_4} = 0$).

Figure 3.12 shows the results ($\dot{Q}_{fm}$ vs $\dot{Q}_{heater}$) belonging to one of the three experimental runs we performed. During this run the still pressure was about 0.3 mbar. Our data are well described by a straight line (red line in figure 3.12) with a slope of 1.01. It confirms eq. 3.7 when the heat is applied by a heater. So we expect that it works also when the heat is applied only by the dilution refrigerator. At $\dot{Q}_{heater} = 0$ mW and with ^{3}He and ^{4}He circulation

[4]During the three $\dot{Q}_{heater}$ sweeps we performed T_{pot} changes slightly: respectively about 5%, 15% and 5%.

measured								calculated		
P_{still} $(mbar)$	Q_{still} (mW)	$T_{pot,\dot{n}}$ (K)	$\dot{n}_3$ $(\mu mol/s)$	$\dot{n}_4$ $(\mu mol/s)$	$\dot{Q}_{fm,\dot{n}}$ (mW)	$\dot{Q}_{fm}$ $\dot{n}$=0 (mW)	$\dot{Q}_{pot,exp}$ (mW)	$\dot{Q}_{pot,\dot{n}_3}$ (mW)	$\dot{Q}_{pot,\dot{n}_4}$ (mW)	$\dot{Q}_{pot}$ (mW)
0.3	0.38	1.28	13.5	378.2	16.81	10.98	5.83	1.37	2.50	3.87
0.3	0.0	1.52	13.0	377.0	21.92	17.17	4.75	1.29	2.21	3.50
5.0	0.0	1.51	9.10	325.2	16.69	12.68	4.02	0.93	2.26	3.19

Table 3.5: Results belonging to the three experimental runs we performed in attempting to estimate experimentally the heat load on the pre-cooling stage by its ^{4}He consumption. In all three cases the data are well described by a straight line (eq. 3.7) of slope 1.08, 1.01 and 0.92 respectively.

($\dot{n}_3$ = 13 μmol/s and $\dot{n}_4$ = 378 μmol/s) the measured heat load $\dot{Q}_{fm,\dot{n}}$ is 21.92 mW. The blue point in figure 3.12 ($\dot{Q}_{fm,\dot{n}=0}$=17.17 mW) is the result for $\dot{Q}_{heater} = 0$ in the absence of ^{3}He and ^{4}He circulation. Part of this heat leak is due to the ^{4}He gas forming after the Joule-Thomson expansion at the exit of the impedance (what is injected in the pot contains only 50% of liquid). The difference between this two points gives an experimental heat load $\dot{Q}_{pot,exp}$ of 4.75 mW.

Using eq. 3.5 and 3.6 we calculate a $\dot{Q}_{pot,\dot{n}_3}$ of 1.29 mW and a $\dot{Q}_{pot,\dot{n}_4}$ of 2.21 mW, giving a total heat load on the pre-cooling stage, $\dot{Q}_{pot}$, of 3.50 mW. In this case, the experimental value is about 26% higher than the value following from equations 3.5 and 3.6. Table 3.5 summarizes the results for the three runs we performed. The heat load (experimental and theoretical) for the first run at 0.3 mbar is higher than the other two values because the pre-cooling temperature is lower (1.3 K compared to 1.5 K). The experimental heat load for the second run at 0.3 mbar is higher than that for 5.0 mbar because of the higher ^{3}He flow rate (13 μmol/s compared to 9 μmol/s).

P_{still} $(mbar)$	T_{load} (mK)	T_{still} (K)	x_v $(fraction)$	$\dot{n}_3$ $(\mu mols^{-1})$	$\dot{Q}_{pot,\dot{n}_3}$ (mW)	T_{fp} (K)	$\dot{n}_4$ $(\mu mols^{-1})$	$\dot{Q}_{pot,\dot{n}_4}$ (mW)	$\dot{Q}_{pot}$+ 25% (mW)
0.3	44.0	0.66	1.00	16.5	1.66	2.01	382.6	2.30(*)	4.95(*)
5.0	45.0	1.08	0.94	18.1	1.80	2.05	332.8	1.79	4.49
10.0	46.7	1.31	0.84	28.4	2.98	2.09	327.8	2.16	6.43
15.0	51.8	1.49	0.71	56.3	6.26	2.12	278.3	2.15	10.51

Table 3.6: The estimated heat loads on the 1.7 K stage for experiments listed in table 3.4. (*) This value is higher than those at higher pressures just because in this set of data T_{pot} was not 1.7 K, as in the other three, but lower (1.4 K). Otherwise, at T_{pot}=1.7 K and P_{still}=0.3 mbar, it would be lower than the corresponding values at P_{still}=5.0 mbar.

In table 3.5 I reported also the applied heating power to the still Q_{still}. Diminishing Q_{still} allows us to operate the pre-cooling stage at a higher temperature, so reducing the heat load on it. It is desirable to heat the still such that it always possible to raise the pre-cooling temperature, decreasing Q_{still}, if we need. This would give us margins to operate. In many of our experiments Q_{still} is already practically zero, preventing us to increase the pre-cooling temperature.

With the information obtained with these experiments we can now estimate the heat load on the other experiments: we calculate the heat load by means of equations 3.5 and 3.6 and then increase the results obtained by 25 % (the discrepancy between the calculated values and the experimental data in two cases in table 3.5). In table 3.6 there are the estimated heat load for experiments listed in table 3.4. The heat load increases dramatically with the still pressure and it is higher than 5.0 mW for P_{still} >5.0 mbar (see explanation in table 3.6 caption for the lowest pressure). In section 3.3.2 I will show that it is possible to reduce it appreciably by decreasing the fountain pump

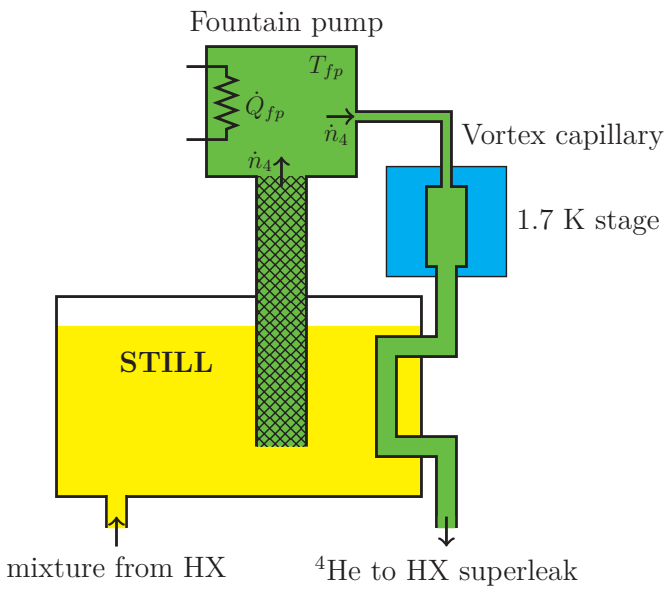

Figure 3.13: The fountain pump and the ^{4}He circulation loop.

temperature and keeping the same ^{4}He flow rate.

The results in table 3.6 are slightly different from those published in [25] for two reasons: firstly, for pedagogical reasons, in [25] we calculated $\dot{Q}_{pot,\dot{n}_3}$ and $\dot{Q}_{pot,\dot{n}_4}$ at the pre-cooling stage nominal temperature (1.7 K) and not at the measured T_{pot} (as I did in this thesis); secondly, here, $\dot{Q}_{pot,\dot{n}_4}$ has been calculated considering the correction on the ^{4}He flow rate, $\dot{n}_4$ (see appendix A)

3.3.2 Fountain pump

As I said in section 3.1, the fountain pump is used to circulate the ^{4}He through the refrigerator. A schematic is shown in Figure 3.13. Applying heat to the ^{4}He in the pump, the ^{4}He in the still is drawn through the superleak into the pump by means of the fountain effect. The ^{4}He flows from the

fountain pump through the vortex capillary to the 1.7 K stage, where it is pre-cooled. Then it is further cooled in the still heat exchanger, and then flows down to the mixing chamber passing through the counter-flow heat exchanger. The ^{4}He flow rate $\dot{n}_4$ can be obtained from the thermodynamic relation:

$$\dot{n}_4 = \frac{\dot{Q}_{fp}}{T_{fp} s_4(T_{fp})} \tag{3.8}$$

where, $\dot{Q}_{fp}$ is the heat input applied to the fountain pump via a resistance heater, T_{fp} is the fountain pump temperature, $s_4(T_{fp})$ is the ^{4}He molar entropy at the fountain pump temperature. Of course the pump has to remain below λ-temperature to function properly.

The role of the vortex capillary is to induce a state where the dominant heat transport mechanism is the mass flow of liquid ^{4}He. This happens when the normal and the superfluid components move together, which means when the fluid is turbulent. There are different hydrodynamics regimes, separated by different critical velocities. This topic is discussed in many text books and articles, see for example [37]. Here I discuss briefly the different regimes and the different criteria to determine the state of the fluid in our vortex capillary. We can distinguish between three regimes, corresponding to different heat transport mechanisms:

- At the low ^{4}He superfluid velocities the heat transport mechanism is the counter-flow between the normal component (which carries entropy) and the superfluid component (which carries no entropy) of ^{4}He. The heat conducted through the capillary $\dot{Q}$ is limited by the viscosity of the normal component and the dimensions of the capillary. In this case

the pressure drop across the capillary is given by the Poiseuille law.

- When the ^{4}He superfluid velocity exceeds the critical velocity[5], the heat transport mechanism is still counter-flow of the normal and the superfluid components, but $\dot{Q}$ is limited by the mutual friction between the superfluid and the normal component. The critical velocity is given by the following empirical law [38]:

$$v_{c1} d^{1/4} = 1cm^{5/4} \tag{3.9}$$

where d is the capillary diameter.

- When the Reynolds number associated to the velocity difference between the normal and the superfluid components exceeds a certain value ($\sim$ 1200-2400), the flow of the normal component becomes turbulent causing the superfluid and normal components to be locked together. In this case, the dominant heat transport mechanism is the mass flow. The pressure drop ΔP_{turb} across the vortex capillary can be calculated by means of the Blasius law:

$$\Delta P_{turb} = 0.241 L \left(\frac{\eta M_4^7 \dot{n}_4^7}{\rho^4 d^{19}} \right)^{1/4} \tag{3.10}$$

where where η is the viscosity of the normal component of ^{4}He, M_4 the molar mass, ρ the density and $\dot{n}_4$ the molar flow rate of ^{4}He and L the length.

[5]Actually for a cylindrical tube there are two critical velocities corresponding to two different turbulent states, but this distinction is not important for our application.

diameter (μm)	v (cm/s)	Re	v_{c2} (cm/s)	$\dot{n}_{4,c}$ (μmol/s)	v_{c1} (cm/s)
72	270.0	19292	21.0	31.1	3.4
136.8	74.8	10154	11.1	59.0	2.9
200	35.1	6913	12.2	131.9	2.7
400	8.8	1264	16.6	720.7	2.2
600	3.9	843	11.1	1081.1	2.0
1000	1.4	505	6.7	1801.9	1.8

Table 3.7: Fluid velocities in the vortex capillary for two different diameters (72 μm and 136.8 μm), in the one-phase heat exchanger (d = 200 μm), in the two-phase heat exchanger (d = 400, 600 μm) and in the cold end (d = 1000 μm) and corresponding Reynolds numbers. The velocities are calculated at 400 μmol/s, the typical value of the ^{4}He flow rate at which we operate our refrigerator. In the last two column the critical velocity and the critical flow rate calculated with a Reynolds number of 2400 are also shown.

The critical velocity is given by the following relation [38]:

$$v_{c2} = \frac{\eta Re}{\rho d} \tag{3.11}$$

where Re is the Reynolds number.

As long as the fountain pump heating power is conducted through the vortex capillary by means of the first or second mechanism, the net ^{4}He flow-rate is zero. When the fountain pump heating power is increased, the ^{4}He flow rate suddenly jumps to a finite value given by eq. 3.8 and the fountain pump can circulate the ^{4}He through the system. Table 3.7 shows the velocities of superfluid ^{4}He in the vortex capillary for two different diameters we used and the corresponding Reynolds number calculated using eq. 3.11. It is evident that the flow is turbulent with both diameters (the Reynolds numbers are much higher than 2400). The table also shows the critical velocity and the critical flow rate calculated using a Reynolds number of 2400. The

typical ^{4}He flow rate at which we operate our refrigerator (350-400 μmol/s) is well above the critical value and the calculated critical flow rates agree to well within a factor two with the observed ones.

To identify the flow regimes in the rest of the dilution refrigerator, we calculated the same quantities (shown in table 3.7) for the one-phase heat exchanger (d = 200 μm), the two-phase heat exchanger (d = 400, 600 μm) and the cold end (d = 1000 μm). For the one-phase heat exchanger the Reynolds number has been calculated considering the viscosity [39] of a 10% mixture at 1.0 K (just before the mixture enters the still). For the two-phase heat exchanger and the cold end I used the viscosity of a saturated mixture at 0.18 K and 8.7% [41] (about 40 μP). The density has been calculated from the molar volume using the data from [40] for the one-phase heat exchanger and the relation in [42] for temperatures below 0.6 K for the two-phase heat exchanger and the cold end. As it is shown in table the vortex capillary is not the only part of our refrigerator where the flow is turbulent: also for the one-phase heat exchanger, at least at high temperatures, the Reynolds number may exceed 2400. In table 3.7 also the first critical velocity v_{c1} calculated from eq. 3.9 is shown: mutual friction can play a role in the two-phase heat exchanger, where the Reynolds number is below 2400 but the flow velocity is higher than v_{c1}.

The still temperature and pressure, T_{still} and P_{still}, and ^{3}He concentration of the liquid in the still, x_{still}, affect the fountain pump very much, because of the equilibrium of the chemical potential of superfluid ^{4}He between still and the fountain pump: $\mu_4(P_{still}, T_{still}, x_{still}) = \mu_4(P_{fp}, T_{fp}, x_{fp} = 0)$, where T_{fp} is the fountain pump temperature and P_{fp} is the total pressure in the fountain

pump. This condition leads to (eq. 2.8 in section 2.1.2):

$$P_{fp} - P_f(T_{fp}) - \Pi(T_{fp}, x_{fp} = 0) = P_{still} - P_f(T_{still}) - \Pi(T_{still}, x_{still}) \quad (3.12)$$

where P_f is the fountain pressure and Π is the osmotic pressure. In the fountain pump there is no ^{3}He ($x_{fp} = 0$), so the osmotic pressure is zero. Therefore, considering also that at the still temperature the fountain pressure, $P_f(T_{still})$, is negligible, $P_f(T_{fp})$ in eq. 3.12 can be rewritten as:

$$P_f(T_{fp}) \sim P_{fp} - P_{still} + \Pi(T_{still}, x_{still}) \quad (3.13)$$

The difference $P_{fp} - P_{still}$ is the pressure drop ΔP in the ^{4}He flow path from the fountain pump through the 1.7 K stage, the still heat exchanger, the counter-flow heat exchanger, the mixing chamber and back up the mixture capillary to the still. In our experiments ΔP is principally due to the turbulent flow in the vortex tube ($P_{fp} - P_{still} = \Delta P \sim \Delta P_{turb}$). Plugging eq 3.10 into eq. 3.13, we get:

$$P_f(T_{fp}) \sim \Pi(T_{still}, x_{still}) + \left(\frac{0.241 L \eta^{1/4} M_4^{7/4}}{\rho d^{19/4}} \right) \dot{n}_4^{7/4} \quad (3.14)$$

The first consideration about eq. 3.14 is that $P_f(T_{fp})$, and so T_{fp}, increases with increasing $\dot{n}_4$ and increasing $P_{still}(T_{still}, x_{still})$ (the osmotic pressure depends on P_{still} through T_{still} and x_{still}). Therefore we cannot increase $\dot{n}_4$, to increase the cooling power, or x_{still}, and so P_{still}, to ease the requirements on the ^{3}He compressor, without taking into account the rise in T_{fp}. A rise in T_{fp} could have two negative effects: firstly T_{fp} could exceed T_λ, rendering

the fountain pump inoperative; secondly it leads to a higher heat loads on the pre-cooling stage.

Another consideration about eq. 3.14 is that the pre-factor multiplying $\dot{n}_4$ scales with $d^{-19/4}$. Therefore, by using a vortex capillary with a larger diameter, the required heat input, $\dot{Q}_{fp}$, to obtain a a given $\dot{n}_4$, is lower. The advantage of running the fountain pump with a lower $\dot{Q}_{fp}$ is that it reduces the heat load on the 1.7 K stage. Figure 3.14 shows our experimental results: the fountain pump temperature and the fountain pressure as a function of the ^{4}He flow rate for the two capillaries we used: 72 μm and 136.8 μm. $P_f(T_{fp})$ is obtained from measurements of T_{fp} and by using the thermodynamic relation:

$$P_f(T_{fp}) = \frac{1}{v_{40}} \int_0^{T_{fp}} s_{40}\, dT \tag{3.15}$$

where v_{40} is the molar volume and s_{40} the molar entropy of pure liquid ^{4}He. s_{40} is obtained using the interpolation from [34].

In figure 3.14 also shown are fits to the data. The fits were chosen to be of the form of eq. 3.14:

$$P_f(T_{fp}) = A + B\dot{n}_4^m \tag{3.16}$$

where A is the osmotic pressure in the still (depending on T_{still}, x_{still}), m is supposed to be 1.75. and the pre-factor B depends on the length and diameter of the vortex capillary, but also weakly on T_{fp}, through the ratio $\eta(T_{fp})^{0.25}/\rho(T_{fp})$. In the fits A and B were set constant, but actually they vary slightly during the $\dot{n}_4$ sweeps because T_{still}, x_{still} and T_{fp} change slightly

[6]When I say overall concentration I refer to the ^{3}He circulating in the whole system (in the refrigerator, in the pump and in the gas handling system). This means that in the still the concentration is smaller than what I call overall concentration.

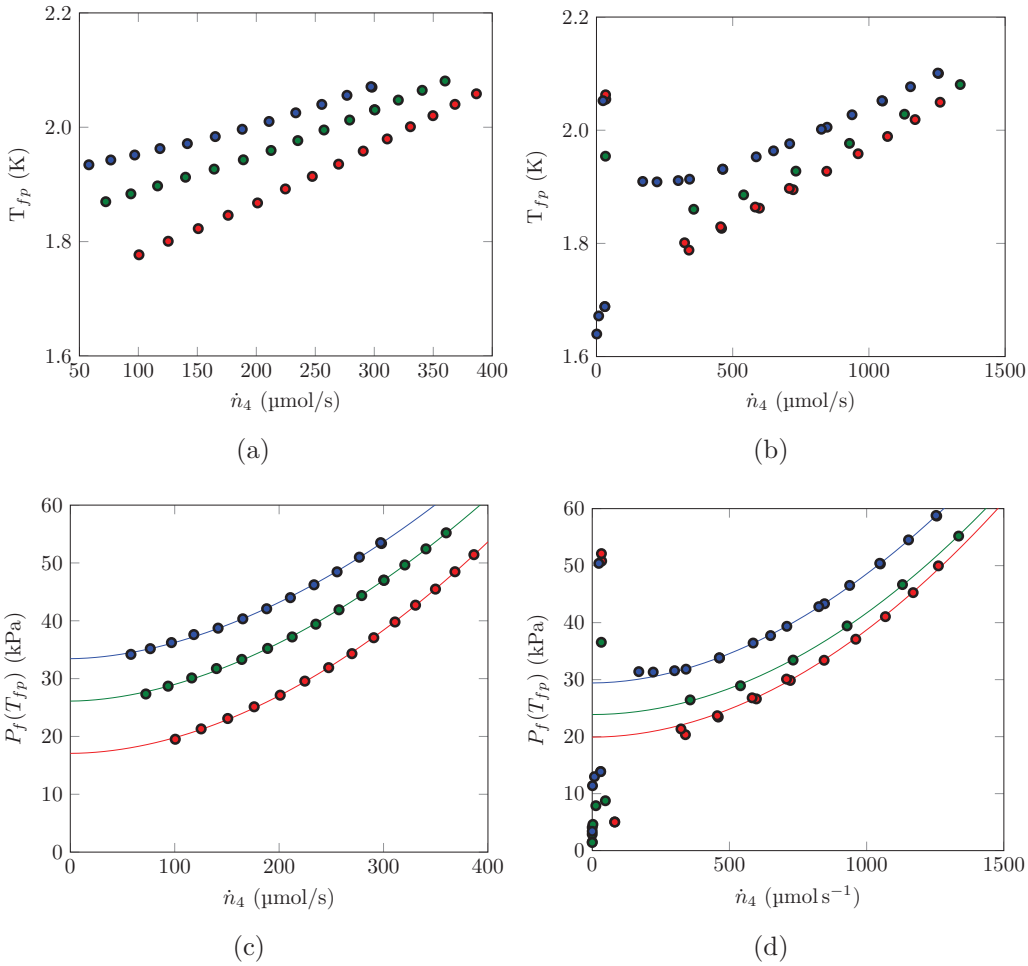

Figure 3.14: The fountain pump temperature as a function of the ^{4}He flow rate for two vortex capillaries of different diameter: 72 μm (a) and 136.8 μm (b). Panel (c) and (d) show the fountain pressure at T_{fp} as a function of the ^{4}He flow rate for the same vortex capillary diameters (c-72 μm, d-136.8 μm). The different colors represent different still pressure (red points - 0.3 mbar, green points - 5.0 mbar, blue points - 10 mbar). Data for the 72 μm capillary are at an overall[6] concentration of 0.1. Data for the 136.8 μm capillary are at an overall concentration of 0.13 (for P_{sill}=0.3 mbar) and 0.07 (for P_{sill}=5 mbar and P_{sill}=10 mbar). In the 136.8 μm curve note at low flow rates the evident change between the second and the third regimes mentioned above.

		fit			calculated		
Capillary (μm)	P_{still} (mbar)	A_f (mbar)	$B_f(*10^{-4})$ $\left(\frac{KPas^{1.75}}{\mu mol^{1.75}}\right)$	m_f	A_m (mbar)	$B_m(*10^{-4})$ $\left(\frac{KPas^{1.75}}{\mu mol^{1.75}}\right)$	m_m
72	0.3	171	4.79	1.88	–	6.43−6.83	1.75
	5.0	261	7.21	1.80	252−270	6.46−6.86	1.75
	10.0	335	7.05	1.80	329−355	6.52−6.81	1.75
136.8	0.3	199	2.90	1.94	–	2.54−2.70	1.75
	5.0	239	2.33	1.96	191−260	2.55−2.72	1.75
	10.0	294	3.98	1.89	268−340	2.54−2.75	1.75

Table 3.8: Parameters (A_f, B_f and m_f) for the fits to the data plotted in figure 3.14 for two vortex capillaries with different diameter. Also shown are the parameters (A_m, B_m and m_m) calculated from the model (eq. 3.14). See footnote to know why I did nott calculate the parameter A for the lowest pressure.

during the $\dot{n}_4$ sweeps. The results for the fits compared to the theoretical values (eq. 3.14) are listed in table 3.8. For the theoretical parameters A[7] and B[8] I give a range of values, considering the change in T_{still}, x_{still} and T_{fp} during the $\dot{n}_4$ sweeps. The parameter A from the fits is well in the range, but not the parameter B: it is from a few percent up to 30 % out of range. m is from 3% up to 10% higher than the value in the model.

Even if the model does not match exactly the reality, the important thing we can learn from these experiments is that we can have the same range of P_f, and so of T_{fp}, with much higher ^{4}He flow rates (up to 1500 μmol/s). Therefore, with the larger capillary, we can circulate, for example, at P_{still}=5.0 mbar about 350 μmol/s of ^{4}He with a $\dot{Q}_{fp}$ of 1.7 mW instead of 3.6 mW

[7] A has been calculated by using T_{still} (measured) and x_{still} and by using a fit to the data from [42]. x_{still} is determined by measurements of T_{still} and P_{still} and by interpolating data from [33]. This method is unreliable for $P_{still} < 1$ mbar because of the pressure drop between the liquid vapour interface and the pressure gauge outside the cryostat.

[8] B has been calculated from measurements of T_{fp} and by using data from [34] for the viscosity η and the density ρ.

(value for the smaller capillary). This means to have a T_{fp} of 1.86 K instead of 2.08 K. This reduces appreciably (by almost two times) the heat load on the pre-cooling stage: from 2.6 mW to 1.4 mW. For the larger capillary, at P_{still}=10 mbar and at the same value of $\dot{n}_4$, the heat load on the pre-cooling stage is 1.6 mW, less than that at P_{still}=5 mbar for the smaller capillary. So, if we decrease by two times the heat load due to the ^{4}He flow calculated in table 3.6 for the still pressure of 10 mbar, we would obtain a total heat load on the pre-cooling stage (about 5.1 mW) comparable to the available cooling power provided by the SPICA ^{3}He Joule Thompson cooler. Table 3.6 shows that at still pressure higher than 5 mbar the main contribution to the total heat heat load is due to the ^{3}He circulation. It would be possible to diminish also this contribution by using a heat exchanger between the outgoing (pumped from the still) and incoming (from ^{4}He bath to 1.7 K stage) ^{3}He gas. In this way the ^{3}He, instead of going directly from the ^{4}He bath at 4.2 K to the 1.7 K pot, would be first pre-cooled at a temperature less the 4.2 K.

Concluding I can say that, by using a vortex capillary with a larger diameter, the heat load on the pre-cooling stage can be kept below 5.0 mW also at pressures between 5 and 10 mbar, with still room for improvement.

3.4 CCDR operational conditions

Here I summarize the conflicting parameters that affect the optimisation of our system:

- for the cooling performance:

- low P_{still}
- relatively high x_{still}

Since in this way the load on the high temperature part of the heat exchanger is lower and the circulating ^{3}He is more pure. Higher P_{still} implies need of higher x_{app} (or higher $\dot{n}_3$ for the same $\dot{n}_4$) which affects negatively the minimum temperature and the heat load on the pre-cooling stage.

- For the fountain pump:
  - low P_{still}
  - low x_{still}

  Increasing both parameters implies higher T_{fp} with two possible consequences: T_{fp} could exceed the λ-temperature and the heat load on the pre-cooling stage is higher.

- For the ^{3}He compressor:
  - high P_{still}
  - low $\dot{n}_3$

At the moment, experimentally, the result of the trade-off is:

- A still pressure between 5.0 and 10 mbar (which means a ^{3}He concentration in the liquid dilute mixture in the still of at least 10%).
- A still temperature between 1.1-1.3K.

- A ^{4}He flow rate between 400 and 350 μmol/s with corresponding values of ^{3}He flow rate between 15 and 30 μmol/s.

Under these conditions the CCDR is presently able to deliver 1 μW of cooling power at a temperature between 45 and 46.7 mK (which means a temperature between 51.4 and 52.6 mK for the load heater), keeping the heat load on the pre-cooling stage below 5.1 mW.

The system can be improved:

- decrease the minimum temperature of the detector simulator improving further the thermal contact between detector and the liquid mixture.

- Optimizing the vortex tube of the fountain pump that reduces the heat load on the pre-cooling stage due to the circulating ^{4}He.

- Pre-cooling the injected ^{3}He gas with the outgoing gas that diminishes the heat load on the pre-cooling stage due to the ^{3}He circulation.

Chapter 4

Negative Gravity Vapor Liquid Phase Separation

A crucial step to demonstrate the feasibility of using a closed-cycle dilution refrigerator in space is to confine the liquid mixture in the still under operating conditions. In order to design a still that can operate in a microgravity environment we built a dedicated setup to study negative gravity vapor liquid phase separation (NG-VLPS) of ^{3}He-^{4}He mixture by means of capillary forces inside porous materials. This chapter describes the NG-VLPS test setup and presents the final results. Some of historic long-winded path are found in appendix B. The output of these experiments has been very important for the design of a gravity-insensitive still.

4.1 Method

The results shown in previous chapter have been obtained with a prototype using a conventional (gravity-sensitive) still to separate the liquid and vapor phases. Even though the performances of the CCDR can be improved further, we had to stop working on it in order to focus on another crucial problem: the confinement of the mixture liquid phase in the still in zero-gravity. This step is essential to demonstrate the feasibility of using a closed-cycle dilution refrigerator in space. We investigated two methods: the first one, based on the interaction among the fountain pressure, the capillary forces, the counterflow of the normal and the superfluid components and the gas flow rate, was ineffective. The second one, that uses capillary forces only to retain the liquid inside porous materials, has been successful. In this chapter I will focus on the second method.

The basic idea is to trap the liquid ^{3}He-^{4}He mixture inside the pores of a porous material (that from now on I will call sponge) by capillarity under negative gravity conditions (the worst case). The confinement has to be compatible with the conditions under which the best trade-off among the best CCDR cooling performance, the operation of the ^{3}He compressor and the constrains on the heat load on the pre-cooling stage has been obtained. Here I recall them:

- A still pressure between 5.0 and 10 mbar.
- A still temperature between 1.1-1.3 K (which implies a ^{3}He concentration in the liquid dilute mixture in the still of at least 10%).

- A ^{4}He flow rate between 400 and 350 μmol/s with corresponding values of ^{3}He flow rate between 10 and 30 μmol/s.

4.1.1 Materials

We built a dedicated setup to study negative gravity vapor liquid phase separation (NG-VLPS) and the output of these experiments led us to the construction of a new negative gravity still (NG-still). With this setup we tested two materials: a bronze sinter[1] and a ceramic foam Procelit P160[2] [43]. These two materials differs in thermal conductivity (bronze conduct better than Procelit 160) and in void fraction (40% for bronze, 90% for Procelit P160).

Table 4.1 summarizes the main characteristic of the two materials we used: the permeability, the void fraction and the volume available for the liquid. The permeability has been determined from the pressure drop caused by a helium flow at 300 K through both materials. The void fraction of the bronze (for that of Procelit we took the value in Afonso thesis [43]) has been measured weighting the sponge box plus the bronze sinter and knowing the volume occupied by the copper box and the bronze and the density of the two materials. The open space in the sponge has been calculated considering the sponge box volume (6.3 cm^3) and the void fraction.

The procelit is a good candidate for our purpose for different reasons: firstly it has already been used in space, with pure ^{3}He, in the sorption

[1]This material has been provided and manufactured by the Federal-Mogul Sintertech SAS.

[2]This material has been provided by Lionel Duband, SBT-CEA (Service des Basses Temperatures of the Commissariat a l'Energie Atomique) in Grenoble.

	Bronze sinter	Procelit 160
Permeability (10^{-12}m^2)	1.70	3.80
Void Fraction (%)	40	90
Open space (cm^3)	2.5	5.7

Table 4.1: The permeability, the void fraction and the volume available for the liquid of the two materials we used for the NG-VLPS experiments.

cryocooler developed by SBT-CEA for the Herschel satellite [44]; secondly its void fraction is higher than that of bronze so that, for a given sponge volume, it can contain more liquid. Moreover it is easier to handle than bronze sinter. For the NG-VLPS setup we prepare ourself the Procelit P160, cutting it with a sharp piece of metal, while for the bronze sinter we had to ask to an industry to manufacture it. On the other hand, being a ceramic, the Procelit P160 is not a good conductor of heat. Therefore, we were afraid that the use of this material would lead to a non-uniform temperature in the still, so causing some issues for the confinement. For this reason we wanted to test a material with higher thermal conductivity, but permeability similar to that of Procelit P160, which already worked in space. We looked for industries that could sinter material with high thermal conductivity and we found the the Federal-Mogul Sintertech SAS, whose bronze sinter had a permeability of the same order of magnitude of Procelit P160.

We calculated the capillary height in the Procelit P160. The capillary height is the maximum height that a liquid is able to climb in a capillary tube. If we assume the porous material is made of small capillaries of radius r and we know the surface tension σ and the density of the fluid ρ the capillary height

h_c is given by:

$$h_c = \frac{P_c}{\rho g} \tag{4.1}$$

where g is the gravitational acceleration and $P_c = 2\sigma/r$ the pressure at which the capillary attracts the liquid. For the surface tension we took the value from Edwards and Saam [36] for a 10 % mixture. For the pore radius of our ceramic we took the values determined by J. Afonso in her thesis [43]: she found for two different cells 21 μm and 15 μm. Using this two values we obtain $P_c = 0.29$ mbar and 0.4 mbar and $h_c = 2.0$ cm and 2.8 cm. These values[3] of h_c are comparable to the distance between the bottom of the stainless steel container and the bottom of the sponge (about 1-1.5 cm). In a static situation to keep the liquid inside the sponge h_c has to be higher than this distance. In our situation the dynamic effects can still keep the liquid inside.

We also tried to find the maximum quantity of liquid we can inject in the system before the sponge overfills. We did it quite carefully with the Procelit P160: the liquid (pure ^{4}He) starts to leak (2.5 mm indicated by the level gauge) between 6.9 and 7.3 cm^3. This is the volume occupied by the liquid if all the gas injected in the system was liquid. This is not the case, because some gas does not liquefy in the cryogenic part of the experiment, but stays in the circulation circuit (pump, liquid nitrogen traps, tubing). Moreover some liquid does not fill the sponge, but stays in the injection capillary. For this reason the maximum quantity of liquid we can inject is higher than the volume available in the sponge. Considering that the level gauge indicates

[3]For the bronze P_c and h_c should be of the same order of magnitude because the permeability is very similar to that of the Procelit.

2.5 mm and the diameter of the hole of the liquid collector is 1 cm, 0.2 cm^3 of liquid are at the bottom; the rest (7.1 cm^3) is the sponge and in the rest of the system. For the bronze we were less accurate: the liquid (pure ^{4}He) does not leak yet at 3.8 cm^3, while it leaks in great quantity (8 mm indicated by the level gauge) at 4.9 cm^3. 8 mm mean 0.63 cm^3 of liquid at the bottom; the rest (4.2 cm^3) is the sponge and in the rest of the system.

4.2 Test setup

4.2.1 Setup description

Figure 4.1 shows a schematics of the two variations of the cryogenic parts of the setup that finally allowed us to demonstrate the confinement of the liquid mixture in a sponge under negative gravity conditions. In appendix B I present the history of the different variations of the setup before arriving at the two final working setups. The sponge (magenta crosshatch) made out of either bronze sinter or Procelit P160 is contained in a cylindrical pot (red) made out of solid copper. Liquid ^{3}He-^{4}He mixture (yellow) is confined in the sponge and fills the injection capillary. The 1 mm diameter orifice at the bottom of the sponge box limits the superfluid ^{4}He film flow out of the sponge box. Assuming a film volume flow ($\dot{V}$) at 1 K of $7{\cdot}10^{-5}$ cm^3/s/cm [17] and the ^{4}He molar volume (v_4) of 27.6 cm^3/mol, I estimate that we can limit the film flow ($\dot{V}\pi D_{orifice}/v_4$) to about 1 μmol/s (see appendix B for more details about the film flow).

The 1 mm diameter orifice at the top of the sponge box in figure 4.1 (a)

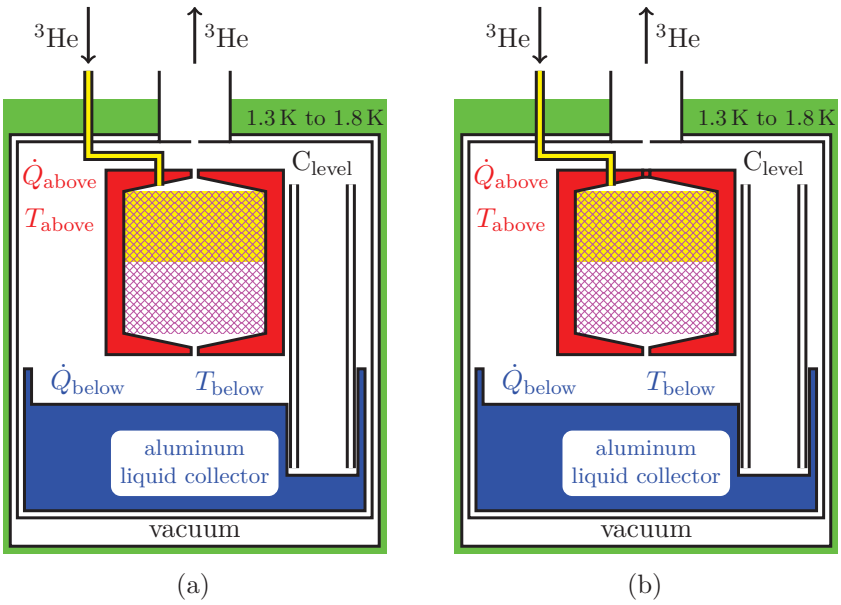

Figure 4.1: The two final working variations of the NG-VLPS test setup (see explanation in the text). The setup (b) is almost completely identical to the setup (a) except for the plugging of the gas escape orifice in the top of the sponge box. Only a sponge out of Procelit P160 has been tested with this setup.

vents eventual helium gas entering the sponge box. In the setup in figure 4.1 (b) we decided to plug the gas escape orifice. The sponge box is mounted against the top of a stainless steel container inside a vacuum can. The can is placed in a pumped ^{4}He bath (green). This is a negative gravity configuration because the liquid is injected in the sponge from the top and the gas, rich in ^{3}He, comes out through the orifice at the bottom of the sponge box. Then the gas is circulated by pumping it through the orifice in the stainless steel container and by condensing it through the injection capillary into the sponge box. A coaxial cylindrical capacitive liquid level gauge serves to detect liquid that might have leaked out of the sponge box. An aluminum liquid collector (blue) at the bottom of the container restricts the space for leaked liquid to a cylindrical hole around the liquid level gauge. The diameter of the hole is 1 cm. Therefore, the liquid collector maximizes the liquid level height around the level gauge per volume of liquid leaked. A resistance heater $\dot{Q}_{\text{above}}$ and thermometer T_{above} are mounted on the top of the sponge box. A resistance heater $\dot{Q}_{\text{below}}$ and thermometer T_{below} are placed on the aluminum liquid collector. The circulation rate of the helium gas depends on the power applied to the heaters. The operation of the capacitive liquid level gauge can be checked by means of heater $\dot{Q}_{\text{below}}$ and thermometer T_{below}, since the thermometer T_{below} reacts differently depending on the presence or absence of liquid helium in the collector when power is applied to heater $\dot{Q}_{\text{below}}$.

The principle of the capacitive liquid level gauge is based on the idea that its capacitance changes if its plates are partially or entirely filled with a dielectric material (in our case the liquid mixture). Its capacitance value when empty,

C_{empty}, is given by:

$$C_{empty} = \frac{2\pi\epsilon_0 h}{ln(D_{outer}/D_{inner})} \tag{4.2}$$

where ϵ_0 is the electric constant ($8.854{\cdot}10^{-12}$ Fm^{-1}), $h = 50$ mm is the height and $D_{outer} = 8$ mm and $D_{inner} = 7$ mm are the outer and inner diameters of the capacitors. The experimental value at 300 K is 19.65 pF in agreement with the value found applying eq. 4.2 (20.83 pF). At low temperatures ($\sim$1 K) it varies slightly: about 19.25 pF.

If the capacitor is partially filled with liquid mixture its capacitance C is given by:

$$C = \frac{2\pi\epsilon_0(h + (\epsilon - 1)x)}{ln(D_{outer}/D_{inner})} = C_{empty}\left(1 + \frac{(\epsilon - 1)x}{h}\right) \tag{4.3}$$

where ϵ is the dielectric constant of the liquid mixture and x the capacitor length filled with liquid. We obtain x from measurements of C using:

$$x = \left(\frac{C - C_{empty}}{C_{empty}}\right)\frac{h}{(\epsilon_{mix} - 1)} \tag{4.4}$$

For ϵ we take the value for ^{4}He because the dilute liquid mixture is composed mostly by ^{4}He (the error we make in the evaluation of the hight is a few percent).

Figure 4.2(a) shows a picture of the sponge box: it is upside-down and without the cap with the orifice to restrict the film flow to show the bronze sinter inside. In figure 4.2(a) also shown are the size of the sponge box and some labels to recognize the different pieces. Figure 4.2(b) shows the setup, without the the cap with the orifice, assembled before closing it in the stain-

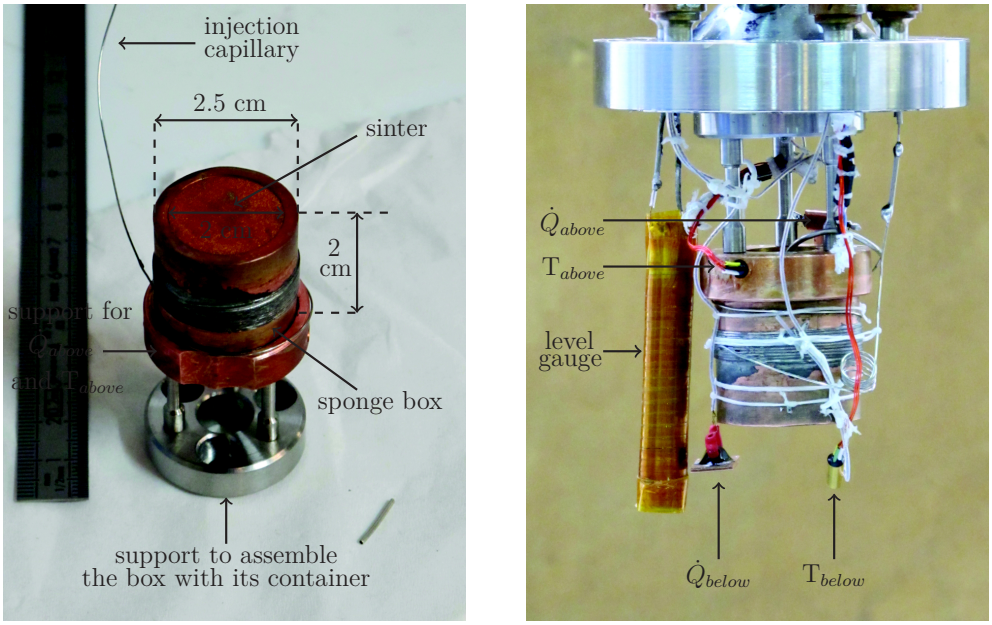

(a) (b)

Figure 4.2: (a) Upside-down sponge box and without the cap with the orifice to restrict the film flow to show the bronze sinter inside. The ^{3}He injection capillary is 140 μm in diameter and it is thermally anchored to the copper box. (b) Setup (without the the cap with the orifice) assembled. The capacitive level gauge is 5 cm in height, its inner diameter is 6 mm and its outer diameter is 8 mm. It is covered with Kapton tape to electrically isolate it. The two thermometers are germanium.

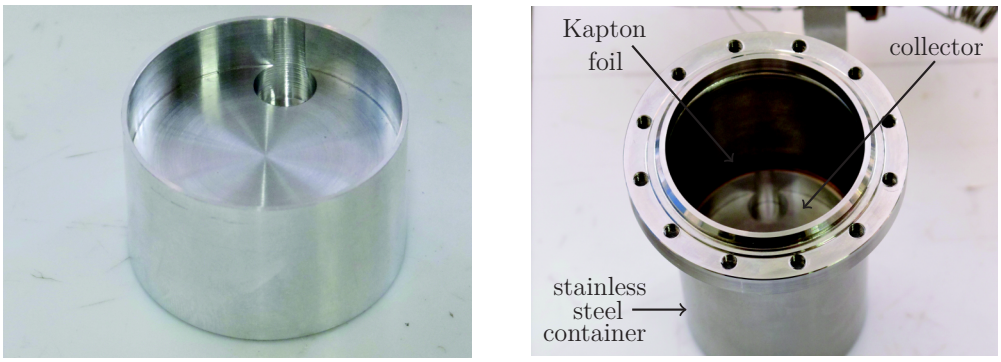

(a) (b)

Figure 4.3: (a) The aluminium liquid collector. It is possible to see the hole in which the capacitive level gauge is inserted. (b) The stainless steel container in which the sponge box is inserted. At the bottom is visible the aluminium collector and the Kapton foil to minimize the the space in the radial direction.

less still container. In figure 4.3(a) the aluminium collector is shown. The hole in the collector is also used to align the capacitive level gauge in vertical position. In figure 4.3(b) it is inserted in the stainless still container and it is also possible to see the Kapton foil filling about 75 % of the space between the aluminum liquid collector and the stainless steel container (about 0.4 mm in radious). The Kapton foil serves to minimizes this space, where the liquid can "hide" without being detected after it has been leaked out of the sponge. Another space below the level gauge where the liquid could "hide" is a gap from 1 mm to 2 mm between the bottom of the aluminum collector hole and the bottom of the liquid level gauge (the gap is partly due to an Araldite spacer to center the coaxial electrodes of the capacitor and partly due to difficulties in assembling the container, the aluminum liquid collector, and the liquid level gauge). The volume of liquid not detected could be significant: imagine that 1 mm of liquid leaks and hide in these spaces. This means that

0.14 cm^3 of liquid is not detected. This volume of liquid not detected is a few % of the maximum liquid that could be contained in the box and in the rest of the system (7.1 cm^3 for Procelit P160 and 4.2 cm^3 for the bronze sinter). It is not a negligible amount.

These spaces where the liquid could go without being detected are the weak point of the NG-VLPS setup. Actually we will see in section 4.2.4 that the liquid level gauge detects the presence of liquid, even when the liquid is below the gauge.

4.2.2 Test equipment

Figure 4.4 shows the test equipment, which consists of:

- A liquid helium cryostat that can be pumped to almost 1.3 K.
- A cryogenic insert implementing the setups already shown in figure 4.1.
- The CCDR ^{3}He-^{4}He gas circulation panel (mentioned in appendix A and described in [45] and [24]), used to handle the helium and to obtain the experimental data related to the amount of gas in the system, pressures and flow rate. The same system was used for experiments on the CCDR.
- A SRS RGA 100 quadrupole mass spectrometer combined with a Pfeiffer HiPace 80 turbo-molecular pump. The RGA has been used for the last experiments on the NG-VLPS setup and it has been proved essential to know the composition of the circulating gas.

- A computer running a data acquisition program consisting of several Python modules to acquire the data from different instruments. The different modules are:
  - a module controlling an Andeen-Haegerlingh AH2550A capacitance bridge to read the capacitive liquid level gauge.
  - a module controlling a Thermometer over Ethernet (ToE), Carte E, to read thermometers T_{above} and T_{below}.
  - a module reading the helium gas flow meter and the pressure gauges on the gas circulation panel from the NI FieldPoint I/O system. The module also controls the heaters $\dot{Q}_{\text{above}}$ and $\dot{Q}_{\text{below}}$ via the NI FieldPoint I/O system.
  - a module reading the ^{3}He and ^{4}He partial pressures from a PPM100 partial pressure monitor connected to a RGA residual gas analyzer.

The measurements taken with the mass spectrometer combined with the turbo-molecolar pump are subject to two systematic errors:

- The mass spectrometer measures the relative heights of the ^{3}He and the ^{4}He signals of a gas mixture that has leaked from the circulating helium through a Kapton membrane. The permeability of ^{3}He is a factor $\sqrt{m_4/m_3}$ higher than the permeability of ^{4}He because of the difference in root-mean-square speed. Here, m_3 and m_4 are the atomic mass of ^{3}He and ^{4}He.

- The helium that has leaked into the mass spectrometer is continu-

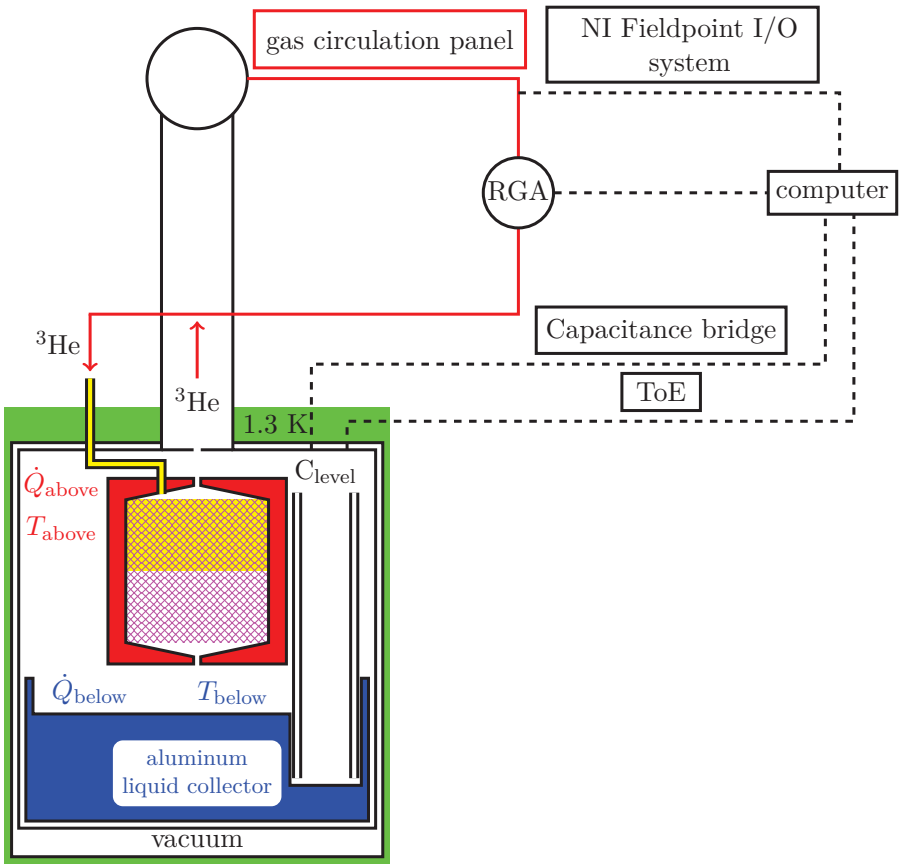

Figure 4.4: Test equipment (see explanation in the text). The dashed lines are the electrical connection.

ally pumped by a turbo-molecular pump. However, turbo-molecular pumps have a higher compression ratio for heavier gases than for lighter gases. The exact values depend on the particular design of the pump. Until further notice, we assume that the correction is another factor $\sqrt{m_4/m_3}$.

For these two reasons the system SRS RGA 100 plus turbo-molecolar pump is a factor m_4/m_3 more sensitive for ^{3}He than for ^{4}He, which means that the height of the ^{3}He signal is systematically a factor m_4/m_3 too high, while that of ^{4}He a factor m_4/m_3 too low. The estimate is also confirmed by the fact that with the this system a ^{3}He-^{4}He ratio of $1.3 \sim m_4/m_3$ has been measured for a prepared ^{3}He-^{4}He mixture with a concentration of 50%. We have corrected our measurements for this factor.

4.2.3 Test procedure

The objective of the NG-VLPS experiments is to establish the confinement of a liquid ^{3}He-^{4}He mixture under conditions (negative gravity, pressure from 5 mbar to 10 mbar, temperature from 1.0 K to 1.3 K, liquid ^{3}He concentration of about 10 %, and circulation rate from 10 µmol s^{-1} to 30 µmol s^{-1}) that are compatible with the operation of the still of the CCDR and of the ^{3}He compressor. When the cryostat has been pumped down to a temperature from 1.3 K to 1.7 K the following procedure has been applied:

- Assure that known quantities of ^{3}He and ^{4}He have been added[4] into

[4]We collect the ^{3}He and ^{4}He gas (150 mbar of ^{3}He and 700 mbar of ^{4}He) in three

the system, consisting of the setup shown in previous section and the circulation circuit (pump, liquid nitrogen traps, and tubing). This allows to calculate a upper limit for the volume V taken by the liquid[5], and the overall ^{3}He concentration x_{in} of the helium gas in the system. In general, the ^{3}He concentration in the low temperature part of the experiment is lower than x_{in} because gas rich in ^{3}He accumulates in the back of the pump and the liquid nitrogen traps.

- Set the pressure, that I will call P_{still}, to a value from 0.3 mbar to 10 mbar to simulate a future space qualified pump with lesser pump specifications than the pump in the gas handling system.

- Use $\dot{Q}_{\text{above}}$ or $\dot{Q}_{\text{below}}$ to apply heating power steps from 0 mW to 2 mW with a duration typically from 3600 to 7200 s. We use $\dot{Q}_{\text{below}}$ not only to verify the operation of the liquid level gauge, but also to test the confinement. In fact, for the design of the new still, we are interested in knowing if there is any difference in heating directly the liquid in the sponge (using $\dot{Q}_{\text{above}}$) or indirectly (using $\dot{Q}_{\text{below}}$). At each step when the setup has reached a stationary state we:

  - Measure the circulation rate $\dot{n}$.

  - Measure the liquid level height h.

storage tanks at room temperature. These three reservoirs (35 L in volume) allow us to inject in the system different amount of ^{3}He and ^{4}He and so to vary the ^{3}He concentration and the volume of liquid in the system. Details about the gas circulation panel are in F. Martin thesis [24] and in the ESA report [45].

[5]This is the volume occupied by the liquid if all the gas injected in the system was liquid. Of course this is not the case, because some gas does not liquefy in the cryogenic part of the experiment, but stays in the circulation circuit (pump, liquid nitrogen traps, and tubing).

- Measure x_{vapor} by means of the RGA gas analyzer.
- Measure the temperature indicated by thermometers T_{above} and T_{below}
- Measure the still pressure.
- Determine x_{liquid} from measurements of P_{still} and T_{above} or T_{below} and by interpolating data from [33]. This method is unreliable for $P_{still} < 1$ mbar because of the pressure drop between the liquid vapour interface and the pressure gauge outside the cryostat.

Another objective of these experiments is to verify the operation of the liquid level gauge. So we "overfill"[6] the sponge and we verify that zero liquid level coincides with the absence of liquid helium in the collector by applying power to heater $\dot{Q}_{\text{below}}$ and looking at the response of thermometer T_{below}.

4.2.4 Results

Figure 4.5 shows an example of the raw data acquired with the setup in figure 4.1(b) when executing the procedure described in section 4.2.3. I remind that we tested this setup only with Procelit 160. It shows the response of stepping the heater $\dot{Q}_{\text{below}}$ upwards from 0.49 mW to 1.44 mW

[6] I use the quotes because the liquid can leak if we entirely fill the sponge or if the pressure is increased.
"Overfilling" also depends on the ^{3}He concentration: when the ^{3}He concentration decreases, a larger volume of liquid can be retained by the sponge. The explanation is that the ^{3}He occupies more space than ^{4}He: its molar volume at low temperatures is about 37.5 cm^3/mol, while that of ^{4}He is 27.6 cm^3/mol. Moreover, the ^{3}He in the injection capillary is more likely to remain gas than ^{4}He. Therefore the dead volume for the ^{3}He could be smaller than that of ^{4}He, meaning that for the ^{3}He is more difficult to remain confined in the sponge.

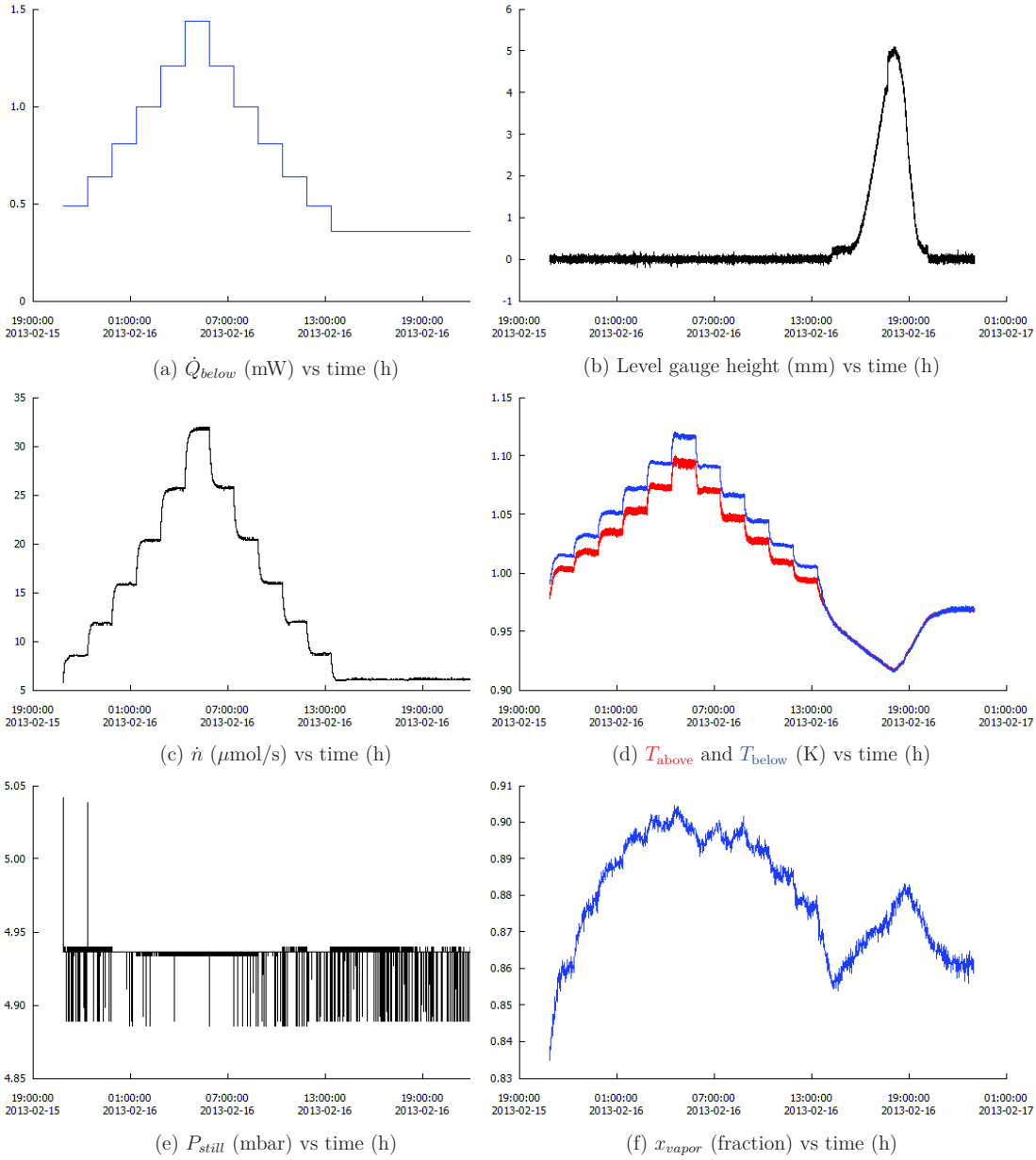

(a) $\dot{Q}_{below}$ (mW) vs time (h)

(b) Level gauge height (mm) vs time (h)

(c) $\dot{n}$ (μmol/s) vs time (h)

(d) T_{above} and T_{below} (K) vs time (h)

(e) P_{still} (mbar) vs time (h)

(f) x_{vapor} (fraction) vs time (h)

Figure 4.5: Raw data taken with the setup in figure 4.1(b). Parameters not given in the figures are: $x_{\text{in}} = 37.38\,\%$, $V_{\text{liquid}} = 5.53\,\text{cm}^3$, and T_{bath} from 1.3 K to 1.4 K. The time step is 1 hour and half.

and downwards from 1.44 mW to 0.36 mW. It is evident, from figure 4.5 (b), that the liquid is successfully confined because, during the $\dot{Q}_{\text{below}}$ sweep, there is no leaked liquid at the bottom (the liquid level gauge indicates 0 mm). The only exception is after 20 hours, when some liquid appears and disappears from the bottom spontaneously, without any notable change of parameters. Considering that the level gauge indicates 5 mm and the diameter of the hole is 1 cm about 0.4 cm^3 of liquid leaked. The interpretation we offer is that the amount of liquid in the sponge is close to "overfilling" and the applied power $\dot{Q}_{\text{below}} = 0.36\,\text{mW}$ is close to the limit necessary to keep the liquid in the sponge. Therefore, we assume that an instability due to an unidentified origin has led a temporary leakage of liquid out of the sponge.

I want to point out two more experimental facts about figure 4.5 (b): the first is that the temperature difference between T_{above} and T_{below} is practically zero while there is liquid at the bottom. Therefore we can verify if the liquid level gauge functions properly, in other words if it indicates liquid at the bottom when the two temperatures are equal and no liquid when the two temperatures are different. The second is that small steps in the liquid level are visible before the liquid leaks in a large quantity and after almost all liquid has gone back into the sponge. We believe, that liquid helium has leaked into space below the liquid level gauge during those small steps and that the steps are a signal of the superfluid ^{4}He film covering all surfaces and therefore also the liquid level gauge. In conclusion, the liquid level gauge detects the presence of liquid, even when the liquid is below the gauge.

Figure 4.6 shows the response to stepping the heater $\dot{Q}_{\text{below}}$ analyzed by averaging the different physical quantities over the last 25 % of each step

		$\dot{Q}_{\text{above}}$			$\dot{Q}_{\text{below}}$			
		$\dot{n}$	T=T	x_l	$\dot{n}$	T	T	x_l
Bronze	P_{still}=4.0	22.3	0.97	11.4	21.8	0.99	1.01	10.0
	P_{still}=10.0	17.6	1.29	8.9	20.0	1.21	-(*)	12.7
Procelit 160	P_{still}=5.0	20.5	1.03	10.8	15.9	1.04	1.05	10.7
	P_{still}=10.0	18.5'	1.19	11.5	17.5	1.23	1.25	10.2

Table 4.2: Data at 1 mW from different experimental runs for the two materials and for different pressures. Units: applied heating power in mW, pressures in mbar, flow rate in μmol/s, temperatures in K (T = T_{above}, T = T_{below}), concentration in %. For all this runs x_{vapor} is between 81 and 92 % (lower for high pressures, higher for low pressures). (*) In this run T_{below} temporarily did not work. Parameters not given in table: for bronze $x_{\text{in}} = 60.98\,\%$ and $V_{\text{liquid}} = 3.30\,\text{cm}^3$. For procelit for the run at 5 mbar $x_{\text{in}} = 47.6\,\%$ and $V_{\text{liquid}} = 4.58\,\text{cm}^3$, while for that at 10 mbar $x_{\text{in}} = 37.38\,\%$ and $V_{\text{liquid}} = 5.53\,\text{cm}^3$.

when the response has reached a stationary state. It shows that for values of $\dot{Q}_{\text{below}}$ between 0.5 and 1 mW the confinement is obtained for a ^{3}He flow rate between 8.7 and 20.5 μmol/s, temperatures between 1.0 and 1.05 K, ^{3}He concentration in the liquid between 10 and 13% and ^{3}He concentration in the vapor phase between 82 and 87%. I remind that for this series of data the pressure is 5 mbar. Those results are compatible with conditions mentioned above.

We also stepped $\dot{Q}_{\text{above}}$ and the results we found are very similar to those obtained with $\dot{Q}_{\text{below}}$. The only difference is that in this case T_{above} and T_{below} are exactly the same. The fact that heating the vapor phase (using $\dot{Q}_{\text{below}}$) the two temperatures are slightly different does not surprise because the vapor conducts heat less efficiently than the liquid. However we observed (figures 4.5 (d) and 4.6 (c)) that this difference is very small (less than 0.03 K), so it is not a concern for our purpose.

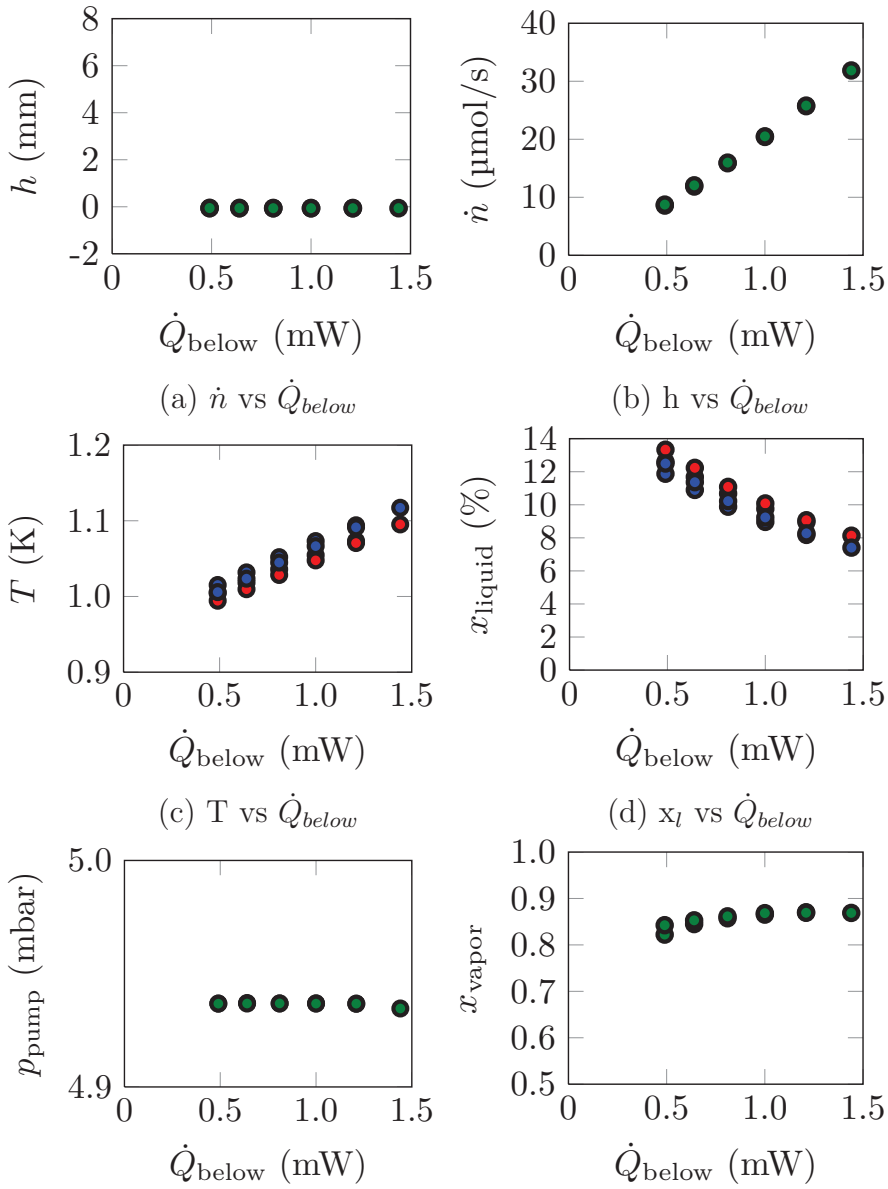

(a) $\dot{n}$ vs $\dot{Q}_{below}$

(b) h vs $\dot{Q}_{below}$

(c) T vs $\dot{Q}_{below}$

(d) x_l vs $\dot{Q}_{below}$

(e) P_{still} vs $\dot{Q}_{below}$

(f) x_{vapor} vs $\dot{Q}_{below}$

Figure 4.6: Results obtained with the setup in figure 4.1(b). Parameters not given in the figures are $x_{\text{in}} = 37.38\,\%$, $V_{\text{liquid}} = 5.53\,\text{cm}^3$, and T_{bath} from 1.3 K to 1.4 K. The red dots in figure (d) and (f) are respectively T_{above} and x_{liquid} calculated on basis of T_{above}. The blue dots in figure (d) and (f) are respectively T_{below} and x_{liquid} calculated on basis of T_{below}

.

We have obtained similar results for P_{still} up to 10 mbar and with the bronze sinter.

Table 4.2 summarizes some data at 1 mW from different experimental runs for the two materials and for different pressures. It shows that the results are similar for the materials and for stepping $\dot{Q}_{\text{above}}$ and $\dot{Q}_{\text{below}}$.

4.3 Test output for NG-still design

The experiments on the NG-VLPS test setup have led to the following points useful for the design of the NG-still:

- The Procelit P160 has been selected for the NG-still, for the reason I mentioned in section 4.2.1. Here I recall them:
  - it has already been used to retain liquid in space.
  - Its void fraction is higher than that of bronze so that, for a given sponge volume, it can contain more liquid.
  - It is easier to handle than bronze sinter.
- There is no significant advantage of heating the sponge pot directly (using $\dot{Q}_{\text{above}}$) or indirectly (using $\dot{Q}_{\text{below}}$). Therefore, we decided to heat the sponge pot indirectly, because it simplifies the NG-still design.
- Almost pure ^{3}He gas is pumped from the sponge through 1 mm holes to limit the ^{4}He circulation due to the evaporation of a creeping superfluid ^{4}He film.

- Successful confinement of the liquid can be checked by means of a concentric capacitive liquid gauge below the porous material.

- The presence of open space above the porous material has no negative effect on the confinement and should therefore allow the connection of the fountain pump superleak. We will see in the next chapter that in the NG-still design there is a space above the sponge forming the entrance for the fountain pump superleak. We designed it hoping that the liquid from the heat exchanger fills this space before being absorbed by the sponge (se section 5.5 for details).

Chapter 5

Negative Gravity CCDR

In this chapter I will present the negative-gravity still (NG-still) design, that builds on the results achieved with the NG-VLPS experiments. This new still is integrated in an "upside-down" version of the CCDR prototype mentioned in chapter 3: in this design the mixing chamber and the heat exchanger are placed above the NG-still. This choice has been made to simulate negative gravity and so to verify if a dilution refrigerator can work in such extreme condition. The main focus of this setup is to test the new still design combined with a fountain pump.

In this chapter I will also describe the experimental protocol, developed in the context of the ESA-ITI contract, to apply during the measurements. Then I will present the experimental results and the problems met during the measurements.

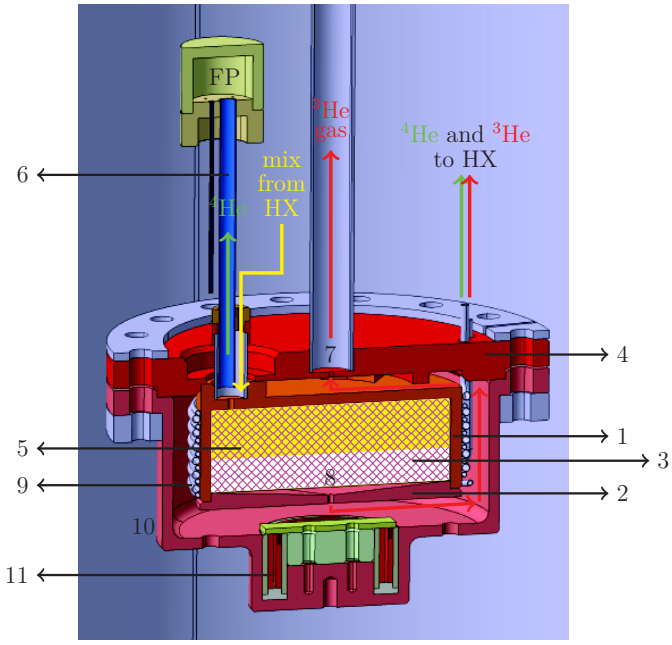

Figure 5.1: CAD cross section of the NG-still and the fountain pump. See the text for explanation. The design, the manufacture and the assembling have been made in collaboration with SERAS (Service Etude et Realisation d'Appareillages Scientifiques)-CNRS and the pôle Cryogénie of the MCBT (Matière Condensée - Basses Températures) department of Institute Néel.

5.1 Negative-gravity still design

Based on the results achieved with the NG-VLPS experiments, we have designed a new still that should work in negative-gravity conditions (NG-still). Figure 5.1 shows a cross section CAD drawing of the principal parts of the still and the fountain pump. The sponge pot (orange container-1 and pink lid-2 at the bottom of the container) contains the Procelit P160 (magenta crosshatch-3) and is soldered against the lid of the still (red-4). The ^{3}He-^{4}He mixture (yellow-5) from the heat exchanger is injected in the porous material from an open space above the sponge box close to the ^{4}He superleak (blue tube-6). Almost pure ^{3}He gas (red arrows) is extracted through the orifices

at the bottom of the pumping line (7), and the orifice at the bottom of the sponge pot (8). The fountain pump (FP) extracts pure liquid ^{4}He (green arrow) from the small open volume above the Procelit P160 box in the still. The two isotopes are then injected, after being pre-cooled in the 1.7 K pot, in the still heat exchangers (grey tubes around the sponge box-9), consisting in two capillaries soldered around the sponge box. The still pot (outer pink container-10) has a capacitive liquid level gauge at the bottom (red and light gray-11). The two holes at the bottom of the still pot are for coaxial cable feed-troughs used to measure the capacitive liquid level gauge. Figure 5.2(a) shows a picture during the mounting: the sponge box, soldered against the lid of the still and without the bottom to show the white Procelit 160 inside the box. Figure 5.2(b) shows the still box open to show, at its bottom, the capacitive level gauge. In figure 5.2(b) also shown are the size of the sponge and still boxes and some labels to recognize the different pieces.

The construction of the still of the NG-CCDR does not allow to check for the presence of liquid at the bottom by heating and checking the thermometer response. However, the still has been constructed to eliminate volume below the liquid level gauge to a maximum. In particular, the capillaries to the feed-troughs of the electrical wiring of the liquid level gauge have been filled with Stycast 2850FT (black spots in figure 5.3).

This NG-still has been integrated in a "upside-down" closed cycle dilution refrigerator. In this setup the mixing chamber and the heat exchanger are above the NG-still. In figure 5.3 (picture during the mounting) the NG-still is closed and assembled with the fountain pump and the heat exchanger.

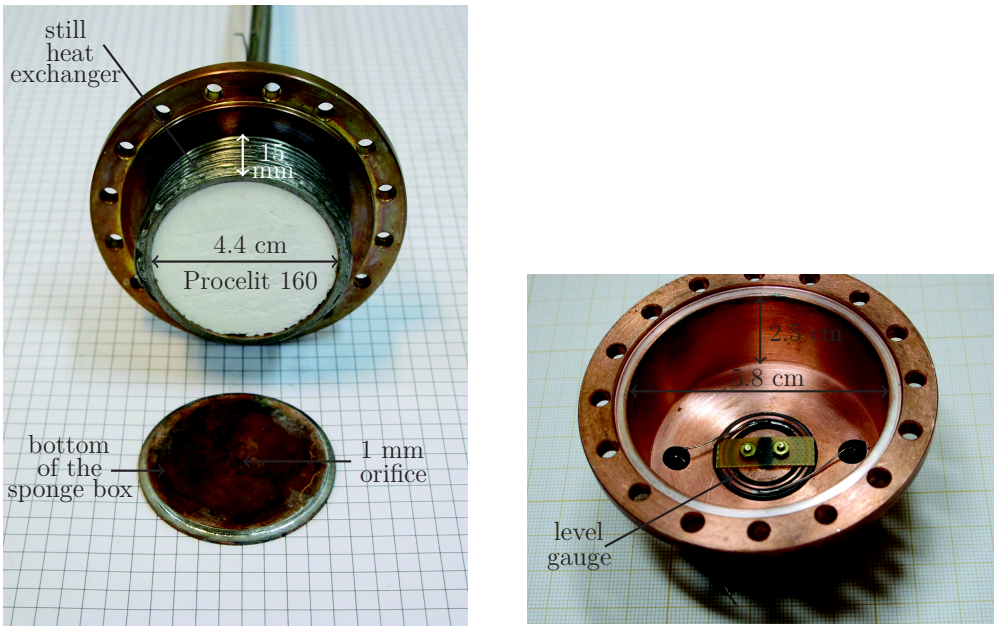

(a) (b)

Figure 5.2: (a) The sponge box, soldered against the lid of the still and without the bottom to show the Procelit 160 inside. The capillary soldered on the sponge box are the ^{3}He and ^{4}He still heat exchanger to pre-cool the two isotopes coming from the 1.7 K pot. (b) The still box open to show at its bottom the capacitive level gauge. Its hight is 1 cm, its outer diameter 2.1 cm and its inner diameter 2.0 cm. Its experimental value at 300 K is 10.75 pF, in agreement with the value found applying eq. 4.2 (11.40 pF).

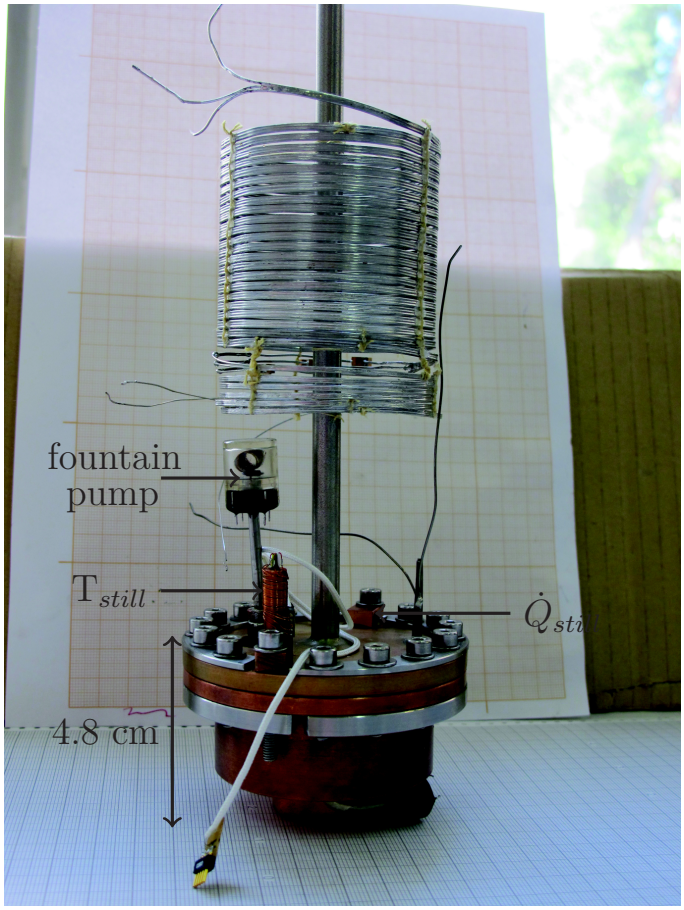

Figure 5.3: The NG-still assembled with the fountain pump and the heat exchanger.

5.2 Negative Gravity CCDR test setup

The objectives of the negative gravity closed cycle dilution refrigerator (NG-CCDR) setup are:

1. To show that a negative gravity closed cycle dilution refrigerator (NG-CCDR) works and to validate the design of the combination of a negative gravity still and a fountain pump.

2. To show that the operation of the negative gravity still is compatible with the conditions under which the best trade-off among the optimum CCDR cooling performance, the operation of the ^{3}He compressor and the constrains on the heat load on the pre-cooling stage has been obtained.

3. To show "reasonable" cooling performance of the NG-CCDR. The "upside-down" design in the existing vacuum can poses serious constraints on the space available for the heat exchanger and the mixing chamber. For this reasons the heat exchanger we designed is smaller than that described in section 3.2.1 and therefore the expected cooling power will be lower and the minimum temperature will be higher. With this setup the main focus is to test the still and the fountain pump to prioritize design decisions, leaving a test with an optimized dilution refrigerator heat exchanger and mixing chamber for later.

Figure 5.4 shows a schematic of the setup inside the 4.2 K vacuum that thermally isolates the dilution refrigerator from the surrounding liquid helium bath. The still (orange container) contains a sponge box (outlined in blue)

filled with Procelit P160 (magenta crosshatch) to confine the liquid mixture (yellow). A ^{3}He pump extracts almost pure ^{3}He through the orifice at the bottom of the sponge box and the orifice at the bottom of the pumping line. The fountain pump FP extracts pure ^{4}He (green) from a small open volume above the sponge box and then it goes towards the 1.7 K POT through the vortex capillary. The total length of the vortex capillary is 0.12 m and its inner diameter is 85.4 µm. This value is larger than that used in the original prototype CCDR. This choice has been made to reduce the required heat input to circulate the ^{4}He, and consequently the heat load on the pre-cooling stage. Almost pure ^{3}He (red) and pure ^{4}He (green) are pre-cooled by heat exchangers in the 1.7 K POT (marked HX-POT-^{3}He and HX-POT-^{4}He) and in the still (marked HX-STILL-^{3}He and HX-STILL-^{4}He). The 1.7 K POT is the same one as used in the original CCDR prototype. After the pre-cooling in the still the circulating ^{3}He and ^{4}He are injected in the counter-flow heat exchanger consisting of a (1-meter long) one-phase heat exchanger (HX-1-DR) with an inner diameter of 0.2 mm and in a (3.5-meter long) two-phase heat exchanger (HX-2-DR) with an inner diameter of 0.4 mm. In this setup the ^{4}He capillary is not replaced by a superleak. The two isotopes are injected in the mixing chamber (MC) and then the mixture makes its way down to the still through the return capillary. The return capillary between the mixing chamber and the two-phase heat exchanger is 1.5-meter long and its inner diameter is 0.6 mm. Figure 5.4 also shows the instrumentation - thermometers, heaters, and a liquid helium detector - needed to perform the tests.

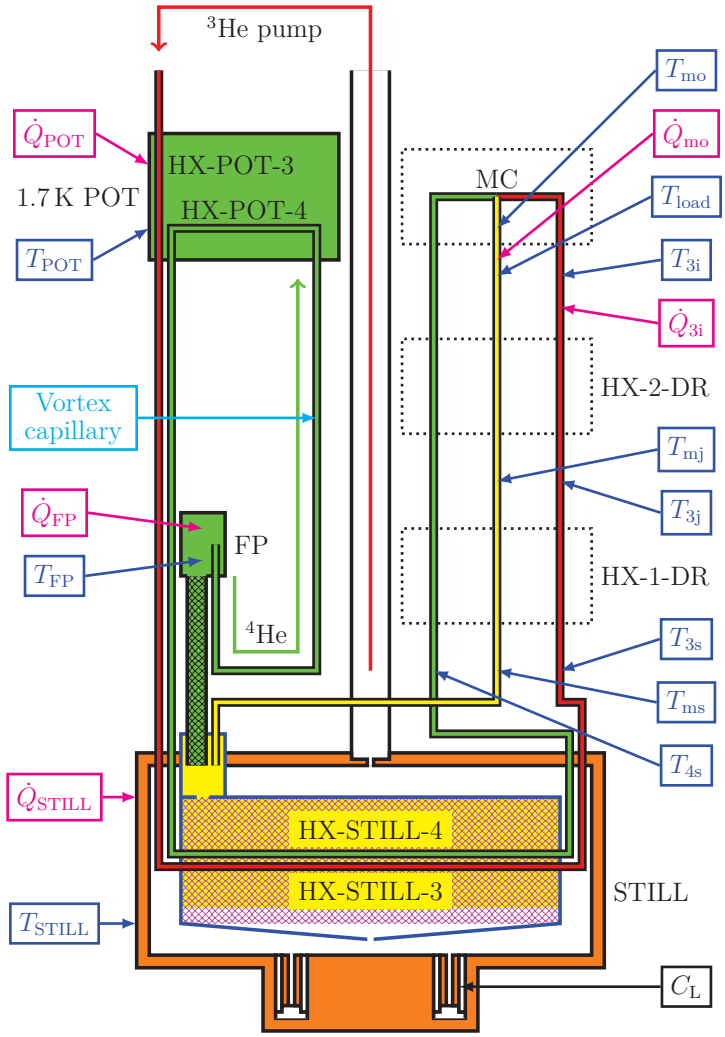

Figure 5.4: Schematic of the setup inside the 4.2 K vacuum that thermally isolates the dilution refrigerator from the surrounding liquid helium bath. See explanation in the text.
Thermometers and heaters: T_{POT} and $\dot{Q}_{\mathrm{POT}}$ are the 1.7 K pot thermometer and heater; T_{FP} and $\dot{Q}_{\mathrm{FP}}$ are the fountain pump thermometer and heater; T_{STILL} and $\dot{Q}_{\mathrm{STILL}}$ are the still thermometer and heater; $T_{3\mathrm{s}}$ and $T_{4\mathrm{s}}$ are respectively the thermometers on the ^{3}He and ^{4}He capillary just after the still; T_{ms} is the thermometer on the mixture return capillary just before the still; $T_{3\mathrm{j}}$ and T_{mj} are respectively the thermometers on the ^{3}He and mixture capillary at the junction between the one-phase and two-phase heat exchangers; $T_{3\mathrm{i}}$ and $\dot{Q}_{3\mathrm{i}}$ are the thermometer and heater on the ^{3}He inlet of the mixing chamber; T_{mo} and $\dot{Q}_{\mathrm{mo}}$ are the thermometer and heater on the mixing chamber outlet; T_{load} is the thermometer on the mixture return capillary between $\dot{Q}_{mo}$ and the two-phase heat exchanger.

5.2.1 Ng-CCDR setup cooling performance

The heat exchanger of the NG-CCDR is not designed to obtain a cooling power of 1 µW at 50 mK. However, two conditions are necessary to obtain this performance with a better heat exchanger in the future:

1. The NG-CCDR must be able to sustain the same circulation rates of ^{3}He (up to 30

ERROR: undefinedfilename
OFFENDING COMMAND: findfont

STACK:

/
/EJVHPN+